J.A.A. Kirsch

Performance Assessment of the Peak RDT for Damping Estimation under Non-ideal Conditions

Figure 1: Rotterdam Future Skyline [1]

TU Delft

TNO innovation for life

MSc Thesis

Performance Assessment of the Peak RDT for Damping Estimation under Non-ideal Conditions

by

Julie Kirsch

in partial fulfilment of the requirements for the degree of,
Master of Science in Civil Engineering,
at Delft University of Technology,
in collaboration with TNO,
to be defended publicly on July 16th, 2025.

Student number:	5855098		
Project duration:	February 10th, 2025 – July 16th, 2025		
Thesis committee:	Dr. E. Lourens,	TU Delft,	Chair
	Dr. A. Cabboi,	TU Delft,	Daily supervisor
	Dr. S. Sánchez Gómez	TU Delft,	Committee member
	Ir. A. J. Bronkhorst,	TNO,	Daily supervisor
	Ir. T. S. J. van Dijk	TNO,	Daily supervisor

TU Delft TNO

Contents

Preface

The completion of this Master's thesis marks the end of seven years of academic studies. Looking back to my first year, I could never have imagined graduating in the field of structural dynamics, having initially started a Bachelor's degree in Architecture, Building Sciences, and Urbanism. It was through my involvement with team VIRTUe that I discovered a passion for tackling complex technical problems and realised the importance of building a stronger technical foundation. This inspired me to pursue a Master's degree in Civil Engineering. Although the pre-master program was nearly as demanding as the thesis itself, I look back on these seven years with gratitude for the knowledge and skills I have acquired along the way.

This thesis has deepened my understanding of structural dynamics and the complexities involved in damping estimation. Through generating synthetic data, implementing the damping identification algorithm in Python, and analysing the results, I gained valuable experience that greatly enhanced my coding skills. Additionally, I developed a genuine interest and appreciation for creating visually engaging graphs for effectively communicating technical information.

I would like to thank my supervisors at TNO for their continuous support throughout my research and the experience gained from working alongside them. I am also grateful to my supervisors at TU Delft for their guidance and insightful feedback, which significantly enriched this thesis.

Finally, I would like to express my appreciation to my parents for their support and encouragement, continually motivating me to pursue the highest level of education possible.

Julie Kirsch
Delft, July 2025

Abstract

Accurately predicting damping in the design phase of high-rise buildings is essential for reliable assessments of occupant comfort. To improve damping prediction models for Dutch high-rise buildings, it is important to assess the reliability of damping estimates derived from measured vibration responses. This thesis aims to evaluate the performance of the Random Decrement Technique ranked by peak amplitude (Peak RDT) in reliably estimating damping, for systems exhibiting constant and amplitude-dependent damping, excited by stationary and non-stationary loading conditions. Since this assessment requires a known ground truth, a series of numerical studies are conducted, producing a distribution of damping estimates.

Under stationary loading conditions, the mean damping estimates are accurate for both systems. However, the precision of damping estimates is significantly reduced at low and high relative amplitude ranges. At low amplitudes, the reduced precision in damping estimates arises because the Random Decrement Signatures (RDS) fail to accurately capture the system's free decay, as segments are sampled at very low response levels. At high amplitudes, the lack of precision in damping estimates is primarily due to insufficient segment counts in the computation of the RDS, which prevents proper isolation of the system's free vibration response.

Moreover, RDS corresponding to the system with amplitude-dependent damping exhibit a non-uniform decay, causing fitting errors when using non-linear Least Squares Minimization to estimate a constant damping value. These errors can be mitigated by reducing the length of the segments sampled by the Peak RDT algorithm.

Three types of non-stationarity are introduced in the excitation: time-varying mean, time-varying variance, and their combination. While the second case yields level-stationary response signals complying with the underlying assumptions of the Peak RDT, the other two introduce time-dependent non-zero means in the response data, leading to significant accuracy errors in mean damping estimates for both linear and non-linear systems.

In conclusion, the Peak RDT yields reliable damping estimates for systems with constant and amplitude-dependent damping only under stationary loading conditions. However, it must be acknowledged that the degrees of non-stationarity considered in this thesis is rather large. The Peak RDT might still produce reliable damping estimates for mildly non-stationary vibration responses.

1 Introduction

The dynamic behaviour of high-rise buildings is an important area of research, particularly given the sensitivity of occupants to accelerations within these slender structures and the ongoing trend of urban densification [2]. Damping describes the amount of energy that is dissipated when a structure returns to its state of equilibrium after being excited [3]. Consequently, it is an import input parameter in the assessment of occupant comfort levels [4].

Determining appropriate damping values in the design phase of new high-rise buildings remains a difficult challenge due to its elusive nature [4]. While various prediction models exist, they do not seem to accurately capture the damping behaviour of Dutch high-rise buildings [5]. This highlights the need for improved empirical models, calibrated using a large dataset of damping estimates derived from measured ambient vibrations.

Yet, damping values estimated from response measurements are known to exhibit considerable variability resulting from the unknown loading conditions, the improper use of response measurements and the sensitivity to settings of the method used to estimate damping.

This thesis focuses on assessing the reliability of damping estimates derived using the Random Decrement Technique ranked by peak amplitude (Peak RDT) under conditions deviating from the method's mathematical assumptions. Assessing the reliability is essential for improving damping predictions models and ultimately, ensure occupant comfort in high-rise buildings.

The research is conducted within the framework of HiViBe [6], an initiative launched by TNO. HiViBe is a consortium focused on advancing knowledge on wind-induced vibrations in high-rise buildings in the Netherlands. A key focus of the research performed in HiViBe is the development of improved damping prediction models.

1.1. Research Context

Wind-induced vibrations of tall slender structures quickly reach the acceptable comfort levels in the serviceability limit state [4]. As seen in figure 1.1, high-rise buildings have inherently low natural frequencies, typically between 0.1 Hz and 1.0 Hz. These low natural frequencies overlap with the dominant frequency range of turbulent wind, which drives the dynamic excitation, and ranges from approximately 0.001 Hz to 0.030 Hz [7]. The proximity in frequency range can lead to resonance effects, causing high-rise buildings to quickly reach the aforementioned acceptable comfort levels. Consequently, high-rise buildings need to be carefully designed with respect to this governing criterion [8].

The modal mass, natural frequency and damping ratio are the main structural parameters that structural engineers use to compute the peak acceleration and assess the vibration comfort in high-rise buildings [5]. Even though all three parameters are difficult to predict accurately in the design phase, the damping ratio is particularly uncertain [4].

The elusiveness of damping can cause problems in the design phase of high-rise buildings, as poorly estimated damping results in inaccurate estimates of the peak acceleration and unreliable comfort

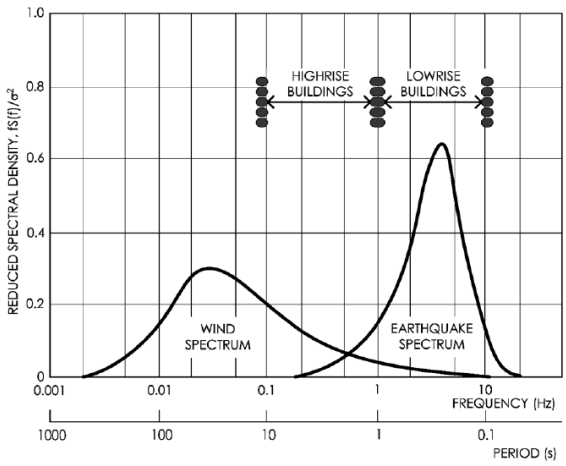

Figure 1.1: Frequency range of structures excited by wind and earthquakes [7]

assessments [9]. Unlike stiffness and mass, which are directly tied to the structure's physical and material properties, damping is a result of complex mechanisms that are not easy to quantify at the design stage [4]. Structural engineers can make use of empirical damping prediction models to estimate an appropriate damping value in the design-phase.

1.1.1. Empirical Estimators for Damping

An important part of the research performed within HiViBe relates to the improvement of damping prediction models, enabling structural engineers to reliably estimate damping in the design stage. This, in turn, allows for more accurate predictions of the peak acceleration and assessments of occupant comfort.

The damping values currently specified in design standards are based on in-situ measurements from existing high-rise buildings. These norms reflect decades of experimental research conducted on a wide range of tall buildings worldwide. In the Netherlands, wind-induced vibration assessments are carried out in accordance with EN 1991-1-4 [10], which provides a framework for evaluating wind actions and includes approximate damping values for different types of structures. The Dutch guideline NEN 6702 [11] provides limit values of acceptable peak acceleration levels.

Although EN 1991-1-4 specifies absolute damping values for high-rise buildings depending on the building material (0.8% for steel, 1.6% for concrete and 1.2% for hybrid structures [5]), research dating back to the 1970s and 1980s shows that damping is in fact amplitude-dependent, meaning that the effective damping increases with the building's response amplitude [3, 12].

The most widely recognized empirical models that do account for this amplitude dependency are Jeary's [13] and Tamura's [14] estimators. These models predict amplitude-dependent damping as a function of the building's fundamental frequency f_0, building width D and the so-called tip drift ratio x_H/h defined as the ratio between displacement at the top of the building x_H and building height h.

Bronkhorst et al. [5] compared damping values predicted by five different prediction models with damping values retrospectively estimated from response measurements, for twelve different Dutch high-rise buildings. One key insight is particularly relevant to this thesis. Figure 1.2 shows that, for most of the twelve buildings, the difference between the predicted and estimated damping values is significant. Considering all five prediction models, the difference between predicted and estimated damping values is consistently greater than 50%. It is noted that, both Jeary's and Tamura's prediction models tend to produce damping values that are lower than the values estimated from measurements. The discrepancy between predicted and estimated damping values suggests that existing empirical models may not fully capture the true damping behaviour of these high-rise buildings.

A possible explanation for the difference between predicted and estimated damping values is given by Gomez et al. [15]. For the soft soils, found in the Dutch delta region, the damping due to soil-structure

interaction greatly contributes to the total damping. This effect is currently not taken into account in the existing models as they are developed using data from other countries with significantly different soil conditions. This highlights the need for a prediction model that accounts for the specific soil conditions commonly found in the Netherlands [5].

Another factor contributing to the discrepancy between predicted and estimated damping is that the deterministic estimates, presented in figure 1.2 in red, are themselves associated with a considerable degree of uncertainty, as damping estimated from ambient response data may not always be reliable. The sources of this uncertainty are discussed in section 1.1.3.

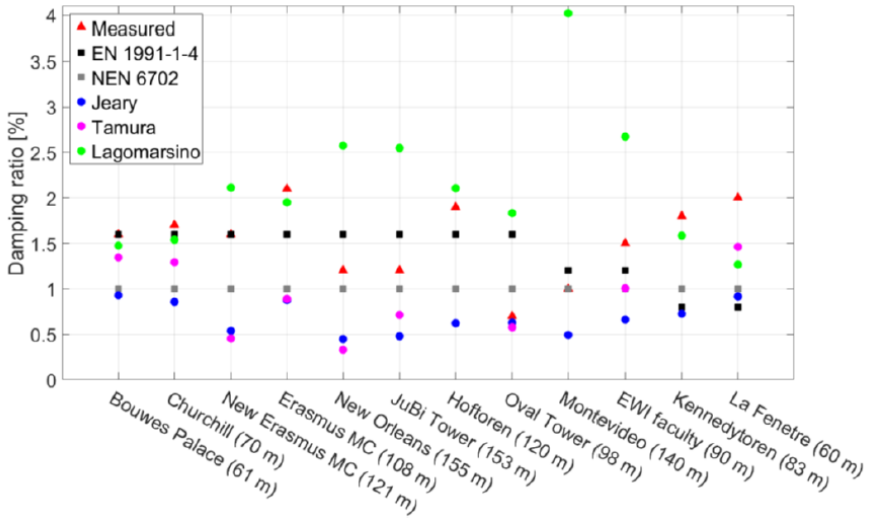

Figure 1.2: Predicted and measured damping for 12 high-rise buildings in the Netherlands (H ≥ 60 m) [5]

1.1.2. Towards Improved Empirical Estimators for Damping

Since current prediction models do not seem to accurately capture the true damping behaviour of Dutch high-rise buildings, there is a need for improved empirical models. New prediction models need to be calibrated using damping values estimated from measured vibrations of the buildings for which they are intended to be valid.

Modal parameters of structures, including natural frequency, mode shape and damping ratio can be identified from in-situ measurements of the structural response to a certain excitation through modal analysis. Many civil engineering structures can be sufficiently excited by ambient excitations such as wind. In that case, operational modal analysis (OMA) is suitable as it can be performed solely on measured response signals and does not depend on knowledge on the excitation [16]. Hence its pseudonym “output-only modal analysis”.

Although operational modal analysis (OMA) enables the estimation of modal parameters with minimal disruption to the structure’s normal use, it has significant limitations due to the unknown nature of the input forces. The absence of information about the input forces affects the reliability of damping estimates, particularly because damping identification is highly sensitive to the characteristics of the input. Additionally, OMA requires the adherence to a set of underlying assumptions which is not guaranteed in practice. Thus, while the natural frequency can usually be estimated with sufficient accuracy, estimations of damping are rather uncertain.

1.1.3. Sources of Uncertainty in OMA-derived Damping

The widespread application of OMA methods to in-situ measurements has, over time, led to the accumulation of large databases of damping estimates. However, the usability of these databases is significantly restricted by the considerable scatter in damping estimates [4]. The scatter in estimated

damping values reflects the inherent uncertainty associated with these estimates. This section outlines the primary sources of uncertainty in OMA-derived damping.

As previously mentioned, damping is sensitive to the input excitations. Since ambient wind induces relatively low excitation forces, the resulting vibration response of high-rise buildings is typically of low amplitude. As a result, the structural response is less sensitive to damping, as opposed to natural frequency. Additionally, OMA methods have to make broad assumptions about the characteristics of the unknown excitation. These assumptions include that the excitation is broadband and stationary, which is generally modelled by white noise. However white noise is often an oversimplified model of the real ambient excitation, which can introduce various errors and complicate accurate damping estimation [4, 17].

The unreliability of damping estimates is partly aggravated by the low natural frequencies typical of high-rise buildings. As a result, long time series of the measured response are needed to obtain reliable results from OMA methods. In practice, the stationarity condition is rarely satisfied over the entire duration of long signals [18].

It is evident that the amplitude dependency of damping also contributes to the scatter in measured damping values [4]. Assigning a single damping value to a building, despite the non-linear behaviour of damping, can lead to confusion and misinterpretation of measured damping values. In fact, significant discrepancies have been reported in damping values measured on the same building but under different response amplitudes. This confusion is aggravated when the response amplitude is not documented along-side reported damping values [19].

Lastly, even under ideal conditions, complying with excitation stationarity and system linearity, damping estimates remain somewhat volatile. This variability arises from the sensitivity of the chosen OMA method to factors such as measurement noise, time history length and parameter settings. As a result, determining the reliability on OMA-derived damping estimates is no easy task, especially since most OMA methods typically yield a single deterministic estimate, meaning that the methods themselves do not provide information on the reliability of the estimates.

In summary, the variability in OMA-derived damping estimates can be attributed to errors introduced by the unknown excitation, the application of OMA methods to response measurements not complying with the underlying assumptions and the sensitivity to settings used in the algorithms. In fact, the blind application of OMA methods to conditions deviating from the underlying assumptions of stationarity and linearity can introduce significant errors and misunderstandings. Yet, the application of OMA methods to data not complying with the underlying assumptions is common practice in the field contributing to the large scatter observed in damping estimates.

1.2. Research Problem

Establishing the reliability of damping estimates from response measurements is necessary for developing new damping prediction models but remains a challenging task. Errors in OMA-derived damping estimates are mainly caused by the unknown excitation, the application of OMA methods to response data that violates underlying assumptions and the sensitivity of damping estimates to algorithm settings. Yet, in practice, OMA methods are commonly applied to response data that does not comply with the underlying assumptions.

The core research problem lies in assessing the reliability of damping estimates in ideal conditions, when no deviations to the underlying assumptions occur, as well as under realistic conditions which includes these deviations from the stationarity and linearity condition.

Given the inevitability of non-ideal conditions in-situ, assessing the reliability of OMA-derived damping estimates under such circumstances is crucial. While the non-linearity of damping, arising from its dependency on response amplitude, is an inherent characteristic of high-rise buildings, wind loads acting on these buildings are inherently non-stationary over extended periods since wind speed and direction vary with time. A method that proved promising in reliably estimating damping under non-ideal conditions is the Random Decrement Technique (RDT).

1.2.1. Potential of the Random Decrement Technique

Even tough numerous OMA methods existed at the time of its invention, the Random Decrement Technique (RDT) demonstrated significant potential due to its greater robustness to non-stationary data, compared to the then commonly used spectral methods, and its ability to capture amplitude-dependent damping behaviour [19].

Spectral techniques fundamentally require data stationarity for extended periods of time to ensure statistical stability. However, as Jeary [19] points out, stationarity of the wind-induced structural response is much less frequent than commonly assumed. While strictly speaking, the RDT also relies on the assumption of stationarity, an important advantage of the method is that it only requires the data to be stationary over short time segments, which is much more realistic.

Additionally, early observations dating back to the 1990s indicate that the technique might be capable of capturing non-linear effects [19]. To address the amplitude dependency of damping, Tamura and Suganuma [20] introduced the RDT ranked by peak amplitude (Peak RDT). This variation of the traditional RDT associates damping estimates with specific amplitude ranges, thereby producing multiple damping values per response measurement. Given these advantages over alternative methods, the Peak RDT is a particularly suitable for assessing the reliability of damping estimates under non-ideal conditions.

1.3. Research Objectives

By assessing the performance of the Peak RDT in reliably estimating damping, and evaluating the reliability of the estimated damping on a set of performance metrics, insights and advancements are provided regarding damping identification using response data not complying with the underlying assumptions.

Accurately assessing this reliability requires a known reference, or ”ground truth”, against which the damping estimates can be compared. Since such a reference cannot be established with in-situ measurements, this thesis will be based on a series of numerical studies.

This research aims to:

1. Evaluate the reliability and limitations of the Peak RDT in identifying constant and amplitude-dependent damping from wind-induced vibrations of high-rise buildings when the excitation complies with the underlying assumptions.
2. Evaluate the reliability and limitations of the Peak RDT in identifying constant and amplitude-dependent damping from wind-induced vibrations of high-rise buildings when the excitation does not comply with the underlying assumptions.
3. Determine and quantify appropriate performance metrics for the reliability of damping estimates derived under non-linear and non-stationary wind-induced vibrations of high-rise buildings.

1.4. Research Scope

This study specifically examines the reliability of damping estimates obtained using the Peak RDT, which was selected for its reported robustness to non-stationary input data and its potential to capture amplitude-dependent damping behaviour.

As noted in previous sections, stationarity and linearity are fundamental assumptions in most OMA methods. These assumptions are discussed in detail in section 2.1.1. Stationarity may refer to both the response data and the structural system itself. In this thesis, the system is assumed to be time-invariant, as the duration of in-situ measurements is generally too short to capture time-dependent variations in modal parameters resulting from degradation or damage.

The non-linearity is addressed solely through Jeary’s amplitude-dependent damping model, which is attributed to a stick-slip mechanism and reflects the contribution of the superstructure alone. As explained in section 2.4.1, total damping also includes contributions from aerodynamic effects, auxiliary systems, and soil–structure interaction. These additional sources of damping are not reflected in the

damping mechanism modelled in this study. Since the objective of this study is to evaluate the reliability of damping estimates rather than to precisely identify the underlying damping mechanisms in high-rise buildings, this simplification is considered acceptable.

2

Literature Review

This chapter presents a review of existing literature relevant to the research topic. In section 2.1, Operational Modal Analysis (OMA), which encompasses methods for deriving modal parameters solely from ambient vibration measurements, is introduced with a focus on its process, assumptions, and limitations. Subsequently, the Random Decrement Technique (RDT) is introduced in section 2.2 as a method for approximating the system's free vibration response. The RDT ranked by peak amplitude (Peak RDT) is specifically developed to identify amplitude-dependent damping and is elaborated on in section 2.5.2. The Least Squares Minimization approach, used for estimating damping from the approximated free vibration response is introduced in section 2.3.2. The two remaining sections provide a foundation for the decisions made in modelling the system and the excitation. Section 2.4 explores various sources of damping specific to high-rise buildings, emphasizing its amplitude-dependency and section 2.6.4 explores various types of non-stationarity.

2.1. Operational Modal Analysis

Modal analysis is an approach used to determine the inherent dynamic characteristics of structural systems. In structural engineering, modal analysis has a lot of applications notably in structural health monitoring, damage detection and in the design of structures exposed to dynamic loading conditions [21]. Modal analysis is based on the assumption that the dynamic response of a linear time-invariant (LTI) system can be represented as a linear combination of its natural vibration modes. Each vibration mode is in turn characterized by its modal parameters: natural frequency f_n, damping ratio ξ and mode shape ϕ_n [22]. Knowing these modal parameters, the engineer is able to fully grasp the dynamic behaviour of a structure.

There are two dominating groups of modal analysis techniques: experimental modal analysis (EMA) and operational modal analysis (OMA) [23]. Traditionally, EMA is used to determine the dynamic characteristics of structures. EMA is based on the relationship between the applied force at one location (input) and the corresponding vibration response at the same or different location (output). Using this relation, a set of frequency response functions (FRF) can be established. EMA thus requires artificially exciting or shaking structures and is best performed in a controlled environment like a lab which poses a problem for many structures in the field of civil engineering [23].

While EMA requires the excitation to be known, OMA methods aim to obtain physical information solely from the vibration response of a structure. OMA methods are therefore often called "output-only" methods and can be performed right after the building delivery or during its lifetime (operational phase), without interrupting the normal usage of building [21]. Fortunately, high-rise buildings can be sufficiently excited by ambient excitations such as wind which diminishes the need for expensive excitation devices.

2.1.1. Underlying Assumptions

The application of Operational Modal Analysis (OMA) relies on a couple of fundamental assumptions [18].

- Linearity
  If the structural system is linear, the principle of superposition applies and the system's response can be expressed as the linear combination of its natural vibration modes. Additionally, the modal parameters are independent of the excitation amplitude.
- Stationarity
  System: If the system is time-invariant, the modal parameters do not change over time and the coefficients of the differential equations describing the dynamic response of the structure (M, C and K) are also independent of time.
  Response: Many OMA methods assume the response to be a stationary stochastic processes in order to derive correlation functions or perform spectral analysis. A process is called stationary if its statistical properties (such as mean, variance, and autocorrelation) do not change over time [24].
- Observability
  This assumption provides that the modes of interest can be observed based on the response time history. For example, the sensor has not been positioned at a node.

2.1.2. Process

Figure 2.1 schematically illustrates the process of OMA. The process can be categorized in two stages, (1) the signal processing stage and (2) modal parameter extraction stage. The measured, or synthetically generated, response time history is the starting point of the procedure. Based on the response time history, the correlation function (CF) and the power spectral density (PSD) are estimated in the time domain and frequency domain, respectively, during the Signal Processing stage.

Subsequently, the modal parameter extraction stage identifies the modal parameters $\hat{f}_n$, $\hat{\xi}$ and $\hat{\phi}_n$ based on the estimated CF or PSD. As shown in figure 2.1, a variety of methods can be applied in the Signal Processing and Modal Parameter Extraction stages. A detailed discussion of these methods is beyond the scope of this thesis.

However, a very promising method for estimating correlation functions is the Random Decrement Technique (RDT). In short, the RDT extracts the free vibration response of a structure from random ambient excitations by averaging time segments of the response that share a common trigger condition. The method is further elaborated on in section 2.2. Unlike other methods, that rely on long and continuously stationary time histories, the RDT only requires stationarity within multiple short periods. By utilizing short time history lengths, the method produces stable damping estimates even when the overall response is non-stationary [25]. Additionally, the RDT has demonstrated potential in identifying amplitude-dependent modal parameters [25].

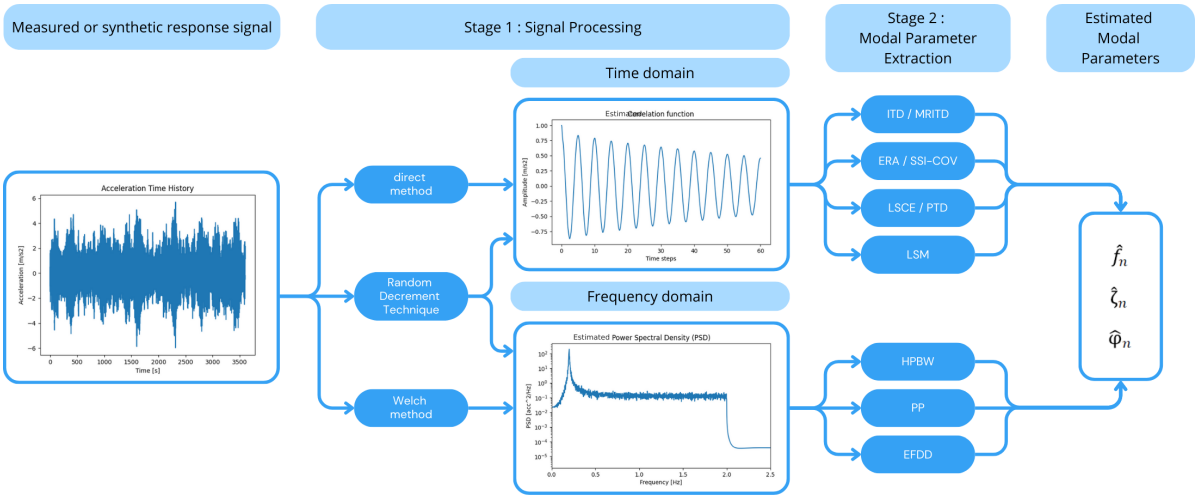

Figure 2.1: Schematic representation of OMA stages

2.1.3. Shortcomings

Although OMA permits the analysis of more complex structures by relying only on response data, it has major drawbacks related to the unknown input forces, affecting the extracted modal parameters.

Since the excitation is unknown, it is difficult to distinguish between natural modes and operational deflection shapes, particularly when peaks in the PSD are caused by the excitation rather than the structure's natural frequencies.[23]. Additionally, closely spaced modes can complicate the identification process. While natural frequencies and the corresponding mode shapes can still be identified if there is sufficient sensor coverage, these mode shapes remain unscaled in the absence of known input forces. The lack of physical significance of mode shapes limits applications in structural health monitoring or computational model validation [23].

Moreover, the results of modal parameter identification oftentimes consist of single value estimates for natural frequency and damping, meaning that the uncertainty associated with those estimates is unknown [26]. OMA might give the impression of a good result, but based only on response data, it is hard to tell whether the estimates are accurate or precise. This emphasizes the need for numerical studies.

2.1.4. Deviations to Underlying Assumptions

The assumptions laid out in section 2.1.1 are rather restrictive with respect to the application of OMA methods to in-situ measurements. Most structures do exhibit some non-linear behaviour given a certain level of excitation. Non-linearities often result from friction between sliding contact surfaces in the building, hysteretic material properties and softening of the soil-foundation system [27]. High-rise buildings, in particular, tend to show amplitude dependent behaviour of modal parameters which is an indicator of non-linearity in the system [28].

Several studies have demonstrated amplitude-dependent damping behaviour in high-rise buildings. As seen in figure 2.2, Jeary [25] analysed a high-rise buildings in Hong Kong using the traditional Random Decrement Technique (RDT), evaluating the Random Decrement Signatures (RDS) at 60 different amplitude levels to assess the amplitude dependency of damping. Similarly, Tamura and Suganuma [20] investigated a 99.35 meter high steel framed observatory tower with a varying cross-section. They applied the RDT ranked by peak amplitude (Peak RDT) to analyse its damping characteristics as a function of acceleration amplitude, as shown in figure 2.3. Lastly, Bronkhorst et al. [5] determined amplitude-dependent damping ratios and natural frequencies using the traditional RDT method, revealing a decrease in damping after reaching the critical tip drift ratio, seen in figure 2.4.

Furthermore, the excitation is generally assumed to be zero-mean, stationary, Gaussian white noise. However, wind has a spectral distribution that is different from white noise. It is also rather unlikely that

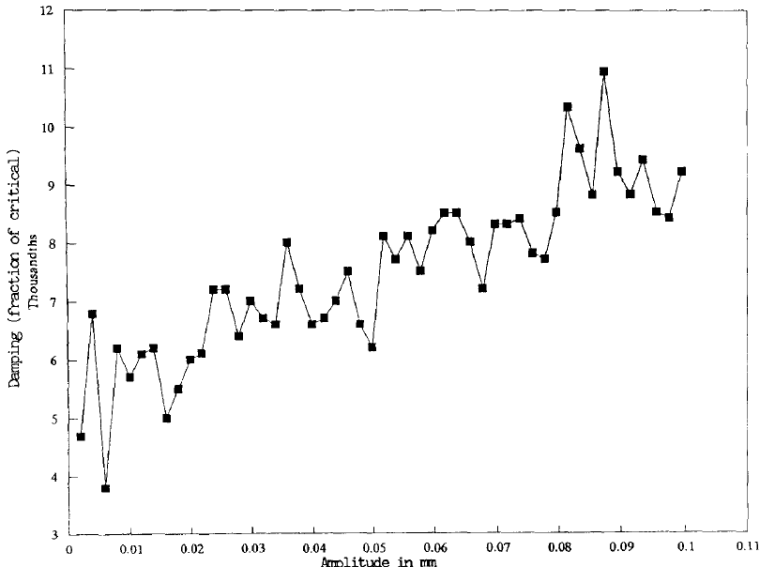

Figure 2.2: Estimated Damping ratio, Hong Kong Tower [25]

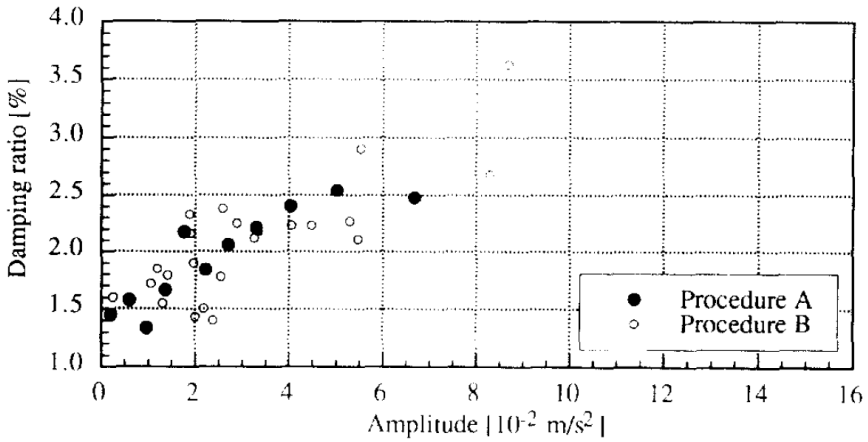

Figure 2.3: Estimated damping ratio, steel-framed observatory tower [20]

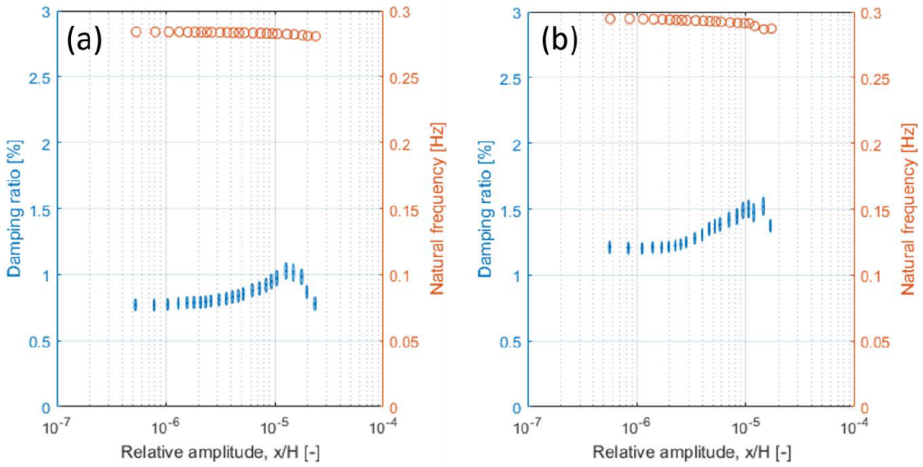

Figure 2.4: Estimated damping ratio and natural frequency, New Orleans Tower [5]

the excitation is stationary for the entire duration of the measurement [29].

In practice, OMA is often applied to in-situ measurements knowing that the conditions deviate from the underlying assumptions. In fact, the blind application of OMA methods, to in-situ measurements containing deviations such as non-stationarity of response signals and amplitude dependency of modal parameters, is often listed as one of the sources of high uncertainty in damping estimates (see section 1.1.3). Knowing that the application of OMA methods to data not complying with the underlying assumptions is common in the field, the aim of this thesis is to analyse the consequences and assess the reliability of the Peak RDT method under such deviations.

2.2. Random Decrement Technique

Henry Cole first developed the Random Decrement Technique (RDT) at NASA in the late 1960s and early 1970s [30]. Ibrahim then extended the method to perform modal identification on civil engineering structures in the late 1970s [31]. The mathematical basis for the method, based on conditional expectation, was worked out by Vandiver et al. in 1982 [32] and Asmussen et al. in 1997 [33]. Nowadays, the method is well established in the field of Operational Modal Analysis [34].

As described in section 2.1.2, modal parameter identification consists of two stages. In the signal processing stage, a Random Decrement Signature (RDS) is computed from the response time history by sampling and averaging significant segments of predefined length τ using a triggering condition. This procedure effectively isolates "decrement events", referring to the time in which the system oscillates freely after being excited. Subsequently, the modal parameters are identified based on the free decay, approximated by the RDS, in the modal parameter extraction stage.

Cole provided an insightful explanation as to why the concept of the RDT intuitively makes sense. In fact, the dynamic response of a linear system to random or ambient loads $x(t)$, is composed of three components at each time step, where x_{x_0} is the response to an initial displacement, $x_{\dot{x}_0}$ the response to an initial velocity and x_F the response to random excitation assumed to be zero mean. By averaging many segments extracted based on a common triggering condition, the response to random excitation x_F is cancelled out. The averaged signal, called the RDS, thus represents the impulse response, or free decay, of the system to a set of initial conditions x_0 and $\dot{x}_0$ [30].

$$x(t_i) = x_{x_0}(t_i) + x_{\dot{x}_0}(t_i) + x_F(t_i) \tag{2.1}$$

2.2.1. Interpreting RDS as Free Decay

In practice, the Random Decrement Signature (RDS) is often interpreted as the free decay of the structural system. However, Vandiver et al. [32] showed that this assumption is not generally applicable. In fact, it is only valid for linear systems excited by a zero-mean, stationary, random process. In that case, the autocorrelation function, which is actually estimated by the RDS, is exactly proportional to the free decay of the system. To understand the origin of errors, it is crucial to recognise the underlying assumptions, summarized in figure 2.5, and critically assess the reliability of the RDT when applied to systems that deviate from these assumptions.

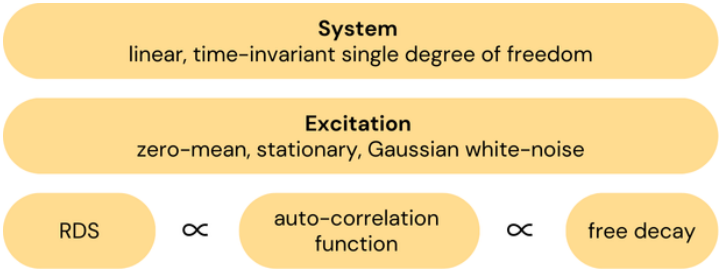

Figure 2.5: Set of assumptions under which the RDS can be interpreted as the system's free decay

2.2.2. Mathematical Expression

Vandiver et al. defined the RDS as the conditional expectation of the segment $x(t+\tau)$ fulfilling the triggering condition C_x, given in equation 2.2.
In OMA, the nature of the response signal is discrete, as it stems from measurements or simulated data. The RDS is thus equal to the average of N_s sampled segments fulfilling the triggering condition C_x at the time points t_n [34]. While equation 2.3 refers to the auto-RDS, Ibrahim extended Cole's algorithm to include the correlation between two response signals of the same structure. The cross-RDS, $\hat{D}_{xy}(\tau)$, is computed by applying the triggering condition to time history $y(t)$ to find the time points t_n fulfilling condition C_y. However, the segments are sampled from $x(t)$ rather than $y(t)$ [35]. The cross-RDS capture correlations between sensors placed at different locations on the structure and can therefore provide more information on modal shapes when used in modal parameter extraction methods such as Ibrahim's Time Domain (ITD) method or Frequency Domain Decomposition (FDD).

$$D_{xx}(\tau) = \mathbb{E}\left[x(t+\tau) \mid C_x\right] \tag{2.2}$$

$$\hat{D}_{xx}(\tau) = \frac{1}{N}\sum_{n=1}^{N} x(t_n+\tau) \mid C_x \tag{2.3}$$

$$\hat{D}_{xy}(\tau) = \frac{1}{N}\sum_{n=1}^{N} x(t_n+\tau) \mid C_y \tag{2.4}$$

2.2.3. Triggering Condition

The triggering condition is an important setting of the RDT, as it defines which, and how many, segments are taken into account in the computation of the RDS. The chosen segments have an effect on the quality of the estimated RDS and, consequently, the reliability of the damping estimate [36]. The more significant segments are extracted from the response time history, the more accurately the RDS can estimate the system's free decay.

There are many different types of trigger conditions used in literature. Cole initially developed the level crossing condition, which is still the most commonly used in practice, illustrated in figure 2.6.a. The use of the level crossing condition is hereafter referred to as traditional RDT. Asmussen proposed the local extremum, positive points and zero crossing condition [36]. A variation of the RDT, called the RDT ranked by peak amplitude (Peak RDT), makes use of the local extremum condition, illustrated in figure 2.6.b. Whereas the level crossing condition samples segments if the response coincides with a specific trigger level (threshold), the local extremum condition only selects local maxima or minima above that threshold. Both trigger conditions are schematically explained in figure 2.6, where the blue line represented the response time history and the red dots indicate the triggered points resulting in a sampled segment.

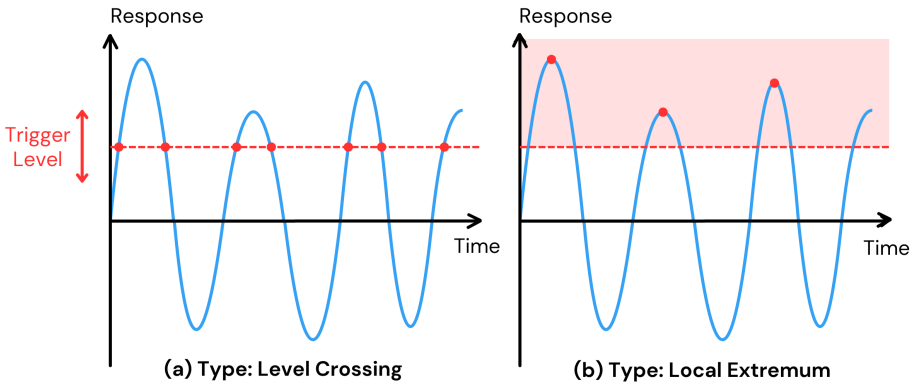

Figure 2.6: Schematic representation of level crossing and local extremum condition

For a structural system, the condition on amplitude can be interpreted as an initial displacement, and the condition on slope can be interpreted as an initial velocity. The trigger condition thus specifies initial conditions [34].

Especially for the traditional RDT, the triggering condition has a large influence on the amount and the significance of sampled segments. The trigger level determines the amplitude of the threshold considered. While a too-high trigger level might lead to a limited number of sampled segments, which is problematic for averaging out the randomness, a too-low trigger level might reduce the relevance of the segments, as they would most likely correspond to insignificant impulses rather than a significant one. An optimal equilibrium needs to be found to balance sensitivity to the signal and segment count.

2.2.4. Segments

The computation of the Random Decrement Signature (RDS) depends on the selection of the segments from the response time history. The two most commonly considered parameters are the segment length and the number of segments sampled and averaged.

Segment Count

The number of segments used in computing the RDS plays a critical role in ensuring reliable damping estimates. Vandiver et al. [32] defined the RDS as the conditional expectation of the segments $x(t+\tau)$ fulfilling the triggering condition C_x (equation 2.2). The discrete formulation (equation 2.3) approximates this mathematical expectation only when N_s, the number of segments, is sufficiently large. Therefore, literature often emphasizes that a high-quality RDS should include a sufficient number of segments to effectively average out the response to the random excitation (assumed to be zero-mean) and isolate the response to initial conditions.

Most existing literature has examined segment counts in the context of the traditional Peak RDT. However, since the Peak RDT further subdivides segments into amplitude ranges, these findings are not directly transferable.

Tamura and Suganuma [20] recommend using up to 2000 segments per RDS for reliable damping estimation, highlighting the sizeable data requirements needed for accuracy. However, Tamura and Suganuma also noted that as few as 700 segments may provide sufficiently accurate results. Kijewski and Kareem [29] applied the local extremum condition to study the impact of correlation between segments. They relaxed the peak amplitude condition in their analysis to include a larger number of segments in the averaging process. Kijewski and Kareem analysed the variance in the RDS for different segment counts, ranging from $N_s = 50$ to $N_s = 350$ and observed that the variance in the RDS decreased as the number of segments increased. Based on their findings, they suggested using approximately 200 segments as a practical balance between statistical reliability and computational effort. The exact number of segments needed is therefore hard to quantify and is strongly case-dependent.

Characteristics Response Time History

The number of sampled segments is closely tied to the length of the response time history considered. A longer time history increases the number of segments, which improves the averaging process and allows the Random Decrement Signature (RDS) to more accurately capture the system's free decay by isolating the free vibration response.

However, especially for in-situ measurements, longer response time histories can be problematic with respect to the stationarity assumption. Although it is generally assumed that wind causes stationary excitations, it is often the case that measurements show the contrary. The longer they are the less likely they are to be stationary.

In addition, the sampling frequency f_s plays an important role in the quality of the RDS. A higher sampling frequency provides a denser time series, increasing the likelihood of detecting valid segments that might otherwise be missed due to strict triggering conditions based on amplitude or slope thresholds.

2.3. Modal Parameter Identification

The second stage of operational modal analysis (OMA) consists of identifying the modal parameters from the estimated correlation functions in the time domain, or alternatively, estimated power spectral densities in the frequency domain. This study focuses only on time-domain methods for identifying modal parameters, while frequency-domain methods are not discussed in detail.

Time domain methods make use of the correlation function and its relation to the system's theoretical free decay to identify the modal parameters. Using the RDT, the free decay can, under certain conditions (see section 2.2.1), be approximated by the Random Decrement Signature (RDS).

2.3.1. Logarithmic Decrement Method

In practice, the damping ratio of an under-damped system is often identified using the Logarithmic Decrement method. The method evaluates the rate of decay between two successive peaks of the Random Decrement Signature (RDS) estimating the free decay. Since the decay is exponential, the logarithmic decrement can be determined by taking the natural logarithm of the ratio of two successive peak displacements in the RDS (equation 2.5) [37].

$$\delta = \frac{1}{n} ln \frac{x(t)}{x(t + nT)} \tag{2.5}$$

Where $x(t)$ is the displacement at a peak in the RDS, $x(t + nT)$ represents the displacement at a peak n cycles later, and T denotes the period of oscillation. For under-damped systems, the damping ratio ξ can be determined from the logarithmic decrement δ using the relation in equation 2.6 [38].

$$\xi = \frac{\delta}{\sqrt{4\pi^2 + \delta^2}} \tag{2.6}$$

2.3.2. Least Squares Minimization Method

The Least Squares Minimization (LSM) method is based on curve fitting to obtain the modal parameters. This method effectively fits the equation of the theoretical free vibration response to the computed RDS using the least squares minimization algorithm. Typically, the theoretical expression of a linear single degree of freedom (SDOF) system is used. The LSM algorithm minimizes the sum of squared differences between the model (free decay) and the data points (RDS). The modal parameters ξ and ω_n are obtained as the optimal values that minimize the cost function during the curve fitting procedure.

Although the LSM algorithm itself does not prioritize any specific time intervals, unless instructed otherwise, the signal's magnitude significantly influences the fitting process. Since the first cycles have a larger amplitude than the later cycles, the squared differences at these points have a disproportionately large impact on the total error. This leads to the algorithm focusing on having a good fit between the model and the RDS in the early cycles, which makes the fit primarily reflect the decay of the first few oscillations rather than the decay at later cycles. The chosen optimization process, together with the estimation limits and initial guess, can also influence the resulting modal parameters.

In contrast to the Logarithmic Decrement method, which relies solely on the amplitude of successive peaks, the LSM fits the entire exponentially decaying sinusoid function. This approach often yields more consistent and robust estimates of the damping ratio, as it is less sensitive to the specific cycles selected for estimation.

For complex systems with many modes, this method can be difficult to implement, but for if the response is governed by only one vibration mode, the implementation is quite simple, due to the simple expression of the free decay [22].

2.4. Damping in High-rise Buildings

Damping plays a crucial role in the dynamic behaviour of high-rise buildings. Accurate damping estimation is essential for structural design, safety assessments, and serviceability evaluations. However, predicting damping in the design of high-rise buildings remains challenging due to its dependence on multiple factors, including material properties, structural connections, and non-structural elements. While various empirical prediction models have been proposed, significant discrepancies exist between predicted and estimated damping values.

This section explores the damping mechanism speculated to govern the behaviour of high-rise buildings, namely the stick-slip mechanism, and explains how it can be effectively modelled using equivalent viscous damping.

2.4.1. Sources of Damping

Generally, damping describes the dissipation of energy by a vibrating system returning to its state of equilibrium [3]. Picozzi et al. [39] distinguish three main sources of damping in high-rise buildings: structural damping ξ_s, aerodynamic damping ξ_a and auxiliary damping ξ_d as described by equation 2.7.

$$\xi = \xi_s + \xi_a + \xi_d \tag{2.7}$$

Structural Damping

The categorization is based on work by Davenport and Hill-Carroll [40], which further identifies three contributions to structural damping ξ_s. The first contribution is attributed to intrinsic material damping in members of the main load bearing structure (MLBS). Material damping occurs within the solid material and is a result of kinetic or strain energy being released during cyclic deformation. These damping effects are non-linear and usually not consistent within the material which makes it hard to analyse their behaviour [41, 42]. The second contribution is a result of frictional damping arising both, between different members of the MLBS, and between structural and non-structural elements, such as architectural finishes. The third contribution is due to foundation damping in the form of radiation of energy and intrinsic damping in the soil. Gomez et al. [15] determined that for the soft soils, found in the Dutch delta region, the damping due to foundation greatly contributes to the total damping.

$$\xi_s = \xi_{s,material} + \xi_{s,friction} + \xi_{s,foundation} \tag{2.8}$$

Aerodynamic Damping

Aerodynamic damping ξ_a refers to the energy dissipation that occurs when a structure moves through a fluid medium such as air. Usually, damping forces are of dissipating nature, reducing oscillations and enhancing stability. However, depending on the relative motion of wind, it can occur that the motion of the structure generates a damping force that further encourages motion. In that case, the aerodynamic damping is negative and leads to aerodynamic instability [42]. Thus, aerodynamic damping can have a large impact on the dynamic behaviour of high-rise buildings.

Auxiliary Damping

Auxiliary damping includes damping that is artificially added to buildings using damping devices. These devices can make use of viscous, friction or hysteretic mechanisms and are easily implemented using hydraulic dampers or mass-tuned dampers [42]. This last source of damping is included for the sake of having a complete picture but falls outside of this thesis' scope.

2.4.2. Stick-Slip Mechanism

In the 20th century, researchers investigated the underlying damping mechanism in high-rise buildings, specifically to understand how the energy is dissipated. Wyatt [12] suggested that all significant energy dissipation within the structure ξ_s could be attributed to friction, and coined the mechanism "stiction". To prove that the proposed mechanism corresponded to the physical processes, it had to be consistent with measured damping data. Eyre and Tilley [43] were among the first to confirm the stick-slip mechanism using damping data gathered from footbridges.

”Stiction” occurs when contact surfaces in the structure are stuck due to friction, until a certain load is applied and a certain displacement reached, after which the contact surface start slipping, thereby dissipating energy. Wyatt assumed these contact surfaces to be randomly distributed with respect to the displacement amplitude. As the load increases and leads to greater displacement amplitude, more contact surfaces begin to slip and dissipate energy, causing the damping to become dependent on the amplitude. The ”stick-slip” mechanism is based on ”stiction” and occurs when contact surfaces alternate between being stuck, due to high static friction, and slipping, which occurs when the applied force overcomes static friction.

Jeary [3] identified three types of contact surfaces and attributed the dissipated energy to: (1) the extension of microcracks within the material of the main load bearing structure (MLBS), (2) the mobilization of joints between members of the MLBS and (3) the mobilization of interfaces between structural and non-structural elements such as architectural finishes. The stick-slip mechanism thus explains only 2 of the 3 components in equation 2.8, neglecting the contribution of the foundation.

Different types of contact surfaces are activated at different response amplitudes. At low displacement amplitudes, the members of the MLBS are primarily mobilized. The amount of energy dissipated in this way is relatively large, leading to an instantaneous, constant damping value at small amplitudes. At larger amplitudes, the smaller elements also undergo differential movement. This is mainly due to elongation of microscopic cracks which is associated with a reduction of strain energy and a dissipation of energy. At some point, all contact surfaces in the system are activated, and the energy dissipation has reached a maximum and remains constant after that point [3].

As a result, Jeary identifies three regimes: a low amplitude regime with constant damping ratio, a high amplitude regime with constant damping ratio and a non-linear regime stretching between the two as seen in figure 2.7. Considering the reduction in stiffness due to slipping contact surfaces, a decrease in the fundamental natural frequency is also expected, as it is proportional to stiffness. The amplitude-dependent modal parameters damping ratio ξ and natural frequency f_n are schematically illustrated in figure 2.7.

It is worthwhile to mention that some researchers have shown that with very high amplitudes, the damping value seems to decrease [16]. The reduction in damping at very high amplitudes can be understood by the ”smoothing” of rubbing surfaces [25]. This reduction of effective damping value beyond a certain amplitude is however not taken into account in Jeary’s model because most measurements don’t reach amplitudes high enough to observe this reduction in damping. It is therefore not sufficiently explored.

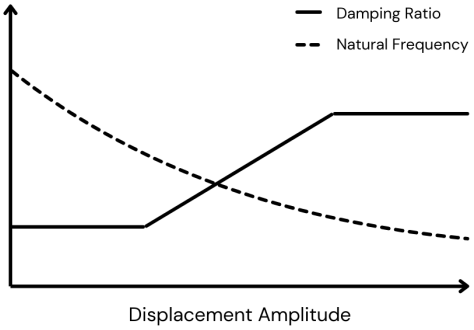

Figure 2.7: Schematic representation of amplitude-dependent damping ratio and natural frequency (Jeary’s model)

2.4.3. Equivalent Viscous Damping

An appealing quality of Wyatt’s model is that it describes a type of behaviour that can be described by ”equivalent viscous damping”. Equivalent viscous damping, describes the combined effect of different dissipation mechanisms in a structure, using a single damping coefficient c. In other words, the numerous stick-slip components, resulting from the contact surfaces discussed in section 2.4.2, can be represented by a single amplitude-dependent equivalent viscous damping function $c(A)$, even though the underlying mechanics are frictional. Figure 2.8 shows the addition of individual stick-slip components, indicated by the parallelogram-shaped force-displacement fields results in the oval-shaped

viscous force-displacement field. It is important to mention that equivalent viscous damping is an approximation meant to simplify the mathematical equations governing the system, and is therefore not exact.

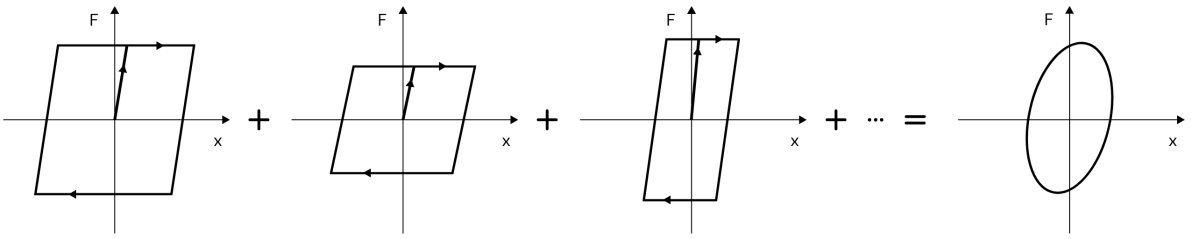

Figure 2.8: Friction damping over a large range of amplitudes gives a viscous damping model, based on Tamura [16]

2.5. Detecting Amplitude Dependent Damping

The mathematical derivation of the Random Decrement Technique (RDT), relies on the assumptions that the system is linear and the excitation is random, stationary, and zero-mean. However, as described in section 2.1.4, deviations from these assumptions are quite common in-situ. Fortunately, researchers recognized the potential of RDT for detecting system non-linearities by varying the trigger level and arranging the corresponding estimated modal parameters by amplitude.

2.5.1. Evolution of Non-Linear RDT

The idea that the RDT could be used to identify non-linear modal parameters was introduced by Ibrahim et al. in 1987 [44]. The authors aimed at identifying damping on a highly non-linear structure assuming that the excitation is an unknown stationary random process, thus excluding any EMA methods and non-linearity tests that require the excitation to be known. The study led to the development of the Multi-Triggering Random Decrement Technique (MT-RDT).

In MT-RDT, a quasi-linear approach is used to deal with non-linearities by repeating the linear identification process (traditional RDT) at different levels of response amplitude, enabling the tracking of amplitude-dependent damping. Subsequently, a linear time-domain modal parameter extraction method is used. The non-linear system is thus linearised by applying the MT-RDT at varying response amplitudes and the resulting RDS describe an equivalent ”linear” system.

This methodology forms the foundation for most non-linear applications of the RDT, including the RDT ranked by peak amplitude. Amplitude-dependent damping cannot be described by a unique damping ratio. In fact, doing so is misleading and associated with large errors.

2.5.2. RDT ranked by Peak Amplitude

A promising approach for identifying amplitude-dependent modal parameters was proposed by Tamura and Suganuma [20]. Similarly to the traditional RDT, the RDT ranked by amplitude, hereafter referred to as Peak RDT, also assumes a zero-mean, stationary, Gaussian process.

Triggering Condition

The Peak RDT utilises the local extremum condition to select segments originating at peak values, allowing for amplitude-specific analysis. Equation 2.2 can be reformulated using the appropriate trigger condition C_x. The adapted formulation for the conditional expectation is presented in equation 2.9, where $\hat{x}$ refers to the amplitude of a local maximum.

However, since it is almost impossible to pick up sufficient segments corresponding to the exact amplitude of $\hat{x}$, amplitude ranges (bins) are adopted. The Random Decrement Signature (RDS) is produced by averaging all N_s sampled segments whose triggering point lies within an amplitude range R. The amplitude dependency of modal parameters can be tracked by arranging the modal parameters by response amplitude.

$$D_{xx} = \mathbb{E}[x(t+\tau) \mid \dot{x}(t) = 0,\ x(t) = \hat{x}] \tag{2.9}$$

$$\hat{D}_{xx}(R;\tau) = \frac{1}{N}\sum_{n=1}^{N} x(t_n+\tau) \mid \dot{x}(t_n) = 0,\ x(t_n) \in R \tag{2.10}$$

Physical Justification

Tamura and Suganuma [20] also provided a physical justification supporting the validity of this method. In fact, the first cycle of the RDS captures the dynamic response of the structure during one oscillation at the specific amplitude range R considered. The response, at a specific amplitude range R, can be directly linked to the hysteresis loop, which characterises the force-displacement relationship of the system throughout one loading and unloading cycle. The size of the loop depends on how far the structure is displaced, so on the amplitude of range R [20]. The area enclosed by the hysteresis loop corresponds to the energy dissipated during that cycle and is thus directly related to the system's damping. The relationship between energy dissipation and oscillation amplitude of the RDS explains why the Peak RDS is appropriate for detecting amplitude dependent behaviour.

Cautions on Peak RDT

It is important to note that the Peak RDT is built on the assumption that damping is amplitude dependent. If the actual damping mechanism is different, the reliability of damping, estimated using the Peak RDT, is not guaranteed. Therefore, the Peak RDT is inherently tied to the validity of the underlying assumption regarding the damping mechanism.

Lastly, Tamura and Suganuma [20] caution that the RDS obtained from a system with amplitude-dependent damping must be interpreted carefully. It does not represent the true free-vibration response of a system with time-varying modal parameters, nor does it correspond to the response of a linearised system with a constant equivalent damping ratio. This can have severe implications for the damping identified from the RDS obtained with Peak RDT contributing to the uncertainty of OMA-derived damping.

Although traditional RDT and Peak RDT are widely used, their accuracy in capturing the amplitude dependency of dynamic characteristics is rarely validated through numerical simulations.

2.6. Non-stationarity of Wind Effects

Wind excitation is inherently variable, and its statistical properties can change significantly over time, especially during extreme weather events such as thunderstorms, hurricanes, or tornadoes [45]. These wind events produce highly non-stationary excitation, characterized by abrupt changes in mean wind speed, turbulence intensity and frequency content.

However, extreme weather conditions do not qualify as ambient excitations and therefore fall outside the scope of this thesis. Their obvious non-stationarity would most likely lead researchers and engineers to omit these measurements when identifying modal parameters using OMA methods. Nonetheless, measurements under extreme weather conditions, and thus large response amplitudes, certainly remain valuable for identifying amplitude dependent modal parameters. Aquino and Tamura [16] pointed out that most measurements available were made under relatively low response amplitude levels, and thus presumably, low excitation levels. As a result, Aquino and Tamura believe that the damping relevant for wind-resistant design (larger response amplitudes) might be lower than predicted by Jeary's model.

2.6.1. Wind Gusts

Under more typical and daily occurring conditions, non-stationarity can arise due to transient wind gusts, diurnal wind patterns (generally over the course of a day), or local disturbances caused by surrounding terrain or built environment. A wind gust is a sudden and brief increase in wind speed, superimposed on the mean wind flow. They typically only last up to a minute and can be generated when wind blows around buildings, trees or other obstacles. These gusts, caused by friction, are generally largest near tall buildings [46].

While individual gusts may not significantly impact the overall structural response of large structures, particularly when analysing long time histories, their repeated occurrence can violate the stationarity of the overall time history.

2.6.2. Types of Stationarity

When analysing wind, two domains are relevant: the temporal domain and the spatial domain. While spatial stationarity refers to statistical properties of wind being consistent across space, temporal stationarity refers to time-invariant statistical properties in time. In this thesis, stationarity is considered only in the temporal domain, as the focus is on a single-degree-of-freedom (SDOF) system and thus limited to along-wind. Stationarity is a somewhat tricky concept, as it always depends on the specific time period being considered. A time series may be stationary during one time frame (20 s) but not in another (1 hour). Additionally, stationarity can be defined and evaluated at different levels.

By definition, a time series exhibits strict stationarity if the joint probability distribution of its values remains unchanged when shifted in time. In other words, the statistical properties of the time series do not change at different time intervals. Strict stationarity is a strong assumption which is very rarely satisfied by real-world data. In practice, weak stationarity, also called second-order stationarity, is often preferred because it defines more relaxed conditions, allowing for some variability in the data while preserving essential statistical properties [47]. For this reason, this thesis will consider violations to the second-order stationarity condition.

A time series exhibits second-order stationarity if the mean and variance of the data remain constant over time, and the auto-covariance between any two time points is only a function of their time lag. Many real-world conditions can be approximated as weakly stationarity, making it a widely used assumption in time series analysis [47, 48]. An even more relaxed condition would be the first-order stationarity which only imposes a time-invariant mean. Other statistical properties like variance or auto-correlation may be time dependent. Lastly, trend-stationary data exhibits fluctuations around a deterministic trend, such as a linear or quadratic time-dependent mean, while difference-stationary data requires one or more differencing operations to achieve stationarity [48].

2.6.3. Stationarity Tests

Although there are many statistical tests for stationarity, testing wind data for stationarity is problematic because the definition of stationarity depends on the time scale upon which the data are considered. This thesis makes use of two stationarity tests with opposite null hypothesis.

Augmented Dickey Fuller ??

The Augmented Dickey Fuller (ADF) test is a statistical significance test commonly used to assess the stationarity of a time series. The test specifically evaluates the presence of a unit root in the time series, which would indicate non-stationarity. A unit root here refers to a disturbance to the system which has a permanent effect on the mean trend of the data. The null hypothesis of the test H_0 is that the series does have a unit root implying non-stationarity. If the p-value is less than the significance level, the null hypothesis is rejected, and the series is considered stationary. If not, the presence of a unit root suggests that the time series is non-stationary [49].

Kwiatkowski–Phillips–Schmidt–Shin

The Kwiatkowski-Phillips-Schmidt-Shin (KPSS) test is another statistical test used to assess the stationarity of a time series. Unlike the ADF, the KPSS assumes data stationarity as the null hypothesis H_0. In fact, it tests for the stationarity of a given series around a deterministic trend, which is called level-stationarity. In addition to a p-value, which can be compared to a significance level, the KPSS test also returns a test statistic which can be compared to a critical value to assess the stationarity of the signal. If the test statistic is below the critical value, the data is stationary [50].

Quantification of Non-stationarity

The KPSS test statistics can however also be used to quantify the degree of non-stationarity. While there is no upper bound, the higher the KPSS statistic, the more non-stationary the data. Logically, this statistic can only be used to quantify how much the response data deviates from the level-stationarity

condition. In existing literature, the method is mainly applied to quantify mildly non-stationary response data, referring to KPSS statistics just above the critical level [51].

2.6.4. Modelling Wind

When assessing the effect of wind on structures, the along-wind $U(t)$ is traditionally modelled as a stationary random process. Furthermore, it is composed of a mean component and a turbulent component, usually described by the Kaimal spectrum, which has a spectral distribution very different from white noise. Wind speed variations in space and time can be defined by equation 2.11, where $\overline{U}(z)$ is the mean wind velocity, generally referring to the mean over 10 minutes, and $u(x, y, z, t)$ is the turbulence components in the wind direction [52, 45]. While the mean wind speed leads to a static response in the building, the time-varying nature of turbulence can excite dynamic behaviour and is therefore more relevant to the study of wind-induced vibrations.

$$U(x, y, z, t) = \overline{U}(z) + u(x, y, z, t) \tag{2.11}$$

Wang and Kareem presented a new approach for analysing non-stationary wind speed time histories [45]. The authors modelled non-stationary wind as a combination of a deterministic time-varying mean wind speed and a stationary fluctuating wind speed. The approach is shown in equation 2.12, where $\overline{U}(z, t)$ is the temporal trend of wind speed and $u'(x, y, z, t)$ is the fluctuating component which can be taken as a zero-mean stationary process.

$$U(x, y, z, t) = \overline{U}(z, t) + u'(x, y, z, t) \tag{2.12}$$

On the other hand, Lin and Chiang [53] performed modal identification from non-stationary ambient response data using an extended random decrement algorithm, modelling the excitation as the product of white noise and a deterministic, time-varying function. Unlike Wang and Kareem, who modulated the mean of the stationary white noise, Lin and Chiang modulated its amplitude, effectively altering the signal's variance over time.

2.6.5. Impact on RDT

In Operational Modal Analysis (OMA), the ambient excitation, given by the turbulent component of wind, is generally assumed to be a zero-mean, stationary Gaussian white noise. This is because OMA methods, such as the Random Decrement Technique (RDT), are designed for stationary processes, making their application to non-stationary input data questionable.

While the need for second-order stationarity of the excitation is commonly stated, it is often implicitly made under the assumption that the system itself is linear and time-invariant. In that case, the response is also second-order stationary [54]. Jeary notes that wind-excited structures rarely exhibit stationarity, even on moderately windy days [19].

When this assumption is violated, the averaging process central to the RDT algorithm can lead to biased or inaccurate estimation of modal parameters as explained in section 2.6.6. As a result, identifying modal parameters under transient, non-stationary conditions remains a challenging task.

Fortunately, a major advantage of the RDT is that it is only necessary for the input data to exhibit stationary characteristics over short sequences. Moreover, the input data can essentially be forced into stationary sets by selecting only those segments of records in which no great changes in amplitude of response occur [19]. This selection of stationary segments from a non-stationary time series is, of course, a laborious process and would reduce length of the useable measurement data. It would be valuable to understand how applying the Random Decrement Technique (RDT) to non-stationary data might impact the accuracy or reliability of the identified damping.

2.6.6. Stationarity Relevance

The assumption for zero-mean, stationary Gaussian excitation in OMA can be understood through the following equations. In this derivation, the important assumption is that $f(t)$ is a zero-mean stationary random process and that the system is linear and time-invariant. Equation 2.13 is also valid for any

time point $t_n + \tau$. By merging the N_s equations and introducing the expression for the RDS, derived in section 2.2, and recalled in equation 2.15, equation 2.15 can be expressed as 2.16.

Only if $f(t)$ is a zero-mean, stationary, random process and for a sufficiently high number of sampled segments N_s, does the ensemble average of the forcing equal to approximately zero. If the ensemble average of the forcing does not approximate zero, the equation of motion doesn't describe the unforced system [55] and the identified modal parameters are incorrect. This derivation also highlights again the importance of sufficient number of sampled segments.

$$m\ddot{x}(t) + c\dot{x}(t) + kx(t) = f(t) \tag{2.13}$$

$$m\ddot{x}(t_n + \tau) + c\dot{x}(t_n + \tau) + kx(t_n + \tau) = f(t_n + \tau), \quad \text{for} \quad n = 1, 2, \ldots, N_s \tag{2.14}$$

$$\delta(\tau) = \frac{1}{N}\sum_{n=1}^{N} x(t_n + \tau), \tag{2.15}$$

$$m\ddot{\delta}(\tau) + c\dot{\delta}(\tau) + k\delta(\tau) = \frac{1}{N}\sum_{n=1}^{N} f(t_n + \tau) \tag{2.16}$$

3

Methodology

This thesis focuses on assessing the performance of the Peak RDT, in reliably estimating damping under ideal and non-ideal conditions, referring to systems exhibiting constant and amplitude-dependent damping, excited by stationary and non-stationary loading. Assessing the reliability of damping estimates requires a known reference, or ”ground truth”, against which the damping estimates can be compared. Since such a reference cannot be established through in-situ measurements, performing numerical studies is essential.

To approach the research objectives systematically, it is important to address each of its parts individually and examine the effects of added deviations one at a time. A systematic approach is essential to understand where errors arise and to attribute them to a specific cause. Therefore, the complete analysis is carried out in multiple phases, for different cases, as described in section 3.1. The reliability of damping estimates is evaluated for each of these cases, based on a distribution of damping estimates. The methodological framework, explained in section 3.2, explains the general steps taken to produce a distribution of damping estimates. While, sections 3.4, 3.3 and 3.5 explain the generation of the synthetic data, sections 3.6 and 3.7 explain the identification of damping in detail.

3.1. Analysis Setup

This section presents the cases analysed in this thesis. It is important to introduce the deviations to ideal conditions one by one in order to identify which errors stem from specific deviations and which are inherent to the damping estimation method used.

In a first phase, the Peak RDT is applied to a linear system with constant damping excited by stationary loading conditions. Case 1, which satisfies all ideal conditions, is referred to as the benchmark case. Since it satisfies all underlying assumptions of the Peak RDT, it is suitable for assessing the method’s inherent ability in accurately identifying modal parameters, providing a baseline for comparison as deviations are introduced. The results from the numerical study (Monte Carlo simulation) help determine which errors can be attributed to the method itself rather than the deviations from ideal conditions. In the second phase, corresponding to case 2, a system with amplitude-dependent damping is tested under stationary loading conditions. The goal is to assess the ability of the Peak RDT to reliably identify non-linear damping behaviour, particularly in the form of the mechanism commonly cited in literature as responsible for amplitude-dependent damping in high-rise buildings. Thus, cases 1 and 2 directly address the first research objective.

In the third phase, the Peak RDT is applied to a linear system with constant damping subjected to non-stationary loading conditions. To assess the sensitivity of damping estimates to different types of non-stationarity, cases 3.a, 3.b, and 3.c are analysed. Each case violates different conditions required for statistical stationarity, allowing the sources of estimation error to be identified. Subsequently, both types of deviations are combined to reflect the complex conditions observed in situ. The combined cases 4.a, 4.b, and 4.c enable an evaluation of the interaction between multiple non-ideal conditions.

Cases 3 and 4 provide a comprehensive response to the second research objective.

- Case 1: Linear System & Stationary Excitation (Benchmark)
- Case 2: Non-linear System & Stationary Excitation
- Case 3.a : Linear System & Non-stationary Excitation (time-variant Variance)
- Case 3.b: Linear System & Non-stationary Excitation (time-variant Mean)
- Case 3.c: Linear System & Non-stationary Excitation (time-variant Variance and Mean)
- Case 4.a: Non-linear System & Non-stationary Excitation (time-variant Variance)
- Case 4.b: Non-linear System & Non-stationary Excitation (time-variant Mean)
- Case 4.c: Non-linear System & Non-stationary Excitation (time-variant Variance and Mean)

3.2. Methodological Framework

Even though multiple numerical studies are carried out to answer each individual research objectives, the procedure is always the same. Given the deterministic nature of damping estimates derived using the Peak RDT, a Monte Carlo simulation is employed to repeat the entire identification process N_{sim} times. From start to finish, three main steps are involved in the numerical studies performed: (1) Data Generation, (2) Damping Identification and (3) Performance Assessment as indicated in figure 3.1.

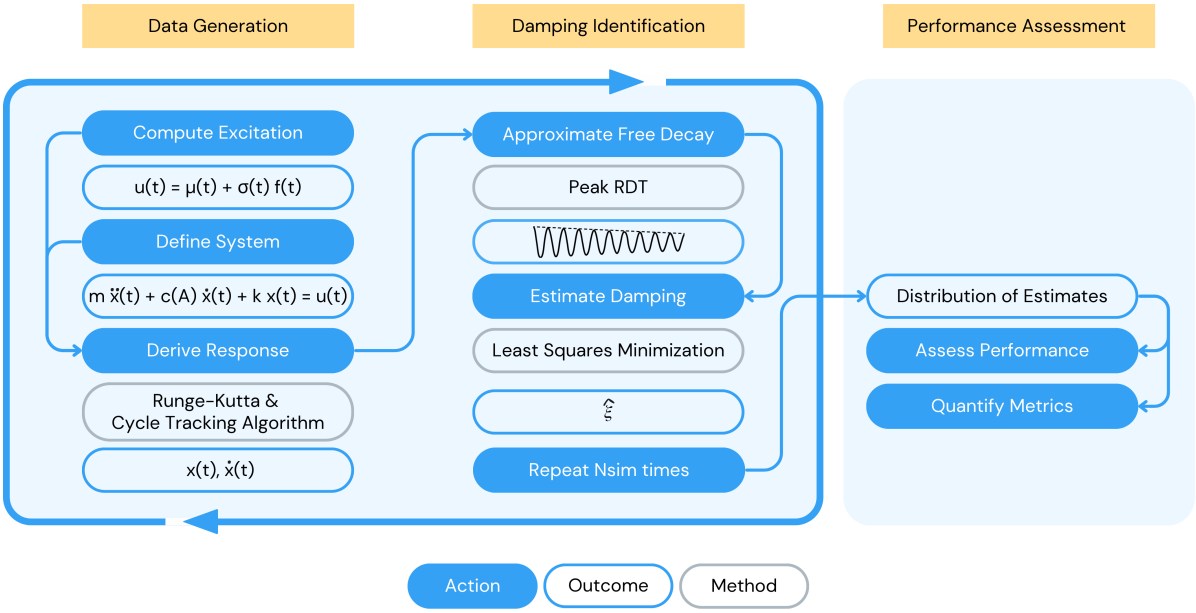

Figure 3.1: Schematic representation of the methodological framework

The first is a preparation phase in which the synthetic response data, representative of (non-)ideal system and excitation conditions, is generated. The preparation phase is explained in detail in sections 3.3, 3.4 and 3.5.

Next, the damping identification process is initiated by applying Peak RDT to the derived displacement responses, in order to approximate the system's free decay. Damping is estimated based on the approximated free decay through the application of a Least Squares Minimisation (LSM) algorithm. Both steps of the damping identification phase are explained in sections 3.6 and 3.7. The Monte Carlo simulation results in a distribution of damping estimates, whose statistical properties can be used to assess their reliability.

Using the distribution of damping estimates, the third research objective can be met. Statistical tools are employed to quantify certain performance metrics by comparing the estimated damping values with the ground truth. The outcome is a comprehensive framework capable of evaluating damping estimation methods under realistic, non-ideal conditions.

3.3. System Definition

The study introduces deviations from the idealised assumptions of OMA methods, capturing system non-linearity and excitation non-stationarity, as detailed in section 2.1.4. By including these realistic deviations, this study aims to produce results that are more relevant and transferable to damping derived from in-situ measurements, thereby enhancing its significance.

For the validity of the numerical study, transparency on the synthetic data is crucial. Since the generation of synthetic data is rarely transparent in existing literature, a significant part of the value of this thesis lies in the detailed documentation regarding the definition of the systems, computation of excitations, and derivation of the responses considered in the numerical study.

This section presents a clear definition of the system under investigation, followed by the procedure used to generate stationary and non-stationary excitation data (see section 3.4), and lastly the numerical scheme used to derive the system's structural response (see section 3.5).

3.3.1. Degrees of Freedom

The system model is chosen to represent the behaviour of high-rise buildings under wind excitation. Since the fundamental mode dominates the wind-induced response, a single degree of freedom (SDOF) system is used to model the first vibration mode [56]. The SDOF shown in figure 3.2 is characterised by the modal mass m, stiffness k, and amplitude-dependent damping $c(A)$ of the first vibration mode and is excited by a (non-)stationary wind load $u(t)$. The system in itself might appear rather simple, but the complexities lie in the inclusion of amplitude-dependent damping and non-stationary excitation.

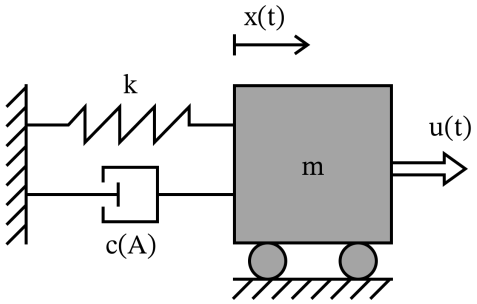

Figure 3.2: Schematic representation of the SDOF

3.3.2. Modelling Amplitude Dependent Damping

In section 2.4.2, the hypothesised damping mechanism governing in high-rise buildings is discussed in detail. Energy dissipation within the structure ξ_s is primarily attributed to friction occurring at contact surfaces. These contact surfaces exist at multiple scales. While, at the microscopic level, energy is dissipated through the mobilisation of microcracks in the material, at larger scales, joints between structural members and interfaces between structural and non-structural components contribute to damping when mobilised. This behaviour can be described using the stick-slip mechanism.

However, the stick-slip mechanism doesn't account for energy dissipated in the foundation $\xi_{s,f}$, which according to Gomez [15], is a relevant contribution to the global damping in Dutch high-rise buildings. Since the focus of this thesis is to assess the performance of the Peak RDT under non-linear and non-stationary conditions, the system is simplified and modelled with the amplitude-dependent stick-slip mechanism, acknowledging that this mechanism represents only a subset of the many sources of

damping described in 2.4.1.

The amplitude dependency of damping, caused by the so-called stick-slip mechanism, is typically characterised by constant damping levels at low and high amplitudes, with a linear increasing damping between the two plateaus (figure 2.7), which is referred to as Jeary's model. Tamura [28] suggests that damping may decrease again once amplitude levels exceed the serviceability limit state. However, few damping models take this into account because measurements at very high amplitudes are limited. Therefore, only Jeary's model is taken into account in this thesis.

The challenge lies in modelling this complex mechanism. Fortunately, Wyatt [12] demonstrated that it can be effectively approximated using equivalent viscous damping. While the stick-slip behaviour at an individual contact surface is inherently complex and non-linear, the combined effect of multiple contact interfaces can be reasonably represented by equivalent viscous damping, as discussed in section 2.4.2. Therefore, for modelling purposes, the system is idealised as a linear SDOF system at constant amplitude A, but since the damping is amplitude-dependent, the system becomes inherently non-linear. The SDOF in figure 3.2 is thus characterised by equation 3.1, its equation of motion (EOM). The amplitude-dependent damping coefficient $c(A)$ can be derived from the unforced EOM, where $\xi(A)$ is the amplitude-dependent damping ratio and A is the maximum displacement is per oscillation cycle.

$$m\ddot{x}(t) + c(A)\dot{x}(t) + kx(t) = f(t) \quad \text{with} \quad c(A) = \xi(A)2\sqrt{km} \quad \text{and} \quad A = \max_{t\in[t_i,t_i+T]} x(t) \tag{3.1}$$

Lastly, as explained in section 2.4.2, Jeary [19] describes that the natural frequency is also amplitude-dependent. However, since damping estimation is the key issue of modal parameter identification of in-situ measurements, and the assessment of its reliability is at the core of this study, only non-linear damping is considered, and the natural frequency in all simulations remains constant at 0.2 Hz.

Amplitude-dependent damping refers to the variation of damping values based on the maximum displacement, velocity, or acceleration of a structure within a cycle. This should not be confused with instantaneous displacement, as amplitude dependence considers the overall response over a full oscillation.

3.3.3. Amplitude Dependent Damping Functions

In the numerical study, two "types" of amplitude-dependent damping are considered. The functions are schematically represented in figure 3.3. The first function shows constant damping across all amplitudes A. It is thus not really amplitude-dependent, but it's represented in this way for consistency. The second incorporates the stick-slip mechanism described by Jeary and outlined in section 2.4.2. It describes linearly increasing damping at low amplitudes, a plateau at mid amplitudes and a linearly increasing damping for high amplitudes.

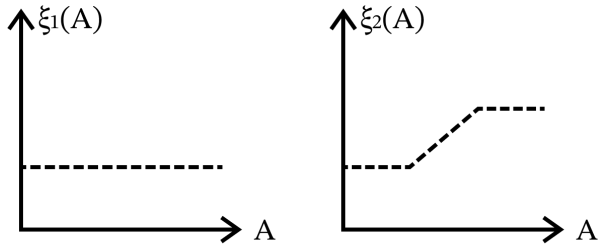

Figure 3.3: Schematic representation of systems considered in numerical study

The two damping functions serve distinct purposes within the numerical study. As outlined in section 3.1, although the Peak RDT is designed to identify amplitude-dependent damping, its validity is first assessed using a linear reference system with known properties. This allows for a clear distinction between uncertainties inherent to the method itself and those introduced by non-linear damping.

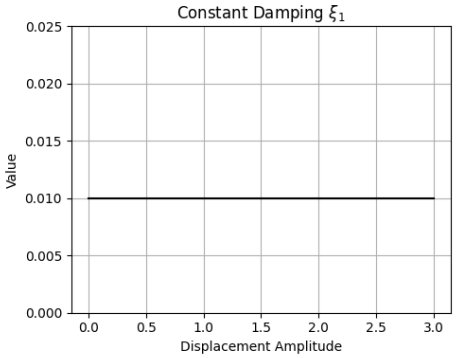

$$\xi_1(A) = 0.01 \tag{3.2}$$

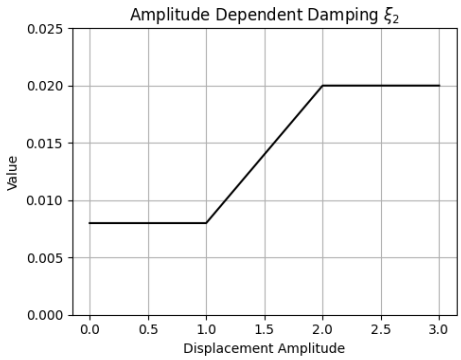

$$\xi_2(A) = \begin{cases} 0.008 & A < 1.0 \\ 0.012A - 0.004 & 1.0 \leq A < 2.0 \\ 0.02 & A \geq 2.0 \end{cases} \tag{3.3}$$

Table 3.1: Amplitude-dependent damping functions and their visual representations

3.4. Computation Ambient Excitation

Accurately modelling the ambient excitations is crucial for generating realistic response data in the numerical study. While section 2.6.4 explains the physical background behind deviations from stationarity, such as those caused by wind gusts or squalls, this section describes the procedure for generating two types of excitation signals: stationary and non-stationary.

3.4.1. Implementation

The turbulent component of wind, which is responsible for the ambient excitation in wind-induced vibrations, is modelled as a zero-mean, stationary, Gaussian white noise. Turbulence is typically characterized by the Kaimal spectrum, which exhibits a spectral distribution that differs significantly from white noise [52]. However, in this thesis, variations in the spectral distribution are not taken into account.

To generate non-stationary excitation signals, two characteristics of the underlying white noise are modified: the mean and the variance. These modifications are inspired by approaches in literature, where non-stationary ambient excitation is modelled as a superposition of a deterministic, time-varying mean wind speed component and a zero-mean, stationary turbulent component [45]. Additionally, the amplitude of the turbulent component can be modulated to simulate temporary increases in turbulence [53]. Accordingly, this thesis investigates the effects of non-stationarity by introducing a time-dependent mean and variance in the excitation, as defined in equation 3.4.

$$\begin{cases} u(t) = \mu(t) + \sigma(t) f(t) \\ \sigma(t) = 1 + k\mu(t) \end{cases} \tag{3.4}$$

With $u(t)$ representing the non-stationary excitation, $\mu(t)$ the time-dependent mean function, $\sigma(t)$ the time-dependent variance envelope, $f(t)$ denoting zero-mean, stationary, Gaussian white noise, and

$k = 0.7$ the scale factor. As can be seen, the variance envelope is also a function of the time-dependent mean function.

As explained in section 3.1, three types of non-stationarity are considered to investigate their individual effects on the reliability of damping estimates. These correspond to (1) a time-dependent mean, (2) a time-dependent variance, and (3) a combination of both, as illustrated in figure 3.4. Throughout this thesis, these cases are referred to as type 1, type 2, and type 3, or abbreviated as NS1, NS2, and NS3, respectively. It is important to note that the time-dependent characteristics remain constant across all simulations and the only variation comes from the white noise input, which is randomly generated and different for each of the N_{sim} simulations. Additionally, for each of the three types of non-stationarity, the degree of non-stationarity is controlled by adjusting the amplitude of the peak P in the mean function, with P taking values of 0.5, 1.0, and 1.5.

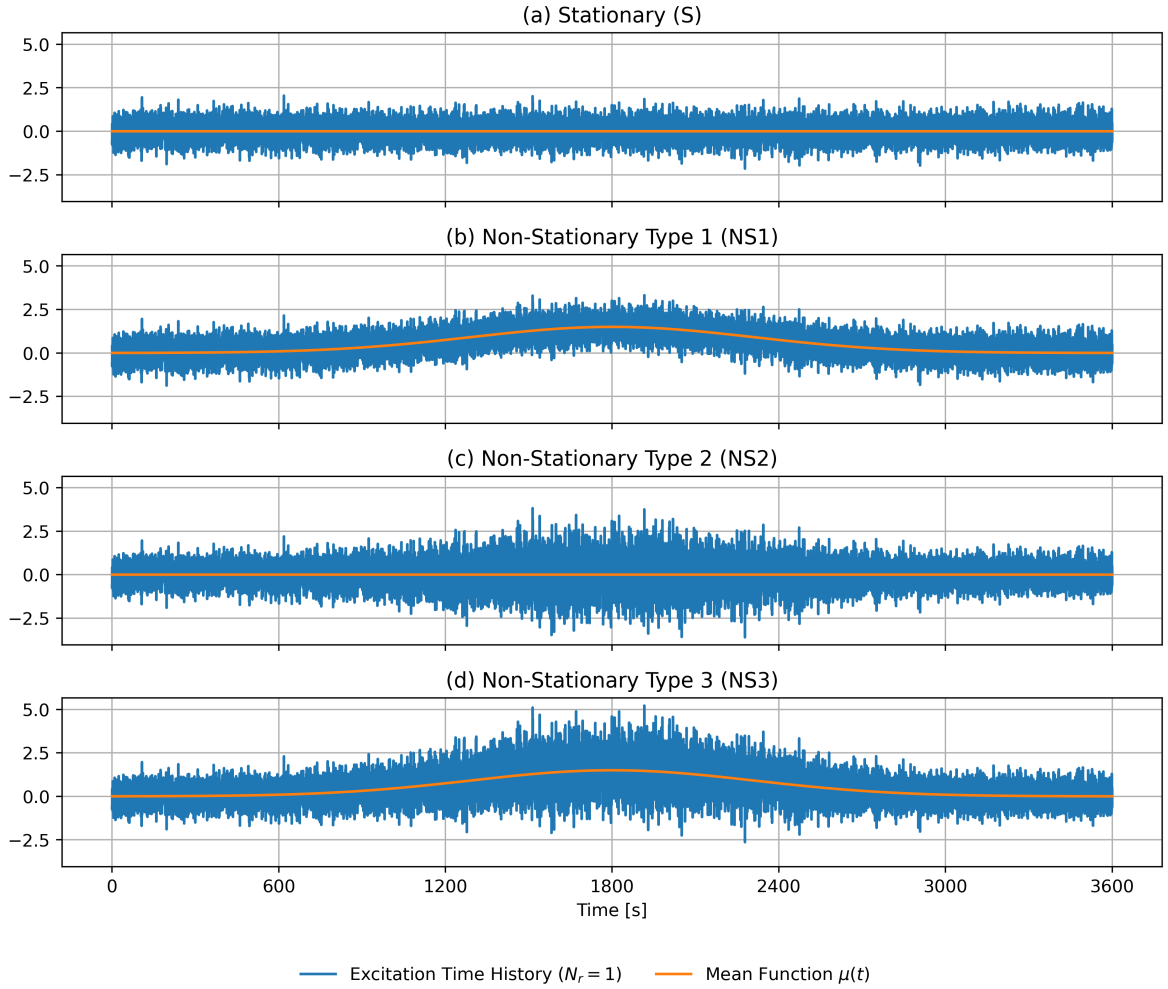

Figure 3.4: Stationary excitation and three types of non-stationary excitation with different time-dependent characteristics;(a) zero-mean stationary Gaussian white-noise; (b) white noise superimposed on a time-dependent mean function; (c) white noise modulated by a time-varying amplitude envelope; (d) white noise superimposed on a time-dependent mean function and modulated by a time-varying amplitude envelope

3.4.2. White Noise Generation

The `white_noise` python function generates a controlled synthetic white noise signal $f(t)$ whose characteristics can be modified. The generated white noise is constrained to a specified frequency range defined by `min_freq` and `max_freq` and can be scaled to have a desired mean (`loc`) and standard deviation (`scale`). Moreover, the function allows reproducibility by specifying a random seed (`seed_num`). The input parameters used in this study are summarized in table 3.2.

Min. Freq. [Hz]	Max. Freq. [Hz]	Loc	Scale
0	2	0	0.5

Table 3.2: Input parameters for the computation of white noise

3.4.3. Mean Function

To model wind gusts or squalls, the mean function $\mu(t)$ is defined as a Gaussian pulse whose mathematical definition is given in equation 3.5. Where $\mu(t)$ is the mean function, P represents the peak value or height of the curve, t_0 denotes the time at which the peak occurs (the centre of the curve), and σ is the standard deviation that controls the width of the curve.

$$\mu(t) = P\, e^{-\frac{(t-t_0)^2}{2\sigma^2}} \tag{3.5}$$

In this thesis, when modelling ambient excitation with a time-dependent mean, one and the same Gaussian pulse is used and superimposed on N_{sim} different white noise signals. As illustrated in figure 3.5, the parameters are chosen such that the pulse width at half amplitude is 20 minutes, and the total pulse duration is 54 minutes, covering nearly the entire length of the hour long white noise signal.

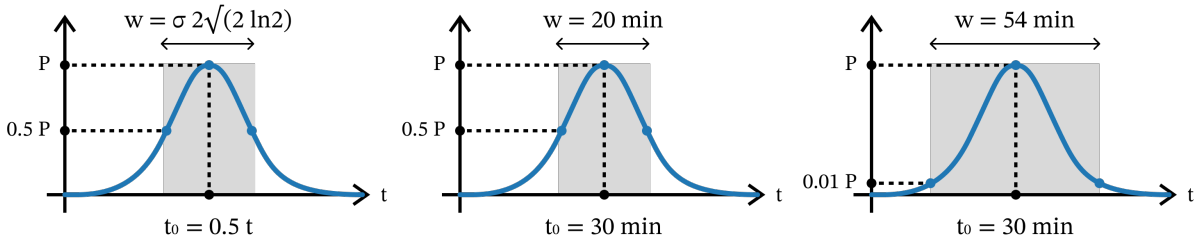

Figure 3.5: Gaussian pulses; (a) mathematical expression; (b) pulse duration of 20 minutes measured at 50% of amplitude; (c) pulse duration of 54 minutes measured at 1% of amplitude

3.5. Numerical Derivation of Response

This section explains the derivation of response data of the system exhibiting amplitude-dependent damping. The Runge-Kutta numerical solver is employed to solve the equation of motion reformulated as an initial value problem. Since the effective value of damping depends on the amplitude of the response, an oscillation tracking algorithm is developed to ensure that the correct damping value is used at each time-step of the derivation.

3.5.1. Runge-Kutta Method

Runge-Kutta (RK) methods are a family of numerical techniques specifically developed to solve ordinary differential equations (ODEs). Their popularity stems from a strong balance between numerical accuracy and computational efficiency. RK methods provide an approximation of the solution to an initial value problem (IVP) by estimating the unknown function of time $y(t)$ based on a known function describing the systems' dynamics $F(t, y(t))$, and an initial condition $y(t_0) = y_0$ [57]. Such an IVP is presented in equation 3.6.

RK methods are iterative time-stepping methods, meaning that they compute the solution at each new time step $y(t + \Delta t)$ based on the value from the previous step $y(t)$, without requiring knowledge of the full solution ahead of time. As shown in Equation 3.7, the computation of the solution at the following time step involves evaluating several intermediate slope estimates, denoted as k values. While their detailed expressions are omitted for brevity, they are computed using the known function describing the system's dynamics $F(t, y(t))$, obtained from the IVP. A weighted average is computed based on these estimated slopes in order to estimate the value at the next time step [57]. While equation 3.7 illustrates

the formulation of the commonly used fourth-order Runge-Kutta (RK4) method, this study employs the RK45 method, which uses a different weighted averaging scheme that is not presented here.

$$\dot{y}(t) = F(t, y(t)) \quad \text{and} \quad y(t_0) = y_0 \tag{3.6}$$

$$y(t + \Delta t) = y(t) + \frac{\Delta t}{6}(k_1 + 2k_2 + 2k_3 + k_4) \quad \text{(RK4)} \tag{3.7}$$

3.5.2. Python Implementation

The numerical integration of the response is performed using the `scipy.integrate.solve_ivp` function in Python. The `solve_ivp` function requires a system of ODEs defined by the initial value problem (`fun`), a time span (`t_span`), and initial conditions (`y0`) [58]. While `solve_ivp` supports various numerical solvers, this study makes use of the Runge-Kutta 4/5 method (RK45). It is an explicit integration technique characterised by a local truncation error of order $\mathcal{O}(h^4)$ and an error estimator of order $\mathcal{O}(h^5)$. In contrast to RK4, RK45 includes a procedure which dynamically adjusts the step size Δt to optimise accuracy and computational efficiency. The exact computation of $y(t + \Delta t)$ using RK45 differs from the expression in equation 3.7. At each time step, two approximations of the solution are made using slightly different variations of the slopes' weighted average and then compared. If the two approximations lie within a specified tolerance, the step size is accepted. If not, the step size is reduced and the process is repeated. If the two approximations agree more closely than needed, the step size is increased to improve efficiency [59].

The IVP of the system considered in this thesis is expressed in equation 3.8. The unknown function $y(t)$ has been replaced by the unknown state-space vector $\mathbf{q}(t)$ with initial condition $\mathbf{q}_0$. The state-space vector contains the displacement $x(t)$ and velocity $\dot{x}(t)$ of the dynamic response and describes the state of the second-order SDOF at any moment in time (eq. 3.9). The derivative of the state-space vector with respect to time $\dot{\mathbf{q}}(t)$, contains the velocity $\dot{x}(t)$ and the acceleration $\ddot{x}(t)$ of the dynamic response and describes how the system evolves in time (eq. 3.9). The acceleration $\ddot{x}(t)$ can be derived by rewriting the system's equation of motion (eq. 3.1) and substituting it into $\dot{\mathbf{q}}(t)$. The result (eq. 3.10) is a system of first-order ODEs which can be used to compute the state at the next time step.

$$\dot{\mathbf{q}}(t) = F(t, \mathbf{q}(t)) \quad \text{and} \quad \mathbf{q}(t_0) = \mathbf{q}_0 \tag{3.8}$$

$$\dot{\mathbf{q}}(t) = \begin{bmatrix} \dot{x}(t) \\ \ddot{x}(t) \end{bmatrix}, \quad \mathbf{q}(t) = \begin{bmatrix} x(t) \\ \dot{x}(t) \end{bmatrix} \quad \text{and} \quad \mathbf{q_0} = \begin{bmatrix} x(t_0) \\ \dot{x}(t_0) \end{bmatrix} \tag{3.9}$$

$$F(t, \mathbf{q}(t)) = \begin{bmatrix} \dot{x}(t) \\ \frac{1}{m}\left[f(t) - c(A)\dot{x}(t) - kx(t)\right] \end{bmatrix} \tag{3.10}$$

Another important consideration when working with measurements is the presence of noise, which can originate from the measurement instrument itself. No noise has been added to the response data in this research.

3.5.3. Challenges regarding Amplitude-Dependent Damping

To estimate the state at the following time step $\mathbf{q}(t + \Delta t)$, the system's state at the current time step $\mathbf{q}(t)$ must be known. This includes the displacement $x(t)$, the velocity $\dot{x}(t)$, the applied force $f(t)$, and the amplitude-dependent damping coefficient $c(A)$. The first three quantities are either known from the initial conditions or computed at the previous time step and do not pose a problem. The computation of $c(A)$, on the other hand, is not as straightforward. The challenge lies in selecting the appropriate damping coefficient when the amplitude A is not known a priori.

Previous numerical studies, investigating the performance of OMA methods in the presence of amplitude-dependent damping, rarely disclose an explanation of how the amplitude dependency is implemented in their synthetic data [56]. Tamura and Suganuma [20] were not transparent on the derivation of the response data used in the validation of the Peak RDT. Furthermore, Li et al. [60] and Wu et al. [61]

used instantaneous displacement-dependent damping $c(|x(t)|)$ to approximate amplitude-dependent damping $c(A)$.

Huang and Gu [56], who introduced the Envelope RDT as an enhancement of the Peak RDT, share similar concerns regarding the lack of transparency in response derivation. The authors provide a detailed description of the iterative method used to compute the dynamic response of a system with amplitude-dependent damping $c(A)$ and stiffness $k(A)$. The algorithm updates the damping and stiffness based on the response's amplitude envelope $A(t)$, derived using the Hilbert transform, until convergence is reached. In this study, a different approach is developed.

3.5.4. Oscillation Cycle Tracking Algorithm

Incorporating the amplitude-dependent damping coefficient $c(A)$ presents a challenge due to the definition of amplitude A. The displacement amplitude is defined as the *maximum displacement within one oscillation cycle*. Since the damping value is required at each time step of the numerical integration, an algorithm was implemented to track and update the evolving amplitude. This enables the `solve_ivp` solver to reference the correct damping value specified by the function $\xi(A)$ (see table 3.1).

In this study, an oscillation cycle is defined as the interval between two successive displacement peaks. Since velocity is the derivative of displacement with respect to time, a peak in the displacement corresponds to a zero-crossing with a negative slope in the velocity. Therefore, the initiation of a new cycle is detected when the velocity at the previous time step $t - \Delta t$ was positive and becomes negative (or equal to zero) at the current time step t. The implementation of these checks is done in Python using function attributes, which track the sign of the velocity at both the previous and current time steps, as well as the maximum displacement recorded within the ongoing cycle. In order to systematically evaluate the damping coefficient at the correct amplitude, the algorithm performs two checks at every time step:

1. Whether a new oscillation cycle has been initiated

$$\text{if} \quad \dot{x}(t-\Delta t) > 0 \quad \text{and} \quad \dot{x}(t) \leq 0 \quad \text{then} \quad A(t+\Delta t) = |x(t)| \tag{3.11}$$

2. Whether a new maximum displacement has been detected

$$\text{if} \quad x(t) > A(t) \quad \text{then} \quad A(t+\Delta t) = |x(t)| \tag{3.12}$$

The implementation of the checks is demonstrated using a simple exponentially decaying sinusoid as illustrated in figure 3.6. The two plots on the right provide a zoomed-in view of the region highlighted by the black dotted frames. While the blue and orange curves represent the numerically derived displacement and velocity, the grey curve corresponds to the expected response based on the systems' analytical solution. Thus, the blue and orange parts are known, and the grey parts are yet to be estimated step by step.

The aim of the demonstration is to compute the response at time step t (the current time step). The state vector $\mathbf{q}(t)$ is estimated using the displacement $x(t-\Delta t)$, velocity $\dot{x}(t-\Delta t)$, and external force $f(t-\Delta t)$, all evaluated at $t-\Delta t$ (the previous time step). As previously stated, the value of the damping coefficient c depends on the maximum displacement of the current cycle. Since, up to the current time step t, the velocity has not crossed zero with a negative slope and no displacement has exceeded the initial value A_1, the amplitude is taken to be A_1 for the computation of $\mathbf{q}(t)$.

However, time step t marks a critical transition point. As the velocity becomes less than or equal to zero, the check performed at the end of the iteration signals the start of a new oscillation cycle. Consequently, the next time step $t + \Delta t$ is computed using an updated amplitude $A_2 = x(t)$. From this point onwards, the updated amplitude will be used to determine the damping until a new cycle is detected.

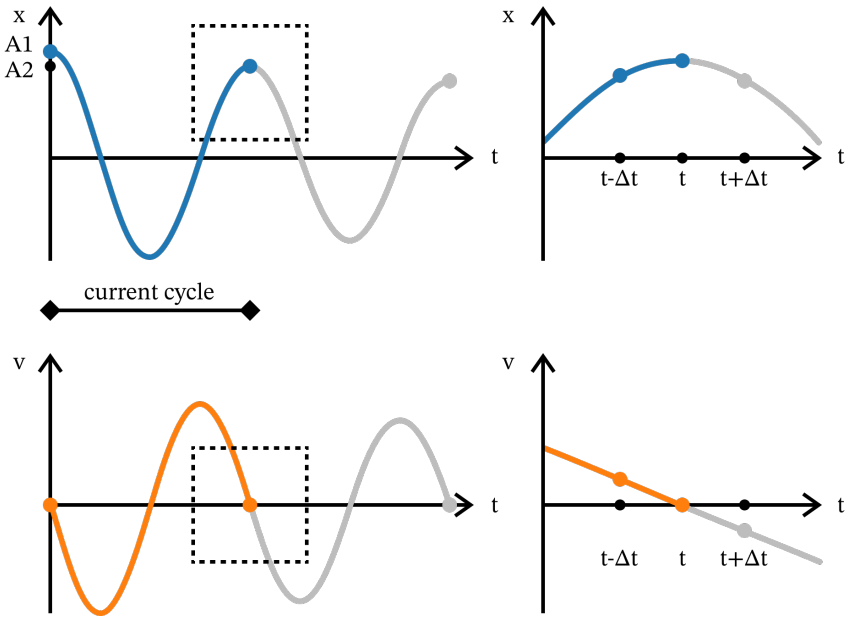

Figure 3.6: Oscillation tracking algorithm

3.6. Approximating the Free Decay

Approximating a system's free decay from its vibration response lies at the core of most time-domain OMA methods and represents the primary goal of the first stage in OMA.

The RDT algorithm approximates the system's free vibration response by sampling and averaging significant segments of pre-defined length. The segments are sampled based on a common trigger condition. The statistical averaging effectively cancels out the forced component of the response, assumed to be zero-mean, and thereby isolates the unforced system response to a set of initial conditions.

The result of this process is called a Random Decrement Signature (RDS) and, under satisfaction of certain conditions (see section 2.2.1), can be interpreted as the system's free decay. Careful execution of the signal processing is essential, as the reliability of damping estimates is highly dependent on the quality of the RDS [34].

3.6.1. Python Implementation

The Peak RDT is a modification of the traditional RDT, mainly with respect to the trigger condition. As mentioned in section 2.5.2, segments are sampled using the local extremum condition, which means that the first point of a sampled segment corresponds to a local peak in the displacement response. The python implementation of the Peak RDT is rather straight forward.

For a given displacement response time series, all peak values are identified using the `scipy.signal.find_peaks` function, which does so by comparing neighbouring values for all time points.

Figure 3.7 illustrates the identification of trigger points from the displacement response of a linear system excited by a stationary force. As explained in section 2.5.2, the triggered points are grouped per amplitude range. In this report, amplitude range and amplitude bin are used interchangeably and refer to the range of amplitudes considered in computing one RDS. For each amplitude bin, segments of predefined length τ are extracted based on the trigger points in that bin. These segments are averaged to create one RDS per amplitude bin.

It is also important to mention that the segments are allowed to overlap in this research which means that they are correlated. Kijewski & Kareem [29] have shown that the effect of correlation between segments have a marginal effect on the quality of the RD function.

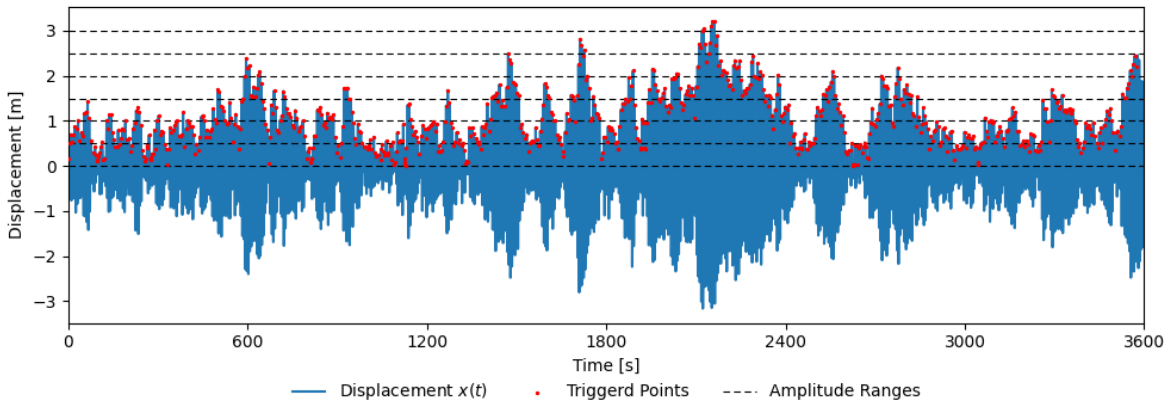

Figure 3.7: Identification and grouping of trigger points in amplitude ranges (Case 1)

3.7. Estimating Damping

The fundamental idea of the Peak RDT is to isolate the free vibration response of the system at multiple amplitude ranges. From the approximated free vibration response, damping can be identified from the amplitude attenuation observed in the free decay. This process corresponds to the second stage of Operational Modal Analysis (OMA), namely modal parameter extraction.

This thesis makes use of non-linear Least Squares Minimization (LSM). As described in section 2.3.2, the LSM method estimates modal parameters by fitting the theoretical free vibration response of a linear single-degree-of-freedom (SDOF) system to the computed Random Decrement Signatures (RDS). It minimizes the squared differences between the model and the data, yielding the damping ratio ξ and natural frequency f_n as optimal parameters.

3.7.1. Free Vibration Response of a Linear System

This section presents the derivation of the free vibration response of a linear SDOF system. The unforced equation of motion (equation 2.16) can be expressed in its canonical form (equation 3.13), where ω_n is the undamped natural angular frequency and ξ is the damping ratio. While he theoretical free decay response of a multi degree of freedom (MDOF) system results from the combined effects of all its contributing modes, a single degree of freedom (SDOF) system only has one vibration mode.

Depending on the value of the damping ratio ξ, three different solutions to the differential equation (equation 3.13) can be found. Since high-rise buildings are generally under-damped ($\xi < 1$), the general solution to the differential equation is given by equation 3.14. It represents an exponentially decaying sinusoidal motion, where the exponent indicates the decay rate and the sinusoidal function represents the oscillatory motion at the damped natural frequency ω_d.

$$\ddot{x}(t) + 2\xi\omega_n\dot{x}(t) + \omega_n^2 x(t) = 0 \tag{3.13}$$

$$x(t) = e^{-\xi\omega_n t}[A\cos(\omega_d t) + B\sin(\omega_d t)] \tag{3.14}$$

$$\dot{x}(t) = e^{-\xi\omega_n t}[(B\omega_d - \xi\omega_n A)\cos(\omega_d t) - (A\omega_d + \xi\omega_n B)\sin(\omega_d t)] \tag{3.15}$$

$$f_n = \frac{\omega_n}{2\pi}, \quad \omega_n = \sqrt{\frac{k}{m}}, \quad \omega_d = \omega_n\sqrt{1-\xi^2}, \quad \xi = \frac{c}{2\sqrt{km}} \tag{3.16}$$

The constants A and B must be determined from the initial conditions. Since this study focuses on the Peak RDT, it is safe to assume that the initial conditions correspond to peak values (equation 3.17). Differentiating equation 3.14 with respect to time yields equation 3.15. Applying the initial conditions $x(0) = 1$ and $\dot{x}(0) = 0$ allows for solving the constants A and B as seen in equations 3.18 and 3.19.

Finally, substitution of A and B into equation 3.14 gives the final expression for the theoretical free decay of a SDOF system under peak displacement amplitude initial conditions (equation 3.21).

$$\begin{cases} x(0) = x_0 = 1 \\ \dot{x}(0) = \dot{x}_0 = 0 \end{cases} \tag{3.17}$$

$$x(0) = e^0(A\cos(0) + B\sin(0)) \quad \rightarrow A = 1 \tag{3.18}$$

$$\dot{x}(0) = e^0((B\omega_d - \xi\omega_n A)\cos(0) - (\xi\omega_n B + A\omega_d)\sin(0)) \quad \rightarrow B = \frac{\xi\omega_n}{\omega_d} \tag{3.19}$$

$$\text{using} \quad \omega_d = \omega_n\sqrt{1-\xi^2}, \quad B = \frac{\xi\omega_n}{\omega_n\sqrt{1-\xi^2}} = \frac{\xi}{\sqrt{1-\xi^2}} \tag{3.20}$$

$$x(t) = e^{-\xi 2\pi f_n t}[\cos(\omega_d t) + \frac{\xi}{\sqrt{1-\xi^2}}\sin(\omega_d t)] \tag{3.21}$$

Given that damping ratio's of high-rise buildings are typically in the magnitude of 10^{-2}, the second term can be negligible. However, it is retained in the numerical study for consistency. Using LSM, equation 3.21 is fitted to the computed Random Decrement signatures, resulting in a deterministic damping estimate.

3.8. Statistical Analysis of Damping Estimates

To assess the reliability of damping estimates, a statistical analysis of multiple realizations of damping estimates is performed. Trough a Monte Carlo simulation it is aimed to produce a distribution of damping estimates on which statistical metrics such as variance or bias can be computed.

3.8.1. Method A vs. Method B

As explained in section 3.2, the first research objective is addressed by conducting a series of Monte Carlo simulations in which the damping identification process is repeated N_{sim} times. Two logical sequences can be followed to perform this repeated identification. They are illustrated schematically in figure 3.8

In the first approach, referred to as method A, the Peak RDT is applied to the displacement response to compute a set of Random Decrement Signatures (RDS) for different amplitude ranges. The Least Squares Method (LSM) is then applied to each RDS to obtain a single damping estimate per amplitude range. Repeating this process N_{sim} times yields a distribution of damping estimates for each range.

This process is detailed in section 3.2 and is adopted throughout this thesis unless stated otherwise. It follows an intuitive sequence and aligns with the primary objective of the study: evaluating the reliability of damping estimates under varying conditions. In this context, generating a distribution of many damping estimates provides deeper insight into the accuracy and precision associated with individual estimates.

In contrast, a second approach, referred to as method B, involves applying the Peak RDT to N_{sim} displacement response signals. Rather than extracting a single damping estimate from each set of RDS, the entire collection of RDS are averaged for each amplitude range to compute a mean RDS. This means that only one mean damping per amplitude range is estimated with the LSM technique. This method provides less insights into the distribution of damping estimates but can be very useful when the behaviour of the RDS per amplitude range is of interest.

It is important to note that both methods require the same total amount of data. In Method A, the mean damping estimates are obtained from N_{sim} individual time traces of 1 hour each. In Method B, the mean damping estimate is effectively derived from a single time trace with a total duration of N_{sim} hours.

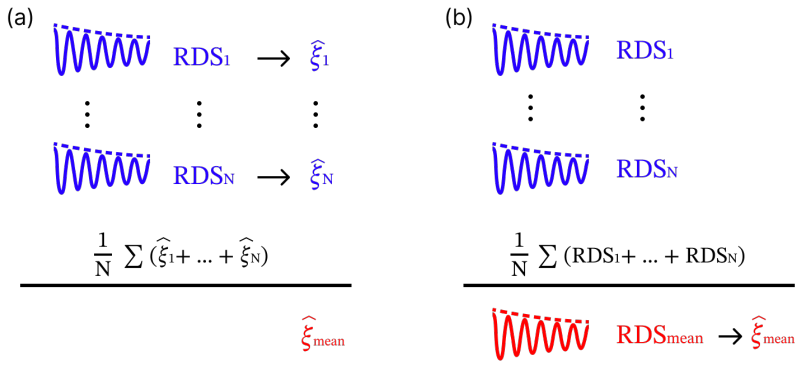

Figure 3.8: Schematic representation of the possible sequences used to obtain the mean damping estimate; (a) Method A, Mean damping obtained from a distribution of damping estimates; (b) Method B, Mean damping obtained from a mean RDS

3.8.2. Statistical Metrics

The reliability of damping estimates is evaluated based on accuracy and precision. These metrics are quantified based on the distribution of damping estimates resulting from the Monte Carlo simulation. While bias and relative error are metrics of accuracy, variance and the 95% confidence interval on the mean provide metrics of precision.

Bias

Bias is a measure of accuracy and refers to the systematic difference between the expected value of an estimator $\hat{\theta}$ and the true value of the parameter θ being estimated. Its mathematical expression is given by equation 3.22, where the expectation operator can be approximated by the mean of the distribution of estimates. A biased estimator consistently overestimates or underestimates the true value, indicated by a positive and negative bias respectively. An unbiased estimator has an expected value equal to the true parameter [62].

$$\text{Bias}(\hat{\theta}) = \mathbb{E}[\hat{\theta}] - \theta \tag{3.22}$$

Relative Error

Relative error is given by the ratio of absolute error to the true value of the parameter being estimated, as shown in equation 3.23. By measuring the size of the error in relation to the true value, it provides a dimensionless metric. This is especially useful when the parameter varies across different orders of magnitude. Therefore the relative error is especially insightful when assessing the accuracy of amplitude-dependent damping.

$$\text{Relative Error} = \frac{|\hat{\theta} - \theta|}{|\theta|} \tag{3.23}$$

Variance

Variance quantifies the spread or variability around its expected (mean) value and is given by equation 3.24. Lower variance indicates more consistent estimates across repeated samples, contributing to precision of the estimator [62].

$$\text{Var}(\hat{\theta}) = \mathbb{E}\left[(\hat{\theta} - \mathbb{E}[\hat{\theta}])^2\right] \tag{3.24}$$

Confidence Intervals

The confidence interval provides a range of plausible values for a parameter being estimates. It is constructed such that it contains the true value with a specified probability, chosen to be 95% in this thesis. The confidence intervals depend on sample size n in each amplitude range. Whereas for large sample sizes, the critical value $z_{\alpha/2}$ is taken from the normal distribution, for small sample sizes the critical value $t_{\alpha/2,n-1}$ is taken from the Student's t-distribution with $n-1$ degrees of freedom [63].

In equations 3.25 and 3.26, $\bar{x}$ represents the sample mean, s is the sample standard deviation, and n is the number of observations. These parameters relate to the samples or damping estimates contained in each bin. The significance level α is set to correspond to a 95% confidence level.

Large Sample Size ($n > 30$) :

$$CI = \bar{x} \pm z_{\alpha/2} \cdot \left(\frac{s}{\sqrt{n}}\right) \tag{3.25}$$

Small Sample Size ($1 \leq n \leq 30$) :

$$CI = \bar{x} \pm t_{\alpha/2,n-1} \cdot \left(\frac{s}{\sqrt{n}}\right) \tag{3.26}$$

4

Evaluating Non-Stationarity of Response Data

When evaluating the Peak RDT's ability to provide reliable damping estimates under conditions that deviate from its mathematical assumptions, it is crucial to understand how these deviations affect the algorithm and the reliability of the resulting estimates. While section 2.6.6 illustrates the relevance of assumptions such as zero-mean, stationarity and normality, this section contextualizes these underlying assumptions with respect to practical applications of the Peak RDT. Additionally, the effects of introducing non-stationary characteristics in the excitation are analysed based on the resulting response signals. The distributions of these responses are presented, along with a discussion of their mean values and overall shapes in section **??**. The degree of non-stationarity is quantified using a statistical test in section 4.3. The quantification of non-stationarity serves as a basis for evaluating the expected reliability of the damping estimates.

4.1. Notes on Stationarity Condition

In the context of the Random Decrement Technique (RDT), both the excitation and the structural response are often assumed to be zero-mean, stationary and Gaussian. In fact, they are standard assumptions in random vibration theory. However, existing literature is inconsistent on whether these assumptions should apply to the ambient excitation or to the structural response.

As outlined in section 2.2, the RDT relies on statistical averaging of sampled segments to approximate the system's free decay. To ensure that this averaging effectively isolates the free vibration response, the excitation must be zero-mean and time-invariant, as discussed in section 2.6.6. Additionally, if the excitation follows a normal distribution, it is ensured that the statistical average converges to zero which simplifies certain theoretical derivations.

Therefore, in its strictest sense, the zero-mean, stationarity and normality conditions apply to the excitation. However, some literature applies the assumptions directly to the structural response, which can be justified by two practical reasons. Firstly, in operational modal analysis (OMA), the excitation is unknown. Secondly, since the RDT directly uses the response signal as input, it is easier to assess whether the underlying assumptions are met based on the response. Directly applying these assumptions to the response signal is valid under the assumption that the system is linear and time-invariant (LTI). In that case, a zero-mean, stationary, Gaussian excitation will produce a zero-mean, stationary, Gaussian response.

On the other hand, given a non-linear system, response stationarity cannot be guaranteed even though the excitation might be stationary. This means that, although theoretically only the linearity condition is violated, the stationarity condition is also affected. Since researchers agree that damping in high-rise buildings is amplitude dependent, it becomes increasingly important to analyse the effect of non-stationary response signals. Nevertheless, examining the impact of non-stationary excitation on a linear system remains important for identifying potential sources of errors in damping estimates.

Figure 4.1 provides an overview of the deviations considered in this thesis as well as their impact on the stationarity of the response. Theoretically, each of the considered deviations results in a non-stationary response which can be problematic for the identification of damping using the Peak RDT.

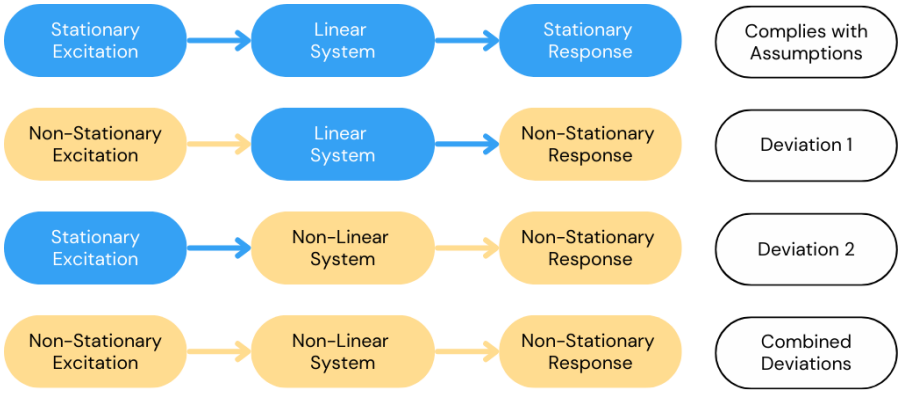

Figure 4.1: Impact of deviations on response stationarity

4.2. Analysis of Response Signals

In this thesis, non-stationarity is primarily introduced in the excitation. However, as discussed in section 4.1, its effects are evaluated based on the characteristics of the resulting response signals, since these serve as the input to the Peak RDT. The statistical properties of vibration responses are analysed using histograms, which represent the distribution of the data points by dividing the data into bins. Each bar indicates the percentage of total data points that fall within that bin. The mean μ and standard deviation σ of the distribution are indicated, and the red line represents a Gaussian distribution fitted to the data.

For all eight cases considered in this thesis, the distribution of a single response realization is analysed. This is deemed sufficient since the only difference between simulations within each case is the randomness of the white noise. The distributions of response signals for the three types of non-stationarity, in both linear and non-linear systems, are shown in figures B.1 and B.2 in Appendix B. Regarding the benchmark case, the distribution of a single response realization is illustrated in figure 4.2. The mean μ and standard deviation σ are included in the figure alongside a red curve, indicating the Gaussian fit to the distribution.

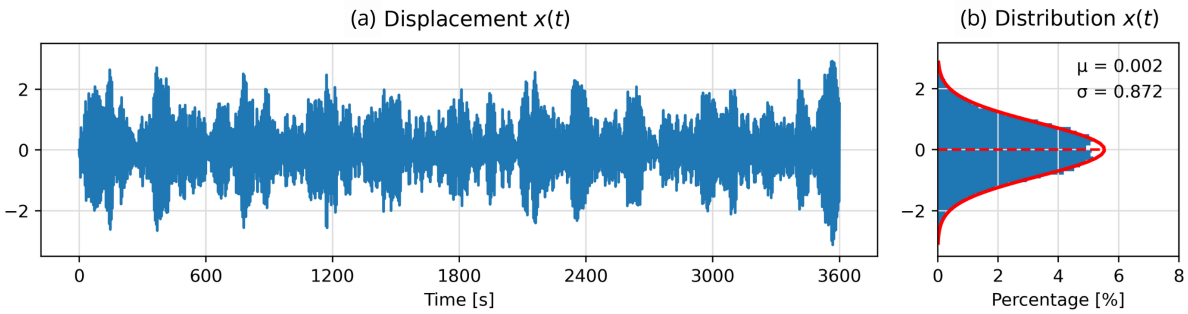

Figure 4.2: One realization of the structural response of the system with constant damping excited by a stationary load; (a) Time-series; (b) Distribution and Gaussian fit

One observation from the benchmark case (figure 4.2) is that the response is not perfectly normally distributed. Specifically, the peak of the distribution appears somewhat flatter, indicating heavier tails compared to a true Gaussian distribution. This suggests that, although the response may visually resemble a Gaussian distribution, it exhibits subtle non-Gaussian characteristics. This is unexpected, as the excitation is zero-mean, stationary, and Gaussian and the benchmark system is linear time-invariant.

The effects of the three types of non-stationarity are analysed for both the linear and non-linear systems. For the first type, which introduces a time-dependent mean in the excitation, a corresponding non-zero mean appears in the response signal. This mean becomes increasingly pronounced with higher values of the Gaussian pulse's peak P. In the non-linear case, the response exhibits slightly more deviation from zero mean, although the differences are marginal. Additionally, the distributions are asymmetric, deviating from the symmetry expected in a Gaussian distribution. The introduction of a non-zero mean in the excitation and resulting response is expected to introduce errors in damping estimates as the RDS would not accurately approximate a free vibration response.

For the second type, which introduces a time-dependent variance in the excitation, the response remains zero-mean for both the linear and non-linear systems. Interestingly, response signals, corresponding to time-dependent variance in the excitation, show a closer adherence to normality compared to the benchmark case, as the peak of the response distribution closely aligns with the Gaussian fit. Damping estimates derived under these conditions are expected to be reliable, as no significant deviations are observed.

Lastly, for the third type, which introduces both a time-dependent mean and variance in the excitation, the response signals exhibit a combination of characteristics combining observed in the first two types. A non-zero mean is present in the response and becomes more pronounced with increasing values of the Gaussian pulse's peak P. As with the first type, the non-linear system shows slightly greater deviations from zero mean, although these differences remain marginal. Additionally, the response distributions are asymmetric, deviating from the symmetry expected in a Gaussian distribution. As a result, it is expected that the application of the Peak RDT to these response signals will produce erroneous damping estimates.

4.3. Quantification of Non-stationarity

In this thesis, stationarity of the response signals is assessed using both the Augmented Dickey-Fuller (ADF) and Kwiatkowski-Phillips-Schmidt-Shin (KPSS) tests, as described in sections **??** and 2.6.3. While the null hypothesis of the ADF test is that the data is non-stationary, the KPSS test assumes stationarity as its null hypothesis, specifically referring to stationarity around a constant mean. Their combined application is well suited for confidently evaluating the stationarity of response data. If the ADF test yields a p-value less than or equal to 0.05, and the KPSS test's p-value is greater than 0.05, stationarity of the data is guaranteed. A binary assessment of stationarity for all N_{sim} responses of all eight cases considered, is summarized in table B.1 in Appendix B. Since the outcome is limited to either stationarity or non-stationarity, it provides little insight into how sensitive the reliability of damping estimates is to deviations from the stationarity assumption.

Assessing the degree of non-stationarity provides insight into the threshold below which damping estimates may still be considered reliable. In addition to the p-value, the KPSS test provides a test statistic, which can be used as a measure of non-stationarity. The KPSS test quantifies non-stationarity by comparing its test statistic to a critical value. A larger KPSS statistic indicates a stronger degree of non-stationarity, while values slightly above the critical threshold typically indicate mild non-stationarity.

Figure 4.3.a displays the distribution of N_{sim} KPSS test statistics, computed for each of the N_{sim} responses across all cases considered in this thesis, while figure 4.3.b provides a zoomed in view. At a 95% significance level, the critical value equals 0.463, marked by the red dotted line.

Contrary to initial hypothesis that the non-linear system would produce non-stationary signals, both the linear and non-linear responses to stationary excitation (S) appear stationary based on level stationarity tests, as the entire distribution of KPSS test statistic is below the critical value. Figure 4.3.b shows that the test statistics are slightly higher for the non-linear case, supporting the initial assumption that non-linearity influences the statistical characteristics of the response. However, this effect appears to be minor.

The second non-stationary type (NS2) also yields KPSS values below the critical threshold for all N_{sim} simulations and all three degrees of non-stationarity for the linear and non-linear system, indicating that the responses are stationary even though a time-dependent variance was introduced in the excitation. However, the KPSS test assesses trends in the mean, meaning that other forms of non-stationarity may

not be captured. Similarly to the stationary case, figure 4.3.b reveals slight reductions in stationarity of the responses corresponding to the non-linear system. This supports the expectation that the Peak RDT will yield reliable damping estimates under these conditions.

For the first and third non-stationary type (NS1 and NS3), where a deterministic time-dependent mean is introduced in the excitation, the KPSS test indicates that the responses become increasingly non-stationarity with higher peak values in the mean function. However, the responses resulting from systems excited with a time-dependent mean only (NS1), exhibit more pronounced non-stationarity than the ones corresponding to time-dependent mean and variance (NS3). This is likely because in the third types, the variance is also modulated, partially compensating for the time-dependent mean. In both NS1 and NS3, the non-linear system generally shows higher non-stationarity compared to the linear system. Additionally, it should be noted that the KPSS test statistics for these cases considered are very high, reaching values as large as 16. As described in the literature review (section 2.6.3, a similar procedure was applied to measured acceleration signals from wind-induced vibrations in high-rise buildings and yielded much lower KPSS values, with an upper bound around 1.2, indicating milder non-stationarity. This raises questions about the realism of the degrees of non-stationarity considered in this thesis.

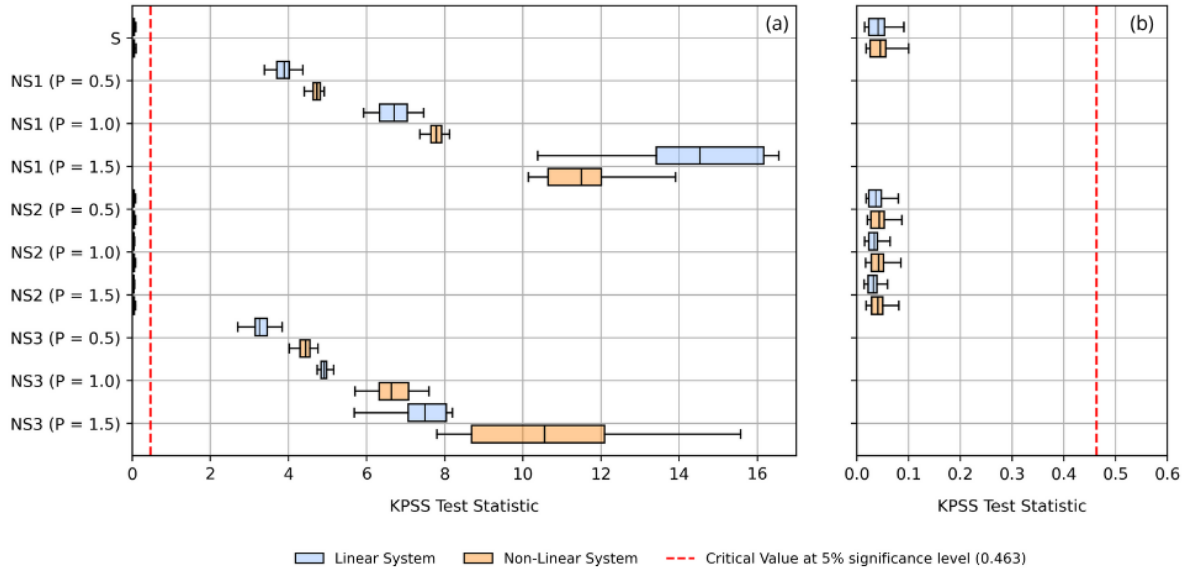

Figure 4.3: Quantification of non-stationarity per case: Boxplots display the distribution of KPSS statistics computed from all N_{sim} response signals. The red dotted line represents the critical value; KPSS statistics below this line indicate stationary time series, while values above indicate non-stationarity; (a) full range; (b) zoomed in

4.4. Conclusion

Since the direct input to the Peak RDT is the vibration response, it is crucial that the responses satisfy the underlying assumptions of zero-mean, stationarity, and normality. This section has demonstrated that introducing a time-dependent mean in the excitation unsurprisingly introduces a time-dependent non-zero mean in the response. This is evident both in the response signal distributions, which show an increasingly non-zero mean, and in the KPSS statistics, which indicate a growing degree of non-stationarity. In contrast, modulating the variance of the excitation results in response data that is level stationary. Furthermore, the non-linearity of the system increases the degree of non-stationarity for all types of excitation considered, although the effect is minor. Therefore, reliable damping estimates are expected for all cases with stationary excitation and modulated variance, while larger errors are anticipated when a time-dependent mean is present (NS1 and NS3). The reliability of the resulting damping estimates is evaluated further in section 7.2.

5

Benchmark Case

In this chapter, the results of the Monte Carlo simulation conducted on the benchmark case are presented. The benchmark case consists of a linear system excited by zero-mean, stationary, Gaussian white noise. It thus fully satisfies the underlying assumptions of the Peak RDT, outlined in section 2.1.1, providing a controlled environment to assess the method's intrinsic capability in reliably identifying modal parameters.

The results of this simulation are essential to evaluate the performance of the Peak RDT before introducing any deviations, hence ensuring that any errors on damping estimates can be attributed to the deviations rather than to limitations of the method itself. Additionally, the benchmark case serves as a reference against which later simulations incorporating deviations from underlying assumptions, can be compared.

In addition to qualitatively evaluating damping estimates derived using the Peak RDT under ideal conditions, this section presents a clarification on the visual representation of the distribution of damping estimates and justifies the use of a trimmed distribution ensuring statistically meaningful results. Furthermore, an explanation is provided on the normalization of the displacement amplitudes. The analysis is completed with a discussion of whether individual or average damping estimates are more appropriate for evaluating peak RDT performance. A quantitative assessment of the reliability of damping estimates is provided in section 7.

5.1. Relative Representation

Figures 5.1.a and 5.1.c illustrate, respectively, a single realization of the stationary white noise excitation $f(t)$ and the corresponding displacement response $x(t)$ of the linear system. Figures 5.1.b and 5.1.d show the distribution of signal values represented as histograms, each overlaid with a fitted Gaussian distribution (red line).

While the system is intended to represent the dynamic behaviour of high-rise buildings, characterized by a natural frequency and damping ratio typical of such structures, figure 5.1.c shows that the magnitude of the displacement response is somewhat exaggerated. This is a result of the chosen magnitude of the excitation. Nevertheless, these displacement responses provide valuable data for identifying the system's damping and evaluating the effectiveness of the peak RDT in reliably estimating damping values.

To analyse the findings independently of the displacement magnitudes observed in the generated data, the amplitude ranges are expressed as normalized values relative to the absolute maximum displacement recorded across the entire set of time series. An alternative approach would have been to normalize each signal by its own maximum absolute displacement. However, this would reduce control over the amplitude ranges, which would be noticed especially in cases including deviations. This choice to normalize with the maximum value recorded in the entire dataset aligns with the way the damping functions are defined and how the peak RDT is computed.

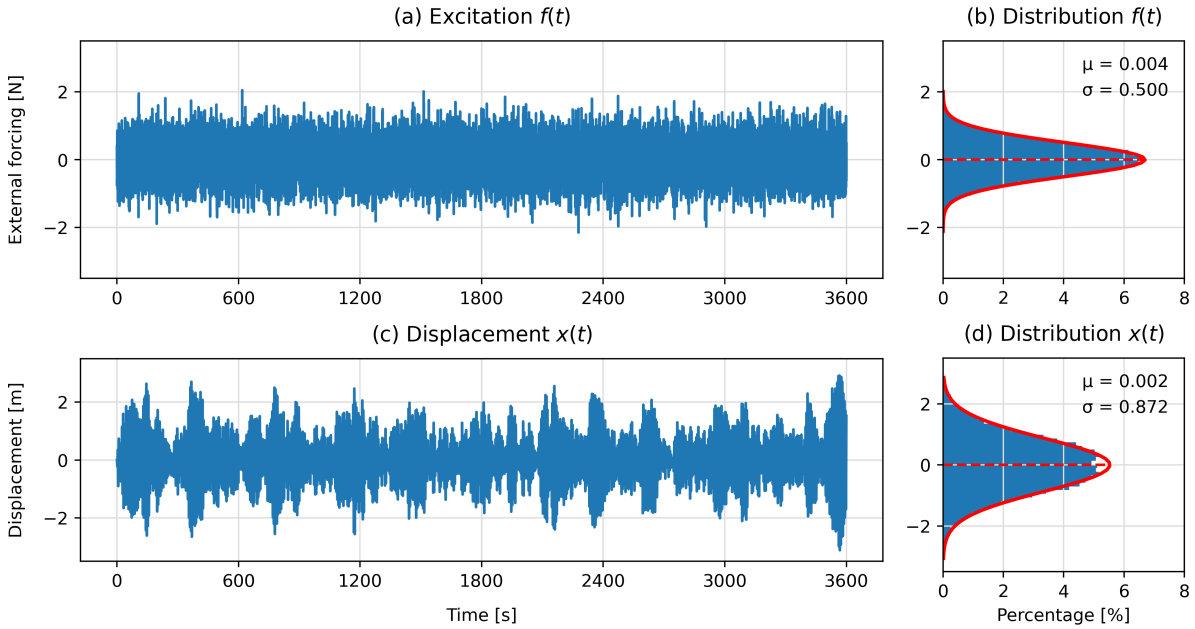

Figure 5.1: Statistical analysis of the excitation and response signals; (a) a single realization of the stationary white noise excitation$f(t)$; (c) corresponding displacement response $x(t)$ of the linear system; (b) and (d) histograms showing the distributions of the excitation and displacement signals
Settings: $t = 3600s$, $f_s = 20Hz$

5.2. Distribution of Damping Estimates

As explained in 3.8.1, the numerical study adopts Method A as the standard approach. The damping identification process is repeated for N_{sim} different displacement response time series. Each response time series produces a set of Random Decrement Signatures (RDS), with each RDS corresponding to a specific amplitude range. In turn, each RDS yields one damping estimate, resulting in a set of damping estimates that vary with amplitude. This phenomenon is known as amplitude-dependent damping. For the linear case, the responses are derived using the constant damping function $\xi_1(A)$ outlined in section 3.3.3. Thus, the damping estimates obtained from the numerical simulation should reflect a constant damping value across all amplitudes.

Horizontal Distribution

Figure 5.2 presents the damping distribution resulting from the Monte Carlo simulation conducted on the benchmark case. While figure 5.2.a displays the entire distribution across all normalized amplitude ranges, figure 5.2.b shows a trimmed version. The relative amplitude range is truncated to maintain the statistical reliability of the distribution of estimates within one bin.

The reduced number of damping estimates in the higher relative amplitude ranges can be attributed to the damping identification method and the chosen approach for dimensionless visualization of the results. Since only the white noise excitation varies from one realization to another, the resulting displacement responses should have the same order of magnitude but it cannot be guaranteed that all response signals will have the same maximum displacement. As a result, it is not be possible to consistently generate damping estimates in the higher relative amplitude ranges.

Throughout this study, it is ensured that each bin contains at least 10% of the total number of realizations N_{sim} used in the Monte Carlo simulation. As shown in table 5.1, the highest amplitude range contains only three damping estimates. However, a distribution with 3 samples cannot provide reliable metrics such as mean or variance, making it inappropriate for meaningful analysis. The trimmed horizontal distribution is referred to as damping distribution throughout this thesis.

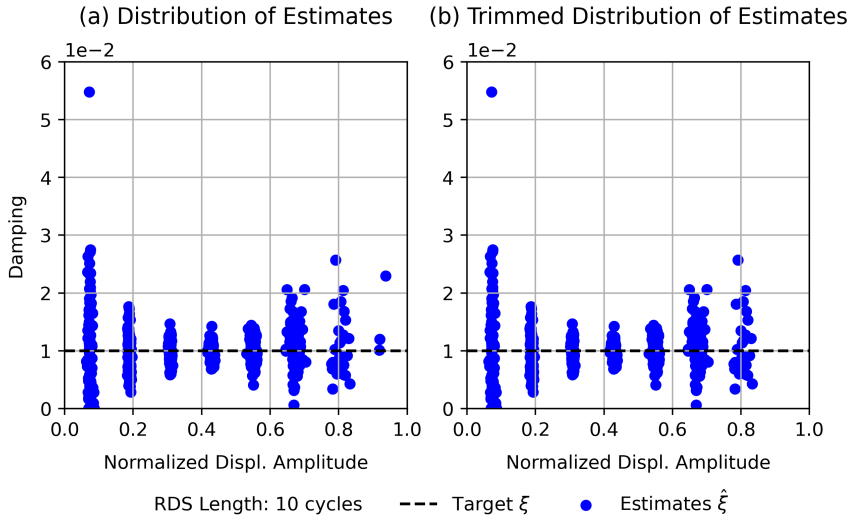

Figure 5.2: Complete and trimmed distribution of damping estimates across relative amplitude ranges
Settings: RDS Length = 10 cycles, $N_{sim} = 100$, $t = 3600s$, $f_s = 20Hz$

Relative Amplitude Range [%]	0-12.5	12.5–25	25–37.5	37.5–50	50–62.5	62.5–75	75–87.5	87.5–100
Realization Count N_r	100	100	100	100	100	86	29	3

Table 5.1: Amount of damping estimates per amplitude range

Vertical Distribution

The vertical distribution of damping estimates within each bin is also of importance and is illustrated using a set of histograms in figure 5.3. The horizontal axes represent the percentage of estimates within each bin that correspond to a specific value. The black dotted line marks the target damping value, namely the true damping value used as input in the system, and the red dotted line indicates the mean value of all estimates. Additionally, a Gaussian curve has been fitted to the data. The fit of the Gaussian distribution to the data is evaluated using the normality test described in section **??**. The corresponding p-value is shown in the top-right corner of each histogram.

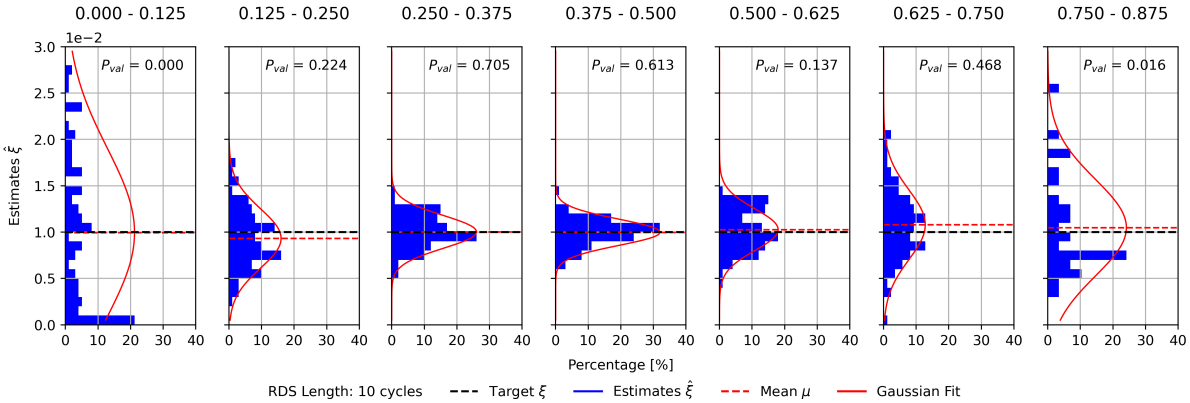

Figure 5.3: Distribution of damping estimates for each relative amplitude range
Settings: RDS Length = 10 cycles, $N_{sim} = 100$, $t = 3600s$, $f_s = 20Hz$

Statistical Metrics

Finally, a statistical analysis can be conducted on the distribution of damping estimates. Figures 5.4.b and 5.4.c show key statistical measures of the damping distribution, namely (1) the mean including 95% confidence intervals and (2) the variance. These metrics are logically computed per bin, thus for each horizontal distribution. The red dots in 5.4.b indicate the mean of the damping distribution for each relative amplitude range. The black dotted line indicates the target damping value given the true damping value used as system input. The red shading indicates the ± 95 % confidence intervals (CI) around the mean. Finally, the black dots in figure 5.4.c illustrate the variance of the distribution which is a measure of the spread in the individual estimates.

The CI is a quantification of uncertainty and provides a range within which the true damping value is likely to fall. For A 95% confidence interval, if the experiment were repeated many times (with different realizations of white noise applied to the same system), 95% of the calculated CI would contain the true damping value. Thus, while a narrow CI indicates high precision on the estimate, a wide CI reflects greater uncertainty. Finally, the black dots in the right plot illustrate the variance of the distribution which is a measure of the spread in the individual estimates.

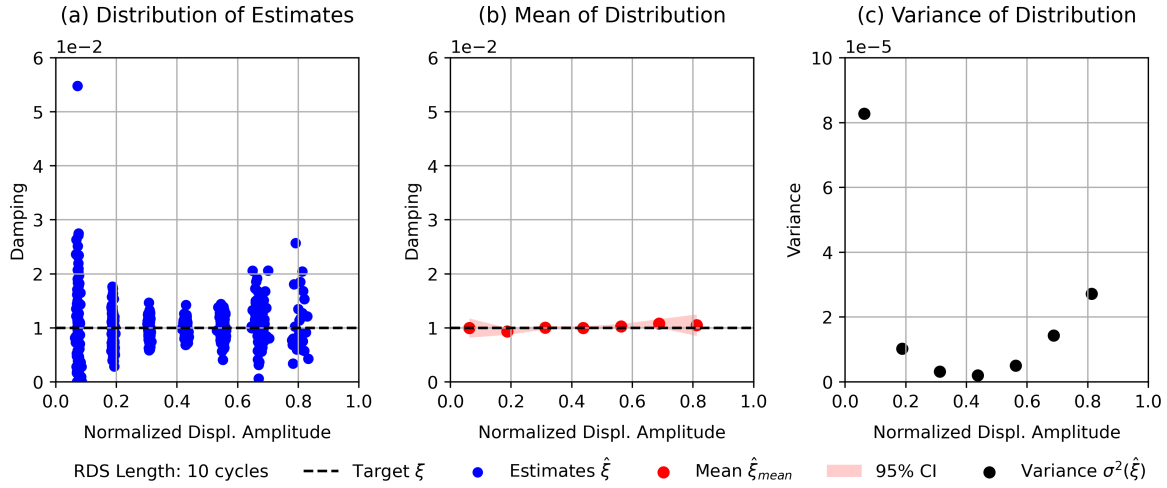

Figure 5.4: Damping Estimates, Linear System & Stationary Excitation
(a) Distribution of Estimates, (b) Mean of Distribution, (c) Variance of Distribution
Settings: RDS Length = 10 cycles, $N_{sim} = 100$, $t = 3600s$, $f_s = 20Hz$

5.3. Observations

The benchmark case involves a linear system with constant damping subjected to zero-mean stationary white noise excitation. Since the system and excitation fully satisfy the method's underlying assumptions, it provides a controlled setting to evaluate the performance of the Peak RDT in estimating damping. Assessing the Peak RDT in such a controlled setting allows for distinguishing between uncertainties inherent to the method itself and those arising from deviations from the ideal conditions. This section outlines the observations made on the distribution of damping estimates using the Peak RDT under ideal conditions.

Variance

The first observation is related to the variance in individual damping estimates across relative amplitude ranges. As seen in figure 5.4.a, distribution of individual estimates, the spread of damping estimates increases notably in both the lower and higher relative amplitude ranges. This pattern is also reflected in figure 5.4.c, which shows the computed variance per amplitude bin. In the lowest relative amplitude range (0% to 12.5%), the variance is especially high. As seen in 5.4.a, this is partially due to an outlier, but the higher variance is also reflected in the wider spread of remaining estimates in that

range. Overall, a U-shaped trend emerges from figure 5.4.a and 5.4.c, indicating lower variance in the intermediate relative amplitude ranges and higher variance at the extremities.

The larger spread of damping estimates at low and high relative amplitude ranges can be observed in histograms in figure 5.3 as well. Moreover, the middle ranges show a denser clustering of estimates that appears approximately Gaussian and distributed around the mean value. This is most evident for the estimates in relative amplitude range 37.5% to 50%. Whether the estimates are actually normally distributed around the mean value can be verified based on the p-values computed in the normality test. The test assumes normality under the null hypothesis. Therefore, rejecting the null hypothesis based on a p-value less than or equal to 0.05 indicates that the data is not normally distributed. The damping estimates are thus normally distributed in all bins except for the two outermost, where the highest variance is observed.

The fact that the damping estimates are not normally distributed at the lower and higher relative amplitude ranges is an interesting observation as a Gaussian distribution usually entails the notion of a random error, meaning that sometimes the estimates are more or less accurate but on average they converge to the target value. However, deviations from normality indicate that the errors may be less random and more systematic in nature. Especially for the lowest relative amplitude ranges it is observed that 21% of the data has a damping value that lies between 0% and 0.01%.

Mean

Secondly, despite the large spread in individual damping estimates, figure 5.4.b reveals that the mean value in each amplitude bin closely aligns with the true damping ratio indicated by the black dotted line. Moreover, the confidence intervals (CI) follow the same trend as the variance: they are very narrow in the middle amplitude ranges, indicating high reliability of the mean estimate, and widen slightly at the extremes, reflecting slight increased uncertainty.

These observations lead to the intermediate conclusion that while the Peak RDT may produce unreliable individual estimates, with a percentage error as high as 450%, the mean of all estimates provides a highly accurate estimate of the true damping value $\xi = 0.01$. The reliable mean estimates are supported by rather narrow CI. Thus, despite considerable variance in individual estimates, the statistical mean effectively captures the ground truth. The strong contrast between reliability of individual estimates $\hat{\xi}$ and the mean of estimates $\hat{\xi}_{mean}$ suggests that the Peak RDT is much stronger when applied probabilistically rather than deterministically.

5.4. Defining Damping Estimates

The aim of the benchmark case is to assess the ability of the Peak RDT in reliably estimating damping under ideal conditions. Before any conclusions can be drawn from regarding this goal, the exact definition of *damping estimate* must be clarified. In fact, the term damping estimate can be interpreted in two ways.

On one hand, each Monte Carlo simulation results in a distribution of individual damping estimates across normalized displacement amplitudes, represented in figure 5.4.a using blue dots. From this distribution, a mean is computed which is represented in 5.4.b using red dots. The crucial question is whether the term *damping estimate* refers to individual estimates $\hat{\xi}$ or to the mean of individual estimates $\hat{\xi}_m$.

Conceptually, this distinction determines whether the damping identification method is applied in a deterministic or stochastic manner. It is noted that the stochastic application of the damping identification method requires substantial amounts of similar data as the identification process has to be repeated N_{sim} times. Given the substantial spread observed in individual damping estimates, the interpretation can significantly influence the conclusions drawn.

To address this question, it is important to consider the context of the measurement campaigns relevant to this research, particularly with regard to the scale at which damping identification is performed. Additionally, it is important to relate it back to the research problem introduced in chapter 1.

The HiViBe consortium [6], led by TNO, is a large-scale monitoring program that includes a diverse range of buildings, some of which have been monitored for several years, others have only been mon-

itored over a couple of days. As outlined in the introduction, this thesis represents one of several foundational contributions towards more reliable comfort assessments of high-rise buildings in the design phase.

This thesis' research findings are therefore rather likely applied in the context such large-scale monitoring campaigns recording the vibration response of high-rise buildings under wind loading at service limit state (SLS) amplitudes. Unlike ultimate limit state (ULS) scenarios, wind levels relevant to comfort assessments occur much more frequently, resulting in a large collection of data to which damping identification methods can be applied.

For this reason, the reliability of damping estimated using the Peak RDT is evaluated based on the mean of individual damping estimates $\hat{\xi}_m$, suggesting that the stochastic application of the damping identification method leads to to more consistent estimates.

Nonetheless, the assessment of the reliability of an *individual* damping estimates can be both relevant and insightful. This involves the use of Bayesian statistics and is discussed in the recommendations for further research (see section 8.3).

5.5. Conclusion

This chapter presents a summary on the findings related to the benchmark case. The reliability of the Peak RDT in estimating damping, when both the system and the excitation satisfy the underlying mathematical assumptions, is investigated in a qualitative manner in section 7.2.2.

Firstly, it is noticed that distribution of damping estimates are Gaussian for the middle amplitude ranges and not Gaussian for the outermost amplitude ranges.

Secondly, Considering the definition of *damping estimates* discussed in section 5.4, the Peak RDT seems to trace the target value of damping properly. The confidence intervals around the mean are wide for the low and high amplitude ranges and narrow for the intermediate amplitude ranges.

A noticeable increase in the spread of damping estimates is observed at both the low and high ends of the relative amplitude range. This results in a U-shaped trend in the variance, which suggests that the variability is not solely due to random noise but may instead be a structural artefact of the estimation method itself. The origins of the U-shaped variance are explored in section 7.1.3. It is important to keep the artefact in mind for the remaining cases considered.

6

System Non Linearity

The first deviation from ideal conditions, examined in this thesis, is the introduction of system non-linearity by the means of amplitude-dependent damping. The effective damping value in the system is thus dependent on the system's displacement amplitude.

In this chapter, the damping identification process outlined in sections 3.6 and 3.7 is applied to N_{sim} displacement response of a system with non-linear viscous damping subjected to zero-mean stationary Gaussian white-noise. The characteristics of the amplitude-dependent damping function are described in section 3.3.3, the nature of the excitation in section 3.4, and the derivation of the displacement response in section 3.5.

The results of the Monte Carlo simulation on the non-linear and stationary case are used to evaluate the performance of the Peak RDT in reliably identifying amplitude-dependent damping, which is precisely the type of behaviour that the method was developed to capture. It is observed that the length of the Random Decrement Signature (RDS) has a significant impact on the reliability of damping estimates. To quantify this effect, a sensitivity analysis is conducted and the sources of error associated with varying RDS lengths are systematically explored in section 6.2.

6.1. Distribution of Damping Estimates

Figures 6.1 and 6.2 are set up the same way as figure 5.4 in section 5.2 and depict the distribution of damping estimates along with two statistical measures, mean and variance. The distribution of individual damping estimates across the normalized amplitude range is shown in figures 6.1.a and 6.2.a, the resulting mean with $\pm 95\%$ confidence intervals (CI) in figures 6.1.b and 6.2.b and the variance in 6.1.c and 6.2.c, respectively.

Both distributions of damping estimates are derived from the same set of displacement responses and the same damping identification methods have been used. The only distinct difference is a different setting in the Peak RDT algorithm, namely the length of the Random Decrement Signatures (RDS).

The length of the RDS is defined in terms of the number of oscillation cycles. The natural frequency of the systems analysed in this thesis is fixed at 0.2 Hz for all cases considered. At this frequency, one oscillation cycle corresponds to a duration of 5 seconds. Accordingly, the RDS lengths used in the estimation of individual damping estimates shown figures 6.2 and 6.1 correspond to 5 seconds and 50 seconds, respectively. These RDS lengths are chosen to present a contrasting result in damping estimates and highlight the effect of settings in damping identification methods.

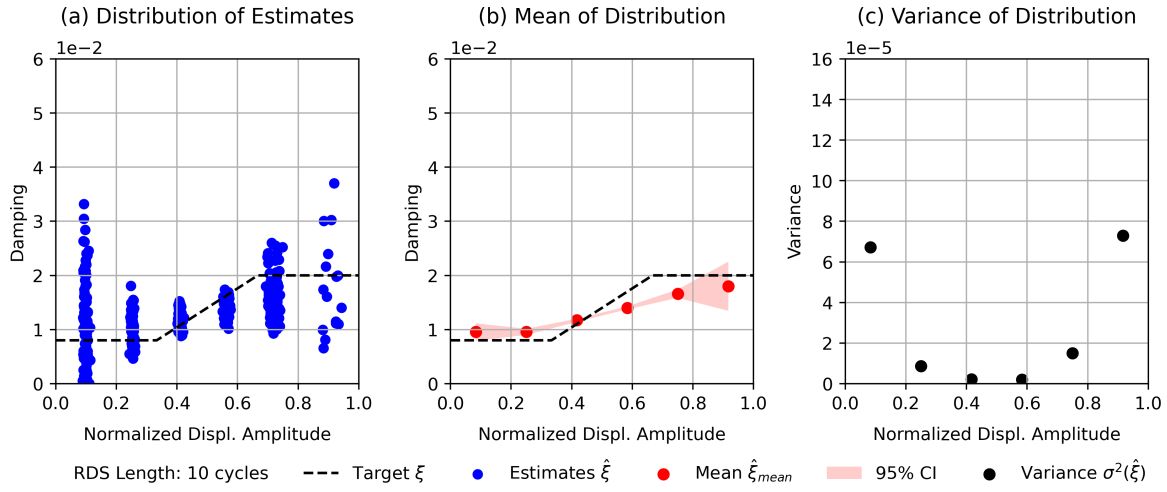

Figure 6.1: Damping Estimates, Non-Linear System & Stationary Excitation
(a) Distribution of Estimates, (b) Mean of Distribution, (c) Variance of Distribution
Settings: RDS Length = 10 cycles, $N_{sim} = 100$, $t = 3600s$, $f_s = 20$ Hz

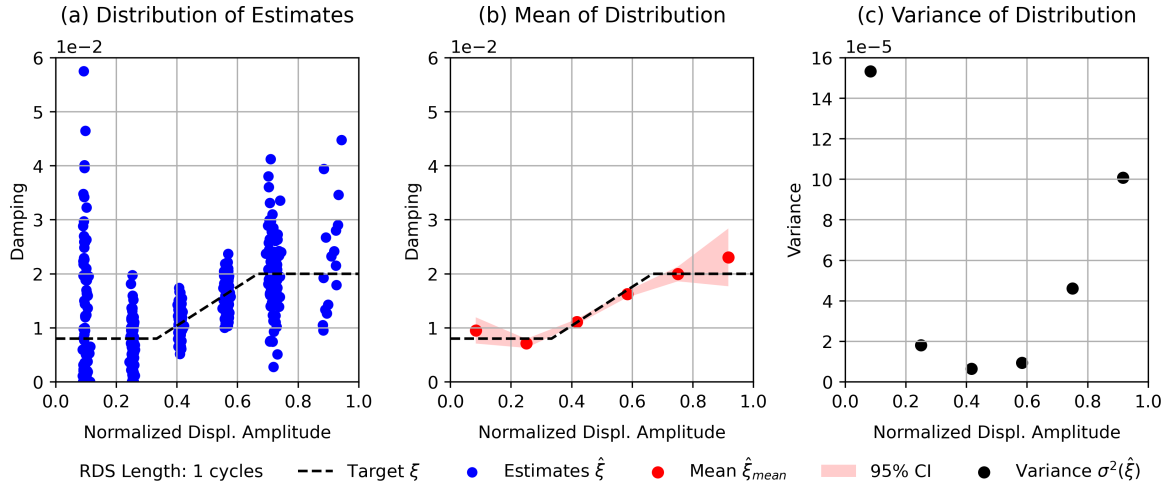

Figure 6.2: Damping Estimates, Non-Linear System & Stationary Excitation
(a) Distribution of Estimates, (b) Mean of Distribution, (c) Variance of Distribution
Settings: RDS Length = 1 cycle, $N_{sim} = 100$, $t = 3600s$, $f_s = 20$ Hz

6.1.1. Observations

This section presents qualitative observations on the distribution of estimates, with a focus on how the distribution of estimates varies with the length of the Random Decrement Signature (RDS).

Mean

The amplitude-dependent damping function, indicated by the black dotted line, is defined by three regions: (1) a low-amplitude plateau, (2) a high-amplitude plateau, and (3) a linearly increasing section in between. Two mean estimates fall within each of these regions. As shown in figure 6.1.b, the mean damping estimates loosely reflect the amplitude dependency of damping across the relative amplitude ranges, as a clear increasing trend is observed with increasing relative displacement amplitude.

Identifying damping using the same settings as for the linear case (10-cycle RDS), reveals that damping is over-estimated in the low-amplitude region and under-estimated in the high-amplitude region. Even though the mean damping values exhibit an increasing trend with increasing relative displacement amplitude, they fail to fully capture the characteristics of the bi-linear input function. While the constant damping in the low-amplitude plateau is mostly reflected, the distinction between the linearly increasing

region and the high-amplitude plateau is not distinguishable.

In contrast, the mean damping depicted in figure 6.2.b, derived with an RDS length of only one oscillation cycle, captures the kinks of the target damping function with more accuracy. Still, the distinction between the linearly increasing region and the high-amplitude plateau remains obscure, as the mean damping continues to increase beyond the defined maximum, indicating a consistent overestimation.

It is also noted that the confidence intervals on the mean damping (CI), given by equations 3.25 and 3.26, show a similar U-shaped pattern for both damping distributions. The confidence intervals (CI) are wider at both low and high relative amplitude ranges and narrower in the middle, indicating greater uncertainty in the estimated damping at the outermost amplitude levels. This behaviour is primarily influenced by the U-shaped variance and the reduced number of samples in the higher relative amplitude ranges, resulting in an especially wide confidence interval. Due to the wider CI, it is more difficult to draw conclusions about the system's amplitude-dependent behaviour in these relative amplitude ranges.

Variance

The benchmark case (see section 5) case revealed that the U-shaped variance is likely an artefact of the damping identification methods used in this thesis, a topic explored in more detail in section 7.1.3. The U-shaped behaviour of the variance can be observed in both figures 6.1.c and 6.2.c, indicating a consistent pattern and reinforcing the claim that higher variance in damping estimates at low and high relative amplitude ranges can, in fact, be attributed to the damping identification method. It's worth investigating whether introducing amplitude-dependent damping amplifies the variance. This is explored further in section 7.2.2.

As seen in figures 6.1.a and6.2.a, What certainly does have an effect on the variance is the length of the RDS chosen in Peak RDT algorithm. The spread in individual damping estimates derived with a 1-cycle RDS (figure 6.2.a) is significantly larger across all relative amplitude ranges compared to the estimates derived using a 10-cycle RDS (figure 6.1.a). The larger spread is, of course, reflected in the variance which seems to have doubled.

6.2. Sensitivity Analysis

Section 6.1.1 highlights significant differences in the distribution of damping estimates obtained using RDS lengths of 1 and 10 cycles. In this section, a sensitivity analysis is conducted by evaluating how different RDS lengths influence the distribution of damping estimates and their statistical metrics.

To assess the influence of RDS length, the damping identification process is carried out for RDS lengths of 1, 3, 5, 7 and 10 oscillation cycles. For each scenario, the distribution of damping estimates is evaluated in terms of the statistical metrics defined in section 3.8.2.

Figures 6.3 and 6.4 show summary statistics of the distribution of damping estimates obtained for different RDS lengths. The relevant metrics are: the mean of damping estimates as well as the $\pm 95\%$ confidence interval on the mean, the variance in the distribution of damping estimates, the bias in the distribution of damping estimates and the relative error computed on the mean damping. For the precise data used in the plots, refer to section B.2.1 in Appendix B.

Precision-Accuracy Trade-off

The sensitivity analysis suggests that there is a trade-off between precision and accuracy in the damping estimates when identifying damping using different RDS lengths. Accuracy describes how close an estimate is to the target value and is typically assessed using the bias. In contrast, precision refers to the consistency of the estimates, as in, how closely they are clustered together. Precisions is typically measured by the variance.

Figure 6.3.a depicts the mean of the distribution of damping estimates as a function of normalized displacement amplitude for multiple RDS lengths. A clear trend that emerges is that, with increasing RDS length, the mean damping seems to flatten out. This indicates a loss of sensitivity to displacement amplitude, meaning that with increasing RDS length, the low-amplitude plateau is increasingly over-estimated and the high-amplitude plateau is increasingly underestimated. This general trend is

also reflected in figure 6.4.a in the computed bias. The loss of sensitivity of the damping estimate to displacement amplitude, when computed using a longer RDS, is a clear indication that the damping is being influenced by contributions from other amplitude ranges. The RDS captures damping behaviour not only at the amplitude of interest but also from segments associated with higher or lower damping values.

Figure 6.3.c shows a clear reduction in variance for increasing RDS length. Although qualitatively, the U-shaped variance remains, the value of variance tends to decrease. The reduction in variance is most pronounced when increasing the RDS length from 1 to 3 cycles, after which it appears to stabilize. The decrease in variance, for increasing RDS lengths, is also reflected in the $\pm 95\%$ confidence intervals (CI). In fact, the CI become progressively narrower as the RDS length increases. The narrowing of CI also seems to stabilize after a length of 4 cycles.

It is important to note that these observations hold generally, although some exceptions occur at the outermost relative amplitude ranges, since these are accompanied with the largest uncertainty as indicated by the widest confidence intervals.

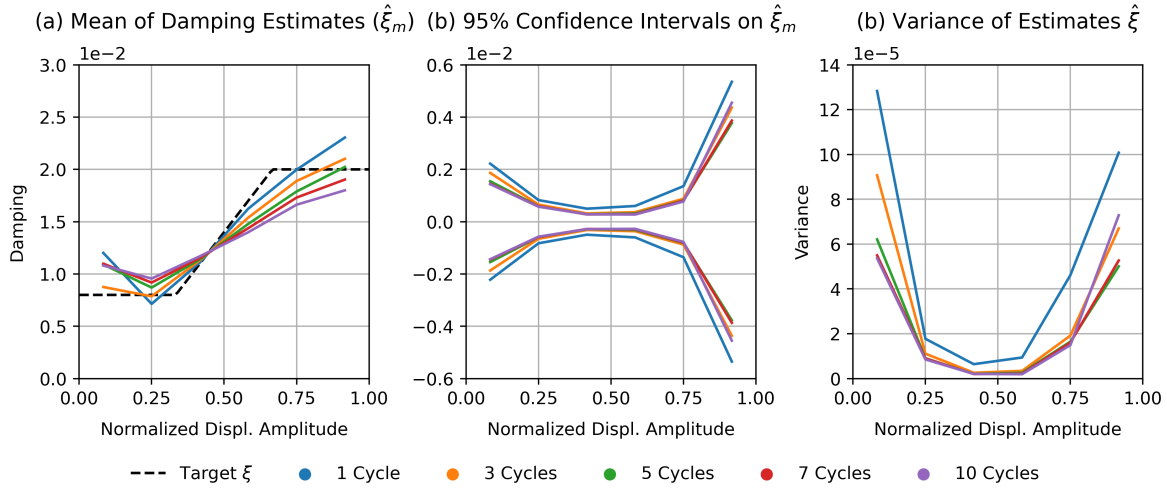

Figure 6.3: Sensitivity Analysis - RDS Length; (a) Mean of Damping Estimates; (b) $\pm 95\%$ Confidence Intervals on Mean; (c) Variance of Estimates

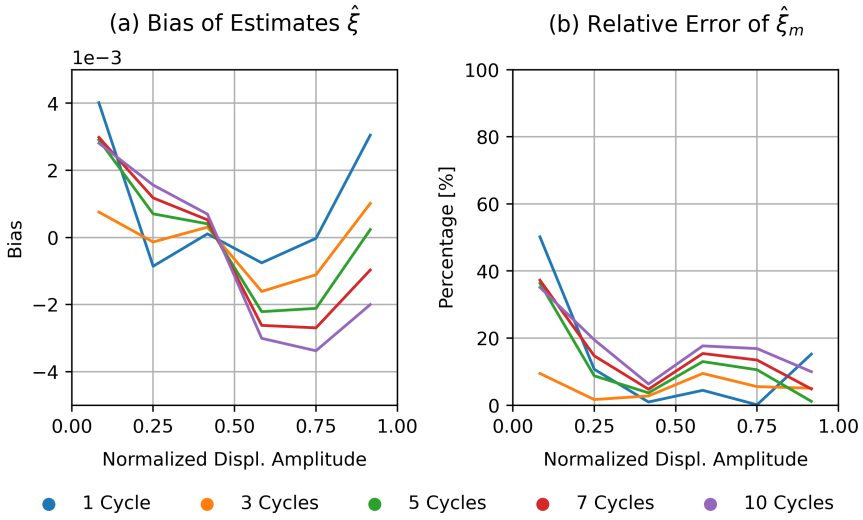

Figure 6.4: Sensitivity Analysis - RDS Length; (a) Bias of Damping Estimates; (b) Relative Error on Mean Estimate

”Optimal” RDS Length

Given the observed trade-off between precision and accuracy, it is natural to consider what the ”optimal” RDS length might be for reliably capturing the amplitude dependency of damping. While this sensitivity analysis certainly provides insights, it is not possible to provide quantitative recommendations on optimal RDS length with sufficient certitude. The discussion is further informed by considering two more key factors.

Firstly, given the discussion on the definition of *damping estimates*, it is concluded that damping identification methods should be applied stochastically rather than deterministically. As a result, less emphasis is placed on the precision of individual estimates while the accuracy of the mean estimate becomes more important. The influence of precision is, of course, still reflected in the width of the confidence intervals surrounding the mean damping. Therefore, settings that yield an accurate mean damping estimate rather than precise individual estimates should be chosen.

Secondly, figure 6.4.b depicts the relative error on the mean damping. The way the relative error is computed is explained in section 3.8.2. As seen in figure 6.4.b, the RDS length that minimizes the relative error varies across different relative amplitude ranges. For normalized displacement amplitudes up to around 30%, the mean damping derived with the 3-cycle RDS consistently shows the lowest relative error, starting below 10% and decreasing further to 2%. For amplitudes between 30% and approximately 85%, the mean damping derived with the 1-cycle RDS demonstrates the lowest relative error, consistently remaining under 5%. Due to large uncertainties in the highest amplitude range, no statement is made regarding the RDS length for this range. However, this demonstrates that different RDS lengths are better suited for capturing the amplitude dependency across different amplitude ranges. In particular, regarding the high-amplitude plateau, using a shorter RDS length is important because most points in the displacement response correspond to lower amplitudes, perturbing the RDS.

6.2.1. Effect of Segment Length

While the section 6.2 summarizes the main findings of the sensitivity analysis, this section focuses on explaining the underlying phenomenon and discussing the implications of segment length on the Random Decrement Signatures (RDS) when the system considered exhibits amplitude-dependent damping.

The concept of the Peak RDT, as outlined in section 2.5.2, is to classify local maxima of the displacement response into distinct amplitude ranges based on their magnitude. Based on these identified trigger points, segments of predefined length are sampled from the displacement response. All segments corresponding to the same amplitude range are then averaged, resulting in a set of Random Decrement Signatures (RDS). Each RDS subsequently yields a single damping estimate representative of a specific amplitude range. By basing the sampling on local maxima, the Peak RDT aims to capture amplitude-dependent damping behaviour. This is because the damping value at a particular amplitude is related to the area enclosed by the hysteresis loop (force-displacement field) during one oscillation of the structure at that specific amplitude.

It becomes clear that longer segment lengths are problematic as they can include system responses from different amplitude levels, and associated with different damping values, within the same signature. When sampled segments reflect the dynamic behaviour of the system at an amplitude range *other* than the range of interest, the resulting RDS becomes contaminated by contributions from multiple damping values. This leads to an RDS that is not truly representative of the system characteristics it is intended to capture.

When the segment length is too long, the RDS no longer reflects the dynamic behaviour associated with the initial conditions of a specific amplitude range. While this is not problematic for linear systems, where damping remains constant across all amplitudes, it becomes a significant issue in the amplitude-dependent case. This implies that, when applying the Peak RDT to systems with amplitude-dependent damping, sampling must be handled with particular care. The flexibility in selecting segment lengths is significantly limited to ensure that the resulting RDS retains physically meaningful information.

6.2.2. Visualization

To visualize the effects of segment length on the behaviour of the RDS and the accuracy of damping estimates, the decay over the entire RDS is analysed. The distortion of the RDS by damping values corresponding to other amplitudes, becomes evident when comparing the approximated free decay (RDS) with the theoretical free decay for the linear and non-linear cases. For this purpose, a mean signature, representative of the mean damping estimate, is derived according to method B. This procedure, outlined in section 3.8.1, is nearly equivalent to estimating damping using a single response signal N_{sim} hours long and can therefore provide more general insights compared to the RDS computed using 1 hour response data.

For the scope of this analysis, the RDS corresponding to two different mean damping estimates are considered in order to derive meaningful conclusions. These points are selected to examine the damping behaviour at the low- and high-amplitude plateaus of the amplitude-dependent case. As seen in figure, 6.1.b, these regions are particularly affected by interference from other amplitude ranges. Given the large uncertainty in the outermost relative amplitude ranges, the second and second-to-last mean damping values are used instead. These are referred to as Points A and B and are illustrated in figure 6.5.

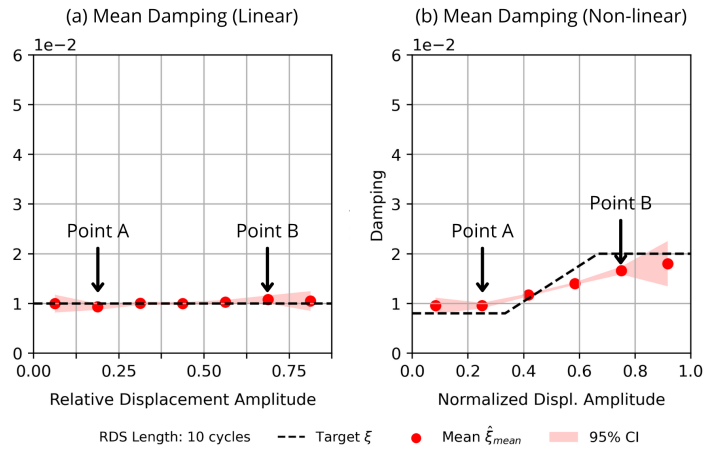

Figure 6.5: Mean damping obtained from response of (a) the linear system and (b) the non-linear system
Settings: RDS Length = 100, $N_{sim} = 100$, $t = 3600s$, $f_s = 20Hz$

Figures 6.6 and 6.7 are structured in the same way. The left side presents results for the linear case, while the right side corresponds to the non-linear case. Sub-figures a. and b. show the computed mean RDS (red line) along with the free decay obtained by plugging the mean damping estimate in the free decay formulated in equation 3.14 (grey line). The RDS is shown in full length (10 cycles) to provide a complete view of the decay. In the remaining sub-figures, the decay behaviour over the complete length of the RDS is examined using the logarithmic decrement (LD) method. Sub-figures c. and d. show the damping estimates corresponding to the 10-cycle RDS, while .e and .f present the 3-cycle RDS. As explained in section 2.3.1, the logarithmic decrement quantifies the rate of decay between two successive peaks in the free decay response. Therefore, the estimated damping depends entirely on the specific pair of peaks analysed, rather than being derived from curve fitting. The value of the decay in terms of damping is illustrated using the red dots. Each value plotted at cycle n captures the decay occurring between the peak at cycle $n-1$ and the peak at n. Additionally, the target value of the damping in that relative amplitude range is indicated by the black dotted line. The grey dotted line represents the estimated mean damping value and its associated $\pm 10\%$ range. The $\pm 10\%$ margin on the mean damping is incorporated to account for potential discrepancies introduced by the LD method.

Table B.5 summarizes the target and mean damping values for all cases considered in this section. The damping estimates obtained through the LD method are compared to the mean damping value in tables B.3 and B.4.

Three aspects are considered for assessment:

1. A close alignment between the mean RDS and the theoretical free decay indicates that the approximated free decay provides a reliable representation of the true dynamic response.
2. A close agreement between the target damping and the mean damping suggests that the mean damping serves as a reliable estimator of the true damping behaviour.
3. The confinement of damping values, estimated using the LD method, within a ±10% range of the mean estimate indicates that the decay behaviour in the RDS is uniformly consistent with the damping obtained through curve fitting.

Point A

In the linear case, shown in figure 6.6.a, the RDS and the free decay response are aligned, indicating that the RDS effectively captures the expected free decay behaviour. In the non-linear case, depicted in figure 6.6.b, the RDS and the free decay response initially align closely, suggesting a good approximation during the early stages of decay. However, a small discrepancy becomes noticeable after the fifth cycle. The rate of decay in the RDS then remains steeper compared to the exponential decay of the free decay curve, highlighting a divergence in the behaviour of the decay during the later cycles.

For the linear case, the mean damping estimate (grey dotted line), obtained from the 10-cycle RDS, closely matches the target value (black dotted line), overestimating it by only 2% (table B.5). The mean damping derived from the 10-cycle RDS is, in fact, more accurate than the one from the 3-cycle RDS, which underestimates the target by 8%. This is consistent with the fact that the LSM performs better when more data points are available for fitting, as long as the system is linear. Moreover, as seen in sub-figures .c and .e, it is observed that all but one of the LD damping estimates (red dots) lie within $\pm 10\%$ of the mean damping obtained through curve fitting. This indicates that the decay along the RDS is relatively uniform and aligns well with the curve-fitted damping value.

In contrast, for the non-linear case, the mean damping estimate from the 10-cycle RDS deviates significantly from the target, overestimating it by 20%, whereas the estimate from the 3-cycle RDS underestimates the target by only 2% (see table B.5). This shows that the application of the LSM leads to a fundamentally different results for the linear and non-linear case. This improved mean damping is due to the shorter RDS, which avoids capturing the dynamic behaviour further away from the point and amplitude of interest. Since the damping is amplitude-dependent, including responses from different amplitude ranges can introduce interference in the RDS construction. By limiting the segment length, the influence of such responses, associated with different damping characteristics, is reduced. As a result, the RDS more accurately reflects the target behaviour.

Furthermore, as seen in figure 6.6.d, almost none of the LD damping estimates (red dots) fall within $\pm 10\%$ of the mean damping value obtained through curve fitting, indicating that the decay along the RDS is not uniform and not consistent with the damping value obtained from curve fitting. The value of the LD estimates increase steadily with each cycle, eventually stabilizing at approximately 1.1% (see table B.3).

It is relevant to mention that, according to the principles of the Peak RDT and the fact that it links the behaviour of the first oscillation cycle to the hysteresis loop, and therefore, to the damping, the decay in the first cycle should theoretically provide an accurate damping estimate. However, as seen in figure 6.6.d, the LD damping estimate at the first cycle underestimates the truth by almost 20%. This discrepancy could be linked to shortcomings of the logarithmic decrement method and the consideration of the specific peaks of RDS that should be used when estimating damping [64]. These shortcomings however, are not further discussed in this thesis.

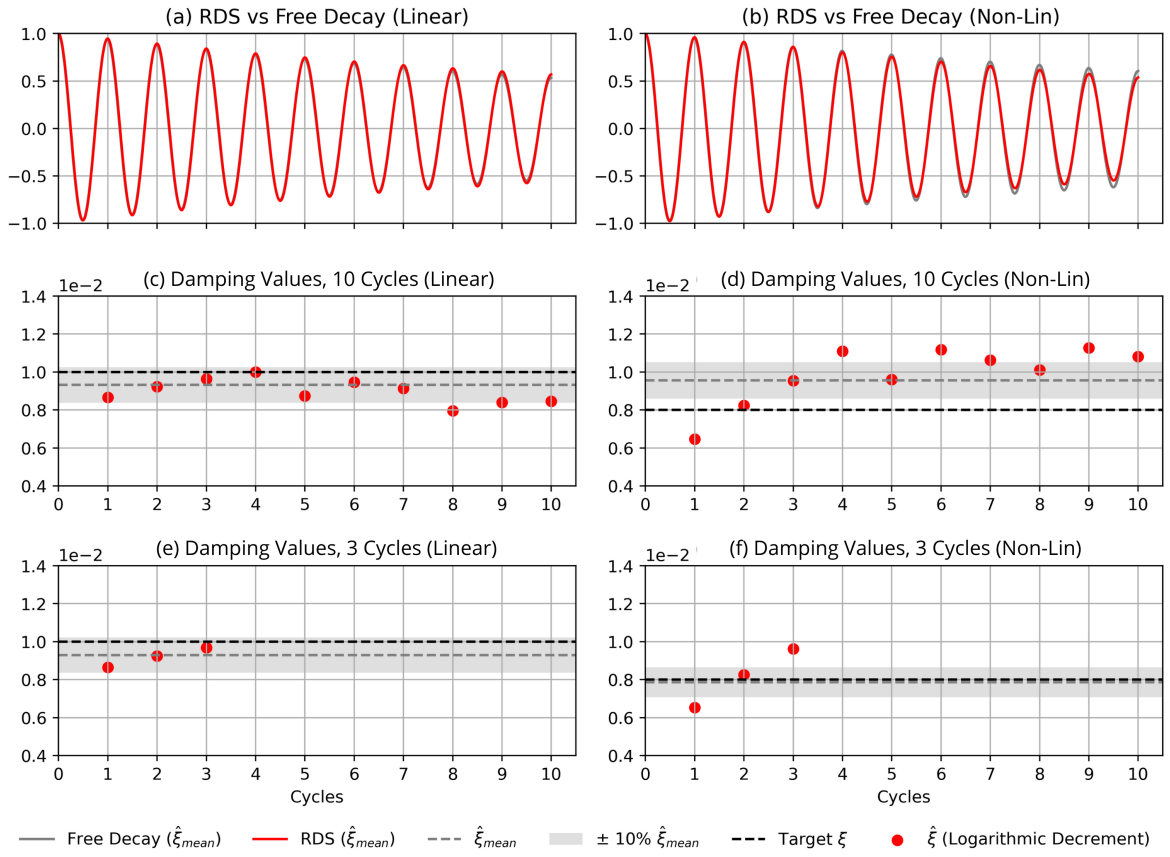

Figure 6.6: Influence of segment length, Point A, comparison of linear (left) and non-linear (right) cases, (a) & (b) Mean RDS vs Free Decay, (c) & (d) Damping Values (10 Cycles), (e) & (f) Damping Values (3 Cycles)
Settings: RDS Length = 100, $N_{sim} = 100$, $t = 3600s$, $f_s = 20Hz$

Point B

For the linear case, the observations remain consistent with those discussed previously regarding point A. Figure 6.7.a shows that the RDS and the free decay computed using the mean damping estimate are completely aligned meaning that the RDS is an accurate approximation of the free decay. This is further supported by the fact that the mean estimate closely aligns with the target value in figure 6.7.c. In fact, the mean damping overestimates the target by only 2% (see table B.5). Moreover, all LD estimates fall within $\pm 10\%$ of the mean damping value obtained from curve fitting, demonstrating that the decay in the RDS is uniform and corresponds to the value obtained from curve fitting.

Regarding the non-linear case, in the earlier analysis of Point A, the RDS exhibited an increased rate of decay relative to the exponential decay of the free decay curve. Figure 6.7.a shows that the RDS decays more slowly than the free decay, once again suggesting that the RDS is not a reliable approximation of the theoretical free decay if the damping is amplitude-dependent.

Moreover, the mean damping estimate deviates significantly from the target value, underestimating the target by 16% and indicating that the damping value obtained through curve fitting on the 10-cycle RDS is not accurate. This discrepancy highlights the limitations of using longer RDS segments in non-linear cases, where amplitude-dependent damping becomes more influential. In contrast, the mean damping corresponding to the 3-cycle RDS underestimates the target by only 5% (see table B.5).

In figure 6.7.d, a clear reduction in LD damping estimates is observed from one peak to the next, throughout the entire RDS. This non-uniform decay pattern emphasizes that, as the RDS length increases, the influence of amplitude-dependent non-linearity becomes more pronounced, resulting in a less accurate representation of the true damping behaviour. Notably, only the first LD estimate lies in close proximity to the target damping value (see table B.4), supporting the earlier statement regarding

the Peak RDT concept and its connection to the hysteresis loop, where the damping is expected to reflect the system's behaviour during the first oscillation cycle.

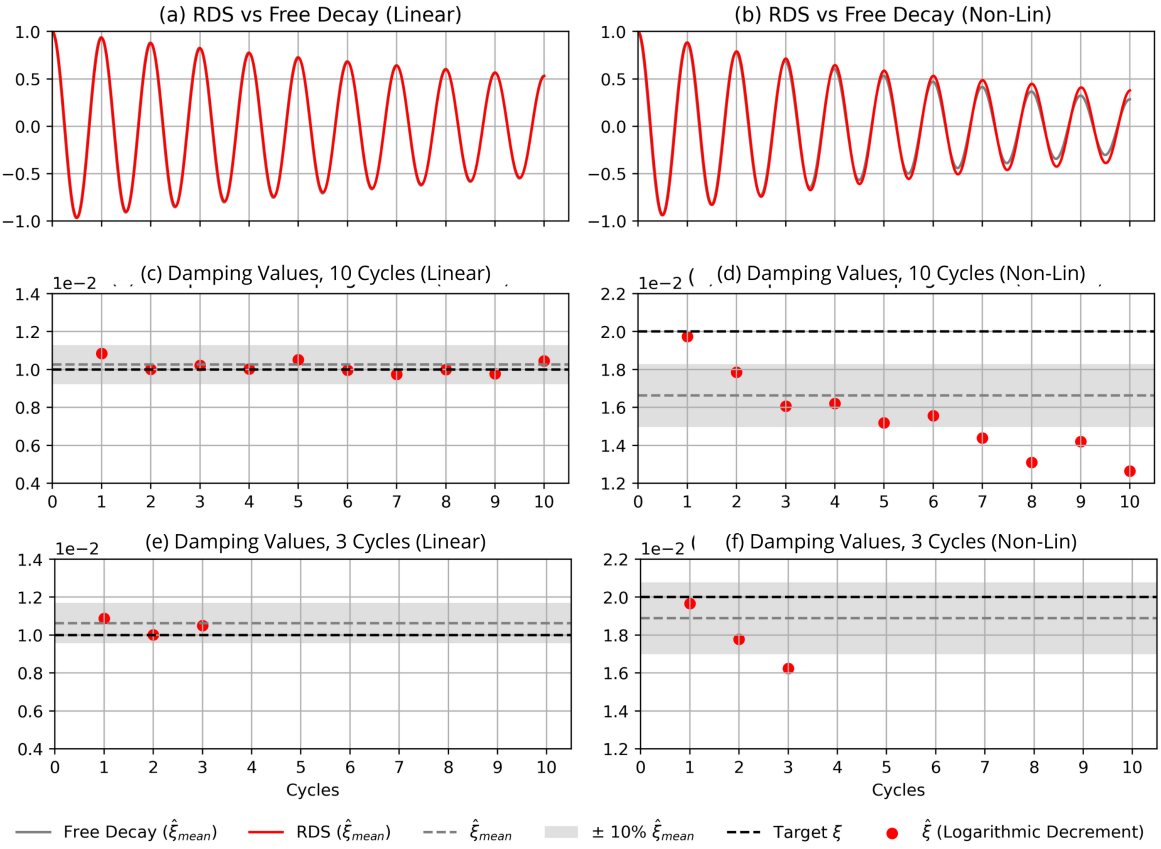

Figure 6.7: Influence of segment length point B, comparison of linear (left) and non-linear (right) cases, .a & .b Mean RDS vs Free Decay, .c & .d Damping Values (10 Cycles), .e & .f Damping Values (3 Cycles)

6.3. Conclusion

This chapter has examined the application of the Peak RDT to the displacement response of systems characterized by amplitude-dependent damping in the form to Jeary's model (see section 3.3.3).

It was observed that a precision-accuracy trade-off exists in the damping estimates obtained using different RDS lengths in the Peak RDT algorithm. As the RDS length increases, the damping estimates become more precise but less accurate. Conversely, shorter RDS lengths yield more accurate but less precise damping estimates. For all RDS lengths considered, the damping identification methods used in this study struggle to accurately detect the kink in the amplitude-dependent damping function, particularly in the transition between the linearly increasing portion and the high-amplitude plateau.

Moreover, the sensitivity analysis shows that the RDS length, which minimizes the relative error in mean damping estimate, varies across amplitude ranges. While in the lower relative amplitude ranges (0 - 0.3), the 3-cycle RDS yields the most accurate mean damping estimate (consistently under 10%), in the higher relative amplitude ranges (0.3 - 0.85), a shorter RDS length of 1 cycle yields the most accurate damping estimate (consistently under 5%).

To capture the variation in damping with respect to amplitude, the Peak RDT effectively linearizes the system within specified amplitude ranges by creating a set of signatures approximating the behaviour of a linearized system. The RDS serves as the basis for applying modal parameter identification methods and estimating the system's modal parameters. However, Tamura and Suganuma, who first introduced the Peak RDT [20], warn that the RDS resulting from this process are not a free decay of the linear

system with corresponding damping ratio. Nonetheless, to estimate modal parameters, Tamura and Suganuma [20], fit the equation of the linear system's free decay (equation 3.14) to the RDS using least squares minimization. The LSM derives the system's modal parameters by curve fitting the theoretical equation of the free decay to the approximated free decay. This approach yields in one deterministic damping estimate per RDS.

A detailed examination of the signatures generated by applying the Peak RDT to the displacement response of a system with amplitude-dependent damping supports the assertion made by Tamura and Suganuma [20]. The RDS, produced in the non-linear case, exhibit a non-uniform decay across the signature. This indicates that the decay in the RDS is itself non-linear, questioning the validity of modal parameter methods based on estimating a constant damping value.

Estimating modal parameters by curve-fitting the theoretical free decay of a linear system to an RDS exhibiting non-linear damping introduces errors, especially when the RDS length is long, as this captures dynamic behaviour across multiple amplitude ranges with varying damping. The errors can be mitigated by reducing the RDS length to ensure that the decay in the resulting RDS is more representative of the damping in the amplitude range of interest.

When segments extend beyond their intended range, the RDS becomes contaminated by data from other amplitude levels, effectively distorting the signatures and reducing the reliability of damping estimates. The computation of the RDS based on longer segments pollutes the RDS with different damping values, making it difficult to extract the correct damping value at a specific amplitude. Using too long RDS effectively ”kills” the non-linearity as the numerous amplitude contributions blend together, resulting in an averaged-out damping effect.

This raises the question of whether curve fitting should instead be based on the free decay of a system with amplitude-dependent damping rather than assuming a constant damping. This is discussed in section 8.3.

7

Performance Assessment

This chapter defines and quantifies performance metrics used to assess the reliability of damping estimates derived using the Peak RDT under non-ideal conditions, and thus directly meets the second research objective outlined in section 1.3.

As explained in section 3.2, the Peak RDT does not directly produce damping estimates, rather, it approximates the system's free vibration response. Subsequently, damping is estimated using non-linear Least Squares Minimization (LSM) and fitting the theoretical free vibration response of a linear system to the approximated free decay. The combination of Peak RDT and LSM constitutes the damping identification method.

The performance of the aforementioned damping identification method can therefore be evaluated on three levels: (1) the quality of the Random Decrement Signatures, which are used as input for damping identification, (2) the reliability of the resulting damping estimates, and (3) the usefulness of the damping identification method with respect to a predictive metric for comfort assessment. These three levels are addressed separately in sections 7.1, 7.2 and 7.3.

7.1. Quality of Random Decrement Signatures

The reliability of damping estimates fundamentally depends on the quality of the computed Random Decrement Signatures (RDS). A damping estimate is reliable only if the RDS accurately represents the system's free vibration response. Understanding the factors that influence the RDS' quality provides critical insight into the algorithm's limitations.

An apparent limitation of the Peak RDT is highlighted in section 5.3. In fact, damping estimates show significantly higher variance in low and high amplitudes ranges compared to moderate levels. Common criteria for high-quality RDS are presented in section 7.1.1 and evaluated in section 7.1.2. Finally, section 7.1.3 presents an explanation for observed U-shaped variance in damping estimates.

7.1.1. Criteria

The system's free decay is approximated using the Random Decrement Signatures (RDS), obtained through ensemble averaging of time-shifted segments sampled according to a common trigger condition, as described in section 2.5.2.

Segment Count

Literature generally states that obtaining a high-quality RDS requires ensemble averaging over a *sufficient* number of segments to effectively cancel out the forcing component, which is assumed to have zero mean. The exact number of segments needed is case-specific and depends on factors such as the signal-to-noise ratio, the damping level or excitation characteristics. Consequently, a single number guaranteeing high-quality signatures cannot be established.

Furthermore, the Peak RDT algorithm divides the total amount of identified trigger points into multiple

amplitude ranges which reduces the amount of segments available for the computation of one RDS, compared to the traditional RDT. To investigate the reason behind the U-shaped variance observed in the distribution of damping estimates (figure 5.4.c), the amount of segments used in the computation of each signature is investigated.

As shown in figure 3.8.a (Method A), each of the N_r damping estimates within each amplitude range is obtained from a single RDS. The number of segments used to compute each of the N_r signatures, is represented by box plots in figure 7.1.b. Each box plot illustrates the distribution of segment count N_s: the whiskers indicate the full range, the box contains the central 50% of the data, and the black line within each box marks the mean value. For example, figure 7.1.b shows that, in the lowest amplitude range, one RDS is on average computed using approximately 120 sampled segments.

Strict Decay

Additionally, visual inspection is often recommended in literature to ensure that the RDS is smooth and exhibits a clear exponential decay. While a lack of smoothness may indicate that the number of segments is insufficient, the presence of a strict decay is particularly emphasized when dealing with closely spaced modes. Nonetheless, a strict decay remains desirable even in systems dominated by a single vibration mode.

Since the theoretical free decay of a linear under-damped system follows an exponentially decaying sinusoid, the RDS is also expected to exhibit a strict decay from one peak to the next. Thus, each peak of the RDS should be lower than the preceding one, indicating a decreasing amplitude with each oscillation cycle.

To test whether the RDS are strictly decaying, a Python function is implemented. The function returns a boolean, `True` or `False`, and qualitatively assesses whether each peak in the RDS is strictly lower than the previous one. Each of the RDS producing one damping estimate in figure 5.4.a is evaluated for strict decay. The results are presented in figure 7.1.a as the percentage of RDS that are strictly decaying (in orange), respectively not strictly decaying (in grey). For example, only 2% of the N_r signatures in the lowest amplitude range exhibit a strict decay.

7.1.2. Evaluation

Figure 7.1 presents the evaluation of the Random Decrement Signatures. The two metrics explained in sections 7.1.1 are compared with the variance observed in the distribution of damping estimates, in an effort to explain the U-shaped variance observed in the distribution damping estimates for the benchmark case.

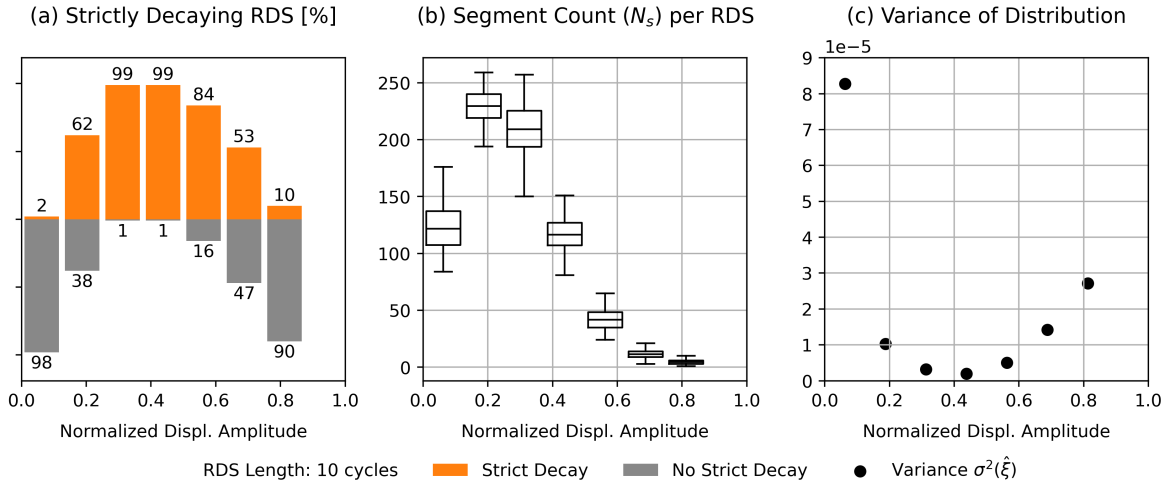

Figure 7.1: Evaluation of Random Decrement Signatures using two criteria (benchmark case);(a) Percentage of strictly decaying RDS, (b) Segments count per RDS, (c) Variance in distribution of damping estimates
Settings: RDS Length = 10 cycles, $N_{sim} = 100$, $t = 3600s$, $f_s = 20Hz$

As shown in figure 7.1.b, the average number of segments used to compute a single RDS exceeds 120 for relative amplitude ranges 0% to 50%, while it drops below 50 for ranges 50% to 100%. Interestingly, despite the first and fourth amplitude ranges having comparable segment counts, the variance in the corresponding damping distributions differs significantly with 8.28×10^{-5} in the first amplitude range compared to 0.20×10^{-5} in the fourth amplitude range (see table B.6). This indicates that a high segment count alone does not guarantee precise damping estimates. When examining the percentage of strictly decaying RDS, only 2% of the signatures in the first relative amplitude range satisfy this criterion, compared to 99% in the fourth range. This indicates that the strictness of decay in the RDS is a strong indicator of the precision of the corresponding damping estimates.

Additionally, the distribution of damping estimates in relative amplitude range 20% to 60% exhibits a variance lower than 1×10^{-5}. While the average segment count in this amplitude range varies significantly, with differences exceeding 150 segments, the RDS produced within this relative amplitude range exhibit the highest percentage of strictly decaying signatures (between 84% and 99%). This observation reinforces the idea that the strictness of decay may serve as a more reliable indicator of quality than the segment count alone.

The analysis of figure 7.1 implies that Random Decrement Signatures, at both low and high relative amplitude ranges do not to accurately capture the system's underlying physical behaviour. An important distinction can be made between the causes at low and high amplitude ranges.

The signatures corresponding to relative amplitude range 60% to 100% are computed using very few segments (fewer than 20). This likely prevents sufficient averaging and hence, the forcing component assumed to be zero-mean, cannot be cancelled out. The signatures in the higher relative amplitude ranges are thus a poor approximation of the system's free vibration response. In contrast, the signatures in the low amplitude range (0% to 15%) contain a sufficient number of segments, suggesting that the issue lies not in the quantity but in the quality of the segments themselves. To investigate this further, the characteristics of the segments composing the RDS are examined.

7.1.3. Segment Inspection

When assessing the quality of Random Decrement Signatures (RDS), it is crucial to understand the influence of sampled segments as they form the basis of the resulting signature. Section 7.1.1 shows that segment count alone is not a sufficient indicator of a high-quality RDS.

In an attempt to explain the difference in variance across amplitude ranges, the exact computation of the RDS across these ranges is examined. In this section, two situations are compared. Firstly, the computation of three different signatures within one amplitude range are compared. Secondly, the computation of three different signatures of different amplitude ranges are compared.

Comparison within one Amplitude Range

The first set of signatures, shown in figure 7.2, corresponds to the lowest amplitude range (0% to 12.5%), where the highest variance in damping estimates is observed (see figure 5.4.c). The high variance in estimates suggests that the signatures do not capture the underlying system behaviour and fail to approximate a clear free decay, which results in considerable fluctuation in the corresponding damping estimates.

Figure 7.2.a corresponds to the highest damping estimate in that range, with a value of 0.055, figure 7.2.b corresponds to an accurate estimate, with a value of 0.010 and figure 7.2.c corresponds to the lowest damping estimate at a value of 0.000. The blue lines depict the individual segments sampled by the algorithm, and the red line represents their average, the unnormalized Random Decrement Signature.

The first observation is that none of the three signatures in figure 7.2 exhibit strict decay. This is unsurprising since figure 7.1.a shows that signatures in this amplitude range typically do not exhibit a strict decay, indicating a deviation from the theoretical free vibration response.

Furthermore, as can ben seen in figure 7.2, the sampled segments corresponding to the three signatures are quite tumultuous. The individual segments do not consistently reflect the same decay behaviour as they align only during the first or second cycle before diverging. In figure 7.2.a, the seg-

ments quickly average out leading to an overestimation of damping while in figure 7.2.c, the amplitude of each peak increases at each oscillation cycle. Since, this cannot be explained by a positive damping ratio it results in a damping estimate of 0.000.

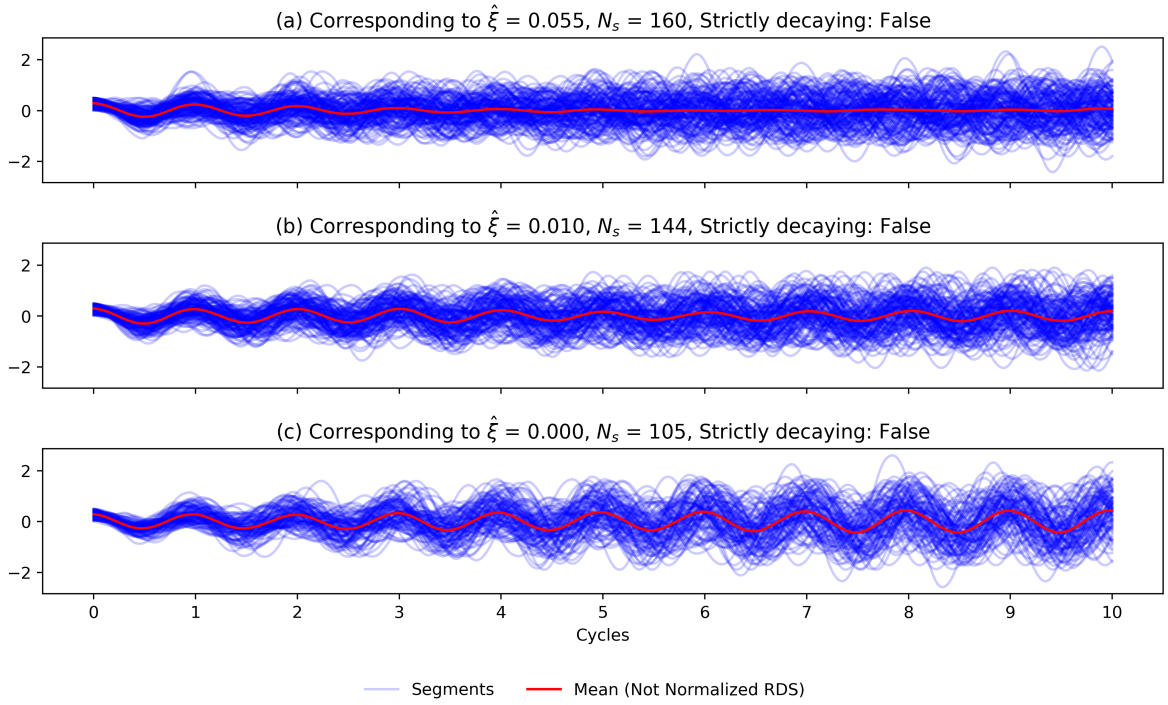

Figure 7.2: Set of three RDS corresponding to amplitude range 0% to 12.5% (benchmark case);(a) Damping estimate $\hat{\xi} = 0.055$; (b) Damping estimate $\hat{\xi} = 0.010$; (c) Damping estimate $\hat{\xi} = 0.000$
Settings: RDS Length = 10 cycles, $t = 3600s$, $f_s = 20Hz$

Comparison across three Amplitude Ranges

Figure 7.3 shows the signatures corresponding to three accurate damping estimates at a value of 0.01. The three amplitude ranges considered are 0% to 12.5%, 37.5% to 50% and 62.5% to 75% respectively. While, figure 7.3.a and 7.3.c correspond to an amplitude range displaying a high variance of 8.28×10^{-5} respectively 1.43×10^{-5}, figure 7.3.b corresponds to a range where a low variance of 0.20×10^{-5} is observed (see table B.6).

A striking difference is visible in the sampled segments between the three signatures produced in different amplitude ranges. Figure 7.3.a displays segments with significant variability. They are not properly conveying the free decay information. In contrast, figures 7.3.b and 7.3.c display segments that consistently reflect a similar free decay behaviour. While the information is most reliable during the first couple of cycles, before the segments begin to diverge slightly, the main trend remains clear, resulting in a good approximation of the free decay. The very few segments in the computation of the RDS in figure 7.3.c also support the fact that the number of segments is less relevant if the segments properly convey the free decay information.

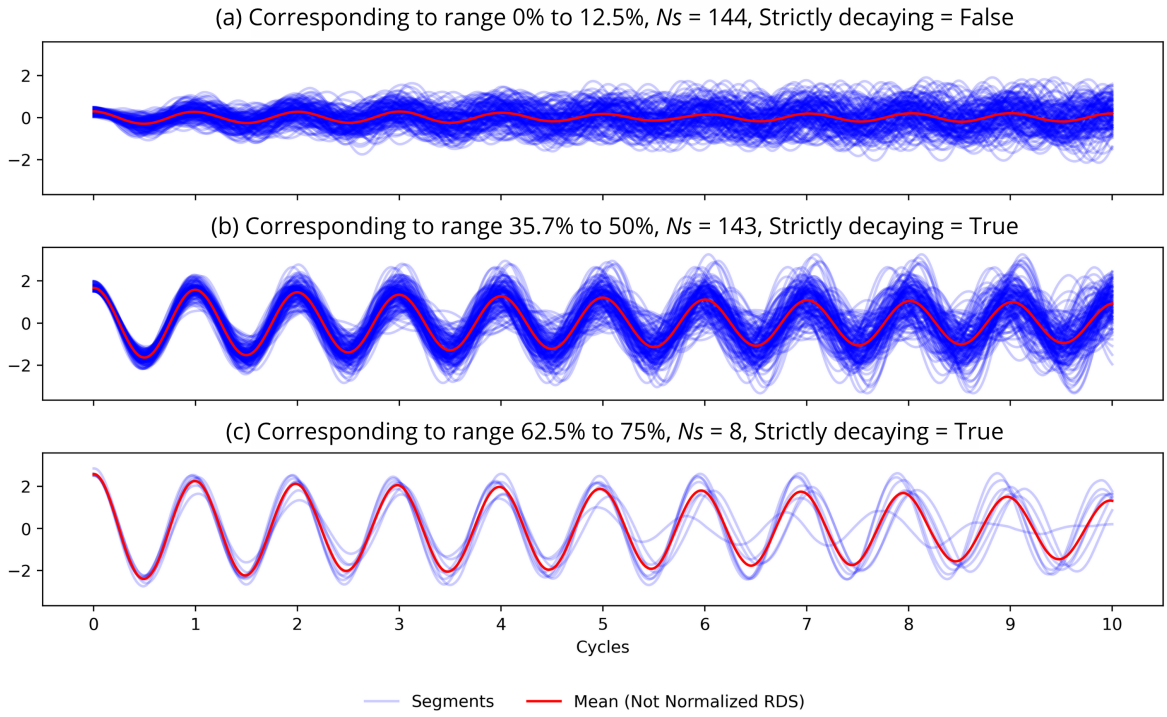

Figure 7.3: Set of three RDS corresponding to damping estimate $\hat{\xi} = 0.010$ for different amplitude ranges (benchmark case);(a) Range 0% to 12.5% ; (b) Range 35.7% to 50%; (c) Range 62.5% to 75%
Settings: RDS Length = 10 cycles, $t = 3600s$, $f_s = 20Hz$

7.1.4. Conclusion

The reliability of damping estimates relies on the quality of the Random Decrement Signatures (RDS) produced by the Peak RDT algorithm. While a sufficient segment count is commonly cited as essential for averaging out the forcing component and isolating the free vibration response, section 7.1.2 highlights that a high segment count is not a sufficient indicator for high-quality signatures derived using the Peak RDT. Visual inspection or qualitative assessment, such as evaluating whether the signatures exhibit a strict decay, can provide a better insight into their quality.

While signatures at low and high relative amplitude ranges do not tend to exhibit a strict decay, those at moderate amplitude ranges typically do. This trend is reflected in the U-shaped variance of damping estimates. Estimates at low and high relative amplitudes show significantly higher variance compared to moderate relative amplitudes. This indicates that signatures at moderate relative amplitude ranges exhibit a more consistent behaviour and shape, striking a good balance between significant and sufficient segments, leading to more precise damping estimates. Therefore, sampling a *sufficient* number of *significant* segments is crucial for obtaining reliable damping estimates.

The U-shaped variance described in section 5.3 is thus a direct result of the Peak RDT. At low relative amplitude ranges, variance is high because the segments are sampled at low response levels, resulting in significant variability in Random Decrement Signatures and a large spread in damping estimates. In fact, using the traditional RDT, low-amplitude trigger points are consciously left out. While this is predominantly due to the presence of measurement noise, which negatively affects the reliability of damping estimates, this thesis demonstrates that another issue at low amplitudes is that the impulse is not significant enough. The sampled segments need to convey the free decay information for a sufficiently long time which usually requires a significantly large impulse.

In contrast, at high-amplitude levels, the sampled segments do convey free decay information. However, since there are so few segments, the forcing component assumed to be zero-mean, is not properly averaged out which introduces errors. Although not investigated in this study, the spread of damping estimates could be reduced with longer response data as this would allow more segments to be sampled.

7.2. Reliability of Damping Estimates

Chapter 1.1 highlights the importance of comfort assessment in the design of high-rise buildings. Occupant comfort is assessed based on peak acceleration, which is strongly influenced by the assumed damping value. Since reliable damping estimates play a crucial role in producing accurate assessments of occupant comfort, it is logical to relate the reliability of damping estimates to this comfort metric. Section 7.2.1 explores the relationship between peak acceleration and damping, establishing a threshold within which damping estimates can be considered reliable.

Subsequently, the reliability of damping estimates is investigated in terms of accuracy and precision, relative to the reliability threshold. While accuracy describes how close an estimate is to its target value, precision indicates how repeatable an estimate is. Assessing both accuracy and precision of estimates is essential for evaluating their reliability and trustworthiness. Sections 7.2.2, 7.2.3, 7.2.4 and 7.2.5 present a quantitative assessment of the reliability of damping estimates corresponding to the systems with constant and amplitude dependent damping excited by the four different loading conditions considered in this thesis (see section 3.4).

7.2.1. Threshold

Appendix A lists the equations used to compute peak acceleration according to appendix C of EN 1991-1-4 [10]. Assuming that all parameters, such as modal mass or the excitation's frequency content, remain constant, then the direct relationship between the peak acceleration and the damping ratio is given by equation 7.1. From the inverse square-root relationship, it can be inferred that an error of $\pm 10\%$ in the damping value leads to an approximate $\pm 5\%$ variation in the predicted peak acceleration (see section A.2).

$$a_{max} \propto \frac{1}{\sqrt{\xi}} \tag{7.1}$$

Bronkhorst et al. [5] analysed the relationship between peak acceleration and damping ratio for a steel building, as illustrated in figure 7.4. The $\pm 10\%$ range on damping (in blue) leads to an approximate $\pm 5\%$ variation in the predicted peak acceleration (in red). The ±5% variation in peak acceleration can determine whether the design complies with the prescribed comfort limits, whose value is indicated by the red dotted line and given by NEN 6702 [11], a Dutch standard that defines comfort limits based on peak acceleration. This sensitivity is particularly important because buildings are often designed close to these thresholds in order to remain economical while still meeting the required comfort criteria. Therefore, in this thesis, damping estimates are deemed reliable if they fall within ±10% of the target value, in order to minimize variance in the peak acceleration.

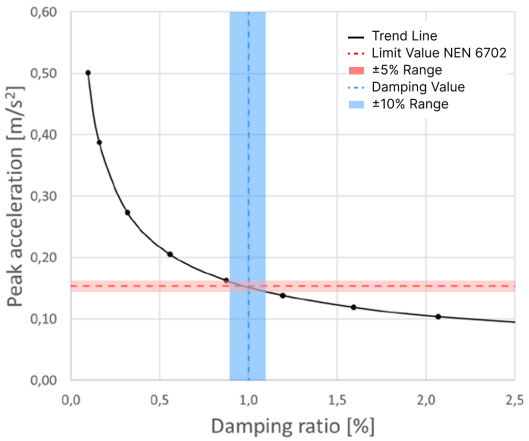

Figure 7.4: Peak acceleration level in a high-rise building at different damping ratios, based on a figure by Bronkhorst et al. [5]

7.2.2. Linear and Non-linear Systems Under Stationary Excitation

This section aims to quantitatively evaluate the reliability of damping estimates obtained through the Peak RDT and non-linear Least Squares Minimization (LSM) methods, applied to systems with constant and amplitude-dependent damping subjected to stationary loads by quantifying the performance metrics outlined in 3.8.2. This section therefore explicitly addresses cases 1 and 2, as outlined in section 3.1. These cases have been thoroughly discussed in sections 5 and 6. The reliability of damping estimates is assessed based on the threshold defined in section 7.2.1.

Figure 7.5 presents summary statistics of the distribution of damping estimates obtained the linear and the amplitude-dependent cases. The relevant metrics are: the mean of damping estimates as well as the $\pm 95\%$ confidence interval on the mean, the variance in the distribution of damping estimates, the bias in the distribution of damping estimates and the relative error computed on the mean damping. While the bias and relative error are a measure of accuracy, the $\pm 95\%$ confidence interval and the variance are a measure of precision. All numerical values supporting figure 7.5 are provided in tables B.6 and B.7 in Appendix B.

As discussed in section 6.2, the RDS lengths can have a significant impact on the reliability of damping estimates in both the linear and non-linear cases. For the sake of this assessment and comparison, it is chosen to use the RDS lengths providing the most accurate mean damping estimates in each case.

Specifically, this means that for the linear case, a 10-cycle RDS is used, whereas for the non-linear case, a 3-cycle RDS is applied. This choice of RDS lengths is informed by the sensitivity analysis discussed in section 6.2. For the linear case, a longer RDS improves the damping estimate by providing more data points to fit the theoretical model. In contrast, for the amplitude-dependent case, a shorter RDS is used to mitigate errors introduced by the non-uniform decay. Figure 6.4.b and table B.2 demonstrate that the relative error remains consistently below 10% when a 3-cycle RDS is employed in the amplitude-dependent case.

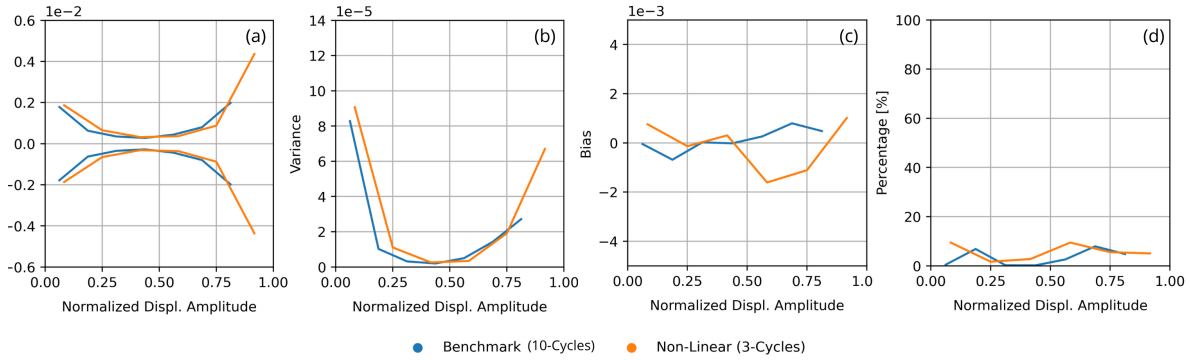

Figure 7.5: (a) 95% Confidence intervals on mean damping; (b) Variance of distribution of damping estimates; (c) Bias of distribution of damping estimates; (d) Relative error on mean damping

Accuracy

Regarding the benchmark case (see section 5),the mean damping estimates remain close to the target value across all relative amplitude ranges. The bias shown in 7.5.c, indicates that the lower amplitude ranges are slightly underestimated while the higher amplitude ranges are slightly overestimated. However, since the bias is consistently lower than 1×10^{-3}, the mean damping in the benchmark case is largely unbiased.

Regarding the amplitude-dependent case (see section 6), the mean damping estimates match the target well at low amplitudes and, as expected, exhibit an increase in damping with increasing amplitude. However, the mean damping does not sufficiently reflect the distinct features of the bi-linear function, especially at the intersection of the linearly increasing section and the high-amplitude plateau, where some discrepancies between the estimated and target mean values are observed.

The bias in figure 7.5.c indicates that damping is significantly underestimated in the relative range of 50% to 83.3%. The bias exhibits a dip in that amplitude range marking the transition between the

linearly increasing section and high-amplitude plateau in the damping function. In this dip, the bias reaches values between 1×10^{-3} and 2×10^{-3}. The origin of this discrepancy is explained in section 6.2.1. Errors arise from fitting the theoretical free decay model of a linear system to signatures exhibiting non-uniform decay.

Moreover, in the highest amplitude range (83.3% to 100%), the estimated mean damping fails to reflect the plateau of the target function and continues to increase. The corresponding bias is also greater than 1×10^{-3}. If the underlying truth was unknown, the mean damping estimates could be interpreted incorrectly, inferring a continuous rise in damping, which could be misleading. It should be noted that a finer resolution of amplitude ranges could help mitigate the systematic errors in relative amplitude range 50% to 100%.

Overall, the mean damping in the benchmark case stays consistently within 10% of the target damping with negligible bias. The mean damping in the amplitude-dependent case reflects the expected amplitude-dependency of mean damping. Some bias errors are introduced due to fitting assumptions in the damping identification process. The variance and 95% confidence intervals behave similarly for both cases, with best precision at moderate amplitudes (20% to 75%).

Lastly, as can be seen in figure 7.5.d, the relative error stays consistently under 10% for both the linear case and the amplitude-dependent case.

Precision

Figure 7.5.b shows the variance in the distribution of damping estimates for both systems. For both the linear and amplitude-dependent system, the variance is U-shaped with significantly larger values in the lower and higher amplitude ranges. The U-shaped variance indicates that low- and high-amplitude estimates are less reliable than mid-range ones due to their reduced precision. In relative amplitude range 0% to 16.7%, the variance equals 8.25×10^{-5} for the linear system and 9.07×10^{-5} for the amplitude-dependent system respectively, while in relative amplitude range 75% to 100%, it equals 2.72×10^{-5} and 6.70×10^{-5}, respectively.

The observed U-shaped variance is an artefact of the damping identification methods used in this thesis and it's origin is in section 7.1.3. While the amplitude-dependent case generally exhibits slightly higher variance than the linear benchmark, the damping estimates in the high-amplitude range for the non-linear system are significantly less precise.

The 95% confidence intervals (CI) in figure 7.5.a mirror the U-shaped trend in the variance. For both cases, the 95% CI are widest at low amplitudes, narrow in the moderate-amplitude region, and wide at high amplitudes. Similar to the variance, the difference between the linear and amplitude-dependent cases are marginal. The largest difference appears in the highest amplitude range (75% to 100%), where the confidence intervals on the mean are $\pm 0.20 \times 10^{-2}$ for the linear case and $\pm 0.44 \times 10^{-2}$ for the amplitude-dependent case. In relative terms, within the lowest amplitude range (0% to 16.7%), the relative uncertainty for the linear system is 18%, while it is 24% for the non-linear system. In the highest amplitude range (75% to 100%), the relative uncertainty is 20% for the linear case and 22% for the non-linear case. Both the benchmark and amplitude-dependent cases exhibit comparable uncertainty in the mean damping estimate across the relative amplitude range, although the uncertainty is slightly higher for the amplitude-dependent case.

Conclusion

Applying the Peak RDT in combination with the non-linear LSM to the benchmark case yields reliable damping estimates, provided the identification is performed stochastically, as described in section 5.4. The mean damping estimates corresponding to 100 hours of response data yield unbiased results. The 95% confidence intervals on the mean are narrow, especially for the moderate amplitude ranges and widen at the low and high amplitude ranges. This is a direct result of the U-shaped variance being significantly higher in the low and high amplitude ranges compared to the moderate amplitude ranges.

The damping estimates derived using the Peak RDT and non-linear LSM for the amplitude-dependent case generally remain reliable. However, compared to the benchmark case, some errors are introduced. A systematic bias arises because the mean damping estimates fail to fully capture the detailed features of the bi-linear damping function. This bias is particularly evident at the transition between the

linearly increasing region and the high-amplitude plateau, as well as within the plateau itself. Without knowledge of the true damping behaviour, these inaccuracies could lead to misinterpretations of the amplitude dependency. These accuracy errors might be mitigated by higher resolution of mean estimates, although this is not explored in this thesis. Additionally, the precision of estimates is marginally reduced, as indicated by slightly larger variance and confidence intervals, especially in the high-amplitude range.

While section 5.4 suggests that a stochastic approach yields more reliable results, such an approach is sometimes not feasible due to limited amount of measured response data. In that case, it is also important to assess the reliability of individual damping estimates. Although this is not further explored in this thesis, Figures 5.4 and 6.1 indicate that the variability of individual damping estimates significantly reduces the range over which the estimates can be considered reliable, thereby limiting the ability to accurately identify amplitude dependency.

7.2.3. Linear and Non-linear Systems Under Non-stationary Excitation of Type 1

Type 1 non-stationary (NS1) excitation signals are computed by superimposing white noise onto a deterministic time-dependent mean function, as described in section 3.4. The effect of this perturbation on the derived response, is discussed in sections 4.2 and 4.3. The resulting displacement responses exhibit a non-zero mean which becomes increasingly non-zero for larger a peak P in the time-dependent mean function. As a result, it is expected that the estimated damping is associated with errors arising from the inability to isolate the free vibration response. Complete summary metrics regarding this case are presented in figure B.3 in Appendix B alongside table **??** providing numerical values.

Accuracy

The main observation is that the accuracy of damping estimates is significantly reduced when the response signals do not exhibit a constant zero mean. Errors in accuracy are evident in both the linear and non-linear cases, as shown by the increasing discrepancy between the mean damping estimates and the target value for with increasing degree of non-stationarity. As can be seen in figure B.3, the bias introduced by the non-zero mean in the linear case remains relatively constant, while in the non-linear case, substantial errors appear particularly in the low relative amplitude ranges (0% to 50%). These accuracy errors are also reflected in the relative error depicted in figures 7.6.a and 7.6.b, where 7.6.a corresponds to the linear case and 7.6.b to the non-linear case. For the linear case, the damping estimates corresponding to the largest degree of non-stationary ($P = 1.5$) are associated with a relative error between 63% and 89%, while the damping estimates corresponding to the lowest degree of non-stationary signal ($P = 0.5$) are associated with a relative error between 18% and 61%.

The non-linear case amplifies errors in accuracy especially in the low amplitude ranges as mentioned previously, with a relative error of 269%, 375% and 325% for increasing degree of non-stationarity in the lowest amplitude range of 0% to 12.5%. The relative error decreases for increasing amplitude range, and stabilizes at values of 22%, 78% and 125% respectively.

Precision

In contrast, the precision of damping estimates is primarily affected in the non-linear case. While in the linear case, the 95% confidence intervals (figure 7.6.c) widen predominantly in the lower amplitude range (0% to 20%), the decrease in precision is marginal as indicated by the variance (figure B.4). At higher amplitude ranges, the second degree of non-stationarity considered (P = 1.0) exhibits wider confidence intervals compared to the other degrees of non-stationarity, although no consistent trend is apparent. Overall, the degree of non-stationarity appears to have only a minimal impact on precision as the confidence intervals exhibit similar behaviour across different levels.

The marginal reduction of precision observed for the linear case, is amplified in the non-linear case. Figure 7.6.d shows that, as the degree of non-stationarity increases, the 95% confidence intervals consistently widen across all amplitude ranges, except for the lowest amplitude range, where as sizeable increase in variance (figure B.4) leads to substantially wider intervals.

Conclusion

As anticipated in section 4.2 and 4.3, the damping estimates resulting from response signals exhibiting increasingly non-zero means are associated with significant errors. While mean damping estimates for the linear case exhibit a constant but significant relative error consistently larger than 10%, mean

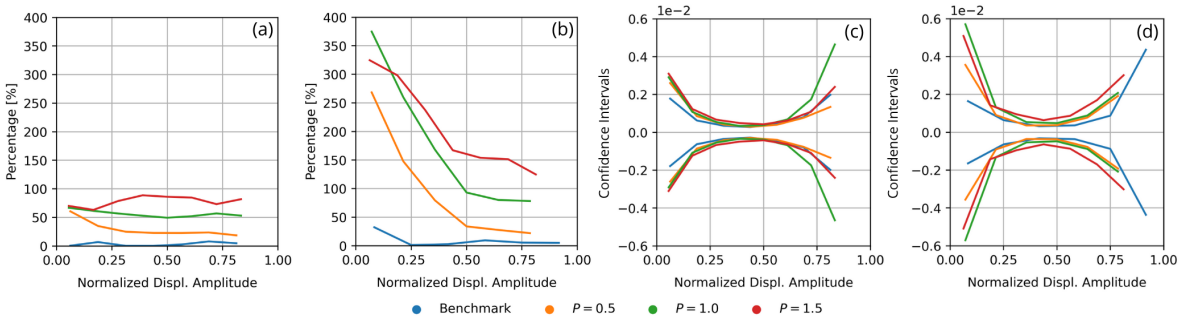

Figure 7.6: Comparison of metrics corresponding to non-stationarity type 1; (a) Relative error on mean damping estimates (linear system); (b) Relative error on mean damping estimates (non-linear system); (c) 95% confidence intervals on mean damping estimates (linear system); (d) 95% confidence intervals on mean damping estimates (non-linear system)

damping estimates for the non-linear case exhibit even larger accuracy errors especially in the lower amplitude range. The precision of damping estimates is not greatly affected for all considered degrees of non-stationarity for the linear case. In the non-linear case however, precision errors become significant.

Damping estimates derived from response data exhibiting a time-varying and non-zero mean value are thus associated with a large bias and are therefore not reliable with respect to the threshold defined in section 7.2.1. Additionally, while damping estimates in the lower and higher amplitude ranges are already associated with a larger variability in the benchmark case, the deviation from the stationarity condition further increases this variability especially if the system at hand exhibits amplitude-dependent damping.

7.2.4. Linear and Non-linear Systems Under Non-stationary Excitation of Type 2

The second type of non-stationarity was modelled by modulating the amplitude of the signal, thus introducing a time-dependent variance. From the quantification of non-stationarity (section 4.3), it was concluded that the displacement responses generated using excitations with time-dependent variance, produced level-stationary responses meaning that the data is stationary around a constant (zero) mean. As a result, the Peak RDT is expected to perform well and reliably estimated damping, since the only deviation from its underlying assumptions is the presence of amplitude dependent damping. The increased excitation variance results in larger displacement magnitudes and a broader amplitude range. In figure B.4, the metrics are normalized using the global maximum across all signals, rather than individual maxima.

Accuracy

The main observation is that both the accuracy and precision of the damping estimates remain largely unaffected across the three cases considered.
Damping estimated from level-stationary response data are generally close to the target value with only minor deviations. Figure 7.7.a and 7.7.b illustrate the relative error on mean damping for the linear and non-linear case, respectively. For the linear case, mean damping generally remains accurate in the lower amplitude ranges. For increasing degree of non-stationarity, the relative error on the mean remain mostly within 10% for amplitude range 0% to 70%, 0% to 54% and 0% to 44%, respectively. The amplitude range for which damping estimates are deemed accurate thus becomes more narrow for increasing degree of non-stationarity. In the higher relative amplitude ranges, a larger discrepancy is observed and reflected in figure 7.7.a. For the non-linear case, the relative error is more constant across all amplitude ranges. All degrees of non-stationarity considered produce damping estimates with a relative error below 10% in amplitude range 25% to 60%.

Precision

Moreover, level-stationary response data only has a minor impact on the precision of damping estimates. Regarding the linear case, B.4 shows that the variance of damping estimates increases especially for the highest amplitude range. It should be noted that the specific amplitude range classified

as ”high” shifts with increasing P, due to the increased magnitude of displacement responses. This tendency is reflected in the 95% confidence intervals as shown in figure 7.7.c. While wide intervals at low and high amplitude ranges is a trend observed in all cases due to the U-shaped variance, the narrow portion of the intervals becomes increasingly narrow for increasing degree of non-stationarity. The 95% confidence intervals however, do not become significantly wider.

In contrast, for the non-linear case shown in figure 7.7.d, as the degree of non-stationarity increases, not only does the narrow portion of the confidence interval becomes smaller, but the intervals also widen significantly in the higher amplitude range. That is likely due to the pronounced U-shaped pattern for the non-linear case (figure B.4). In particular, for the $P = 1.5$ case, the variance reaches values as high as 17×10^{-5} in the relative amplitude range of 60% to 80%.

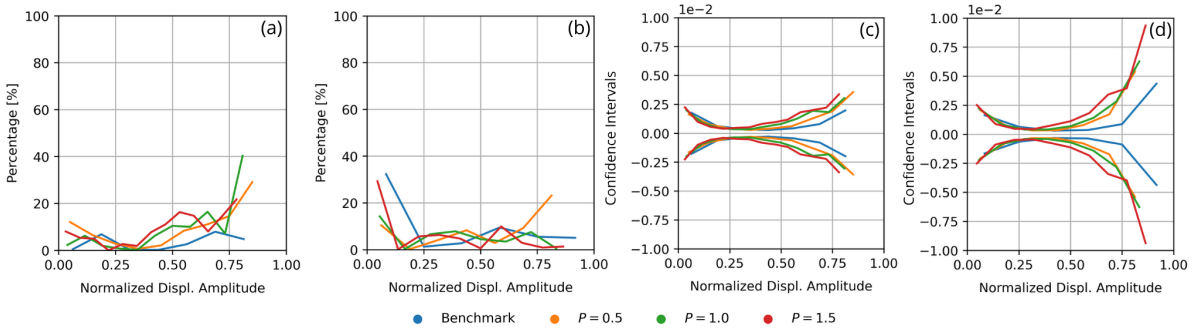

Figure 7.7: Comparison of metrics corresponding to non-stationarity type 2; (a) Relative error on mean damping estimates (linear system); (b) Relative error on mean damping estimates (non-linear system); (c) 95% confidence intervals on mean damping estimates (linear system); (d) 95% confidence intervals on mean damping estimates (non-linear system)

Conclusion

No clear trend is observed in the accuracy of the damping estimates. Although the introduction of time-dependent variance in the excitation leads to minor accuracy errors compared to the benchmark case, these effects are considerably smaller than those observed when a time-dependent mean is introduced. Most damping estimates exhibit a relative error below the 10% threshold, especially in the moderate amplitude range. While section 4.3 confirms that the response data is level-stationary, other tests for stationarity have not been performed. It is noticeable that the time-dependent variance slightly affects precision of damping estimates. While the shape of the confidence intervals are also affected by other parameters such as sample size, the increased variance in higher amplitude ranges observed for both the linear and non-linear case in figure B.4 suggests a consistent effect.

7.2.5. Linear and Non-linear Systems Under Non-stationary Excitation of Type 3

Similarly to the first type of non-stationarity, displacement responses from a system excited by loading conditions with time-dependent mean and variance are classified as non-stationary according to the KPSS test (see section 4.3). Additionally, since the third type of non-stationarity is a combination of the previous two, similar errors are observed. The statistical metrics observed closely resemble those of the other cases, almost as if the errors are superimposed.

Accuracy

The time-dependent, non-zero mean in the response introduces a large bias in the damping estimates. As can be seen on figures 7.8.a and 7.8.b., While for the linear case the relative error is constant across all amplitude ranges, for the non-linear case, substantial errors are introduced especially in the lowest amplitude range. This error then stabilizes for the higher amplitude ranges, remaining far above the 10% threshold.

Precision

Regarding the precision of damping estimates, the errors introduces are very similar to the case with time-dependent variance. For increasing levels of non-stationarity, the narrow portion of the 95% con-

fidence intervals is reduced significantly. Additionally, for the non-linear case, the intervals widen considerably for the non-linear case.

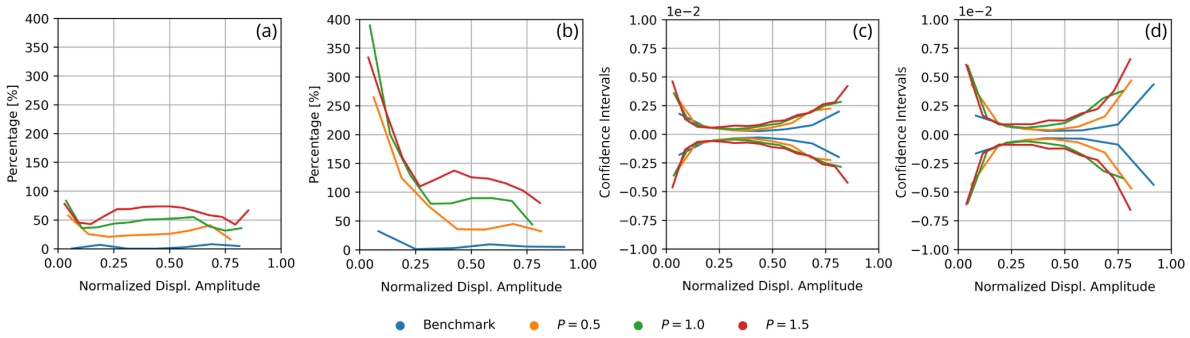

Figure 7.8: Comparison of metrics corresponding to non-stationarity type 2; (a) Relative error on mean damping estimates (linear system); (b) Relative error on mean damping estimates (non-linear system); (c) 95% confidence intervals on mean damping estimates (linear system); (d) 95% confidence intervals on mean damping estimates (non-linear system)

Conclusion

Due to the large bias introduced in both the linear and non-linear case, the damping estimates produced are not reliable. The precision of damping estimates is also reduced significantly for increasing degree of non-stationarity especially for the higher amplitude ranges.

7.2.6. Conclusion

The main difference between the linear and non-linear cases, when excited by stationary load, lies in the accuracy of damping estimates. The mean damping for benchmark case remains consistently within 10% of the target damping with negligible bias. The maximum relative error observed for the benchmark case is 7.9%, occurring in the relative amplitude range 62.5% to 75%. For the amplitude-dependent case, the mean damping exhibits the expected increase in damping with increasing amplitude, aligning well with the target at low to mid amplitudes. While the linear case demonstrates high accuracy, the non-linear case exhibits relative errors above the 10% threshold primarily due to inaccuracies around the kink the damping function between the linearly increasing portion and the high amplitude plateau. This leads to a noticeable dip in bias in that region. It is possible that increasing the resolution, by introducing more finely divided amplitude ranges, could improve the accuracy of mean damping at such transitions. However, this would reduce the number of segments per range, which could negatively affect the Random Decrement signature and thus the reliability of the estimates.

When looking at the cases with non-stationarity, it is apparent that the largest errors are introduced when the response data does not have a constant zero mean. The fundamental principle of the RDT is to average out the component to the forcing ans isolate the free vibration response, which can only be completed if the excitation has a stationary zero mean as described in section 2.6.6. Excitation type 1 and 2 both exhibit time-dependent means in the excitation and therefore produces unreliable damping estimates for all degrees of non-stationarity considered. Since for the linear case, the introduced bias seems to be rather constant across all amplitude ranges, it would be interesting to investigate a link between degree of non-stationarity, regarding only level stationarity, and the relative errors introduced. Furthermore, it seems that damping estimates in the lower amplitude ranges exhibit larger accuracy errors for the non-linear case. Excitation type 2 primarily introduces precision errors, though these are less pronounced than the accuracy errors observed in the other cases. The precision errors are reflected mainly in the narrowing of the confidence range around the mean estimate. As the degree of non-stationarity increases, this confidence range narrows further.

7.3. Prediction Metric

The numerical studies presented in this thesis are carefully designed to accurately reflect wind-induced vibrations of high-rise buildings. Therefore, the computation of the (non)-stationary excitation, the modelling of the structural system and the derivation of the response are informed based on existing literature. Following the literature review, it was chosen to model damping according to the approaches of Jeary [3] and Wyatt [12], which are limited to structural damping, although damping due to soil-structure interaction greatly contributes to total damping in Dutch high-rise buildings.

As explained in section 2.4.2, Wyatt proposed that all significant energy dissipation within the structure could be attributed to friction. Subsequently, Jeary identified three regimes of energy dissipation, associated with friction in different structural components, and linked the dependency of damping to displacement amplitude. While their approaches are based on physical principles, the exact mechanism responsible for energy dissipation in high-rise buildings is hard to verify since the process is very complex. Therefore, the true damping mechanism in high-rise buildings is not known with absolute certainty.

While identifying the true damping mechanism in high-rise buildings lies beyond the scope of this thesis, the assumed damping mechanism remains relevant for assessing the reliability of damping estimates. In fact, the exact value of estimated damping relies on the assumptions that damping identification techniques themselves have about the nature of damping. For instance, the Peak RDT assumes that the damping mechanism is amplitude-dependent and is specifically designed to identify the variation of damping with response amplitude. It does so by producing a set of Random Decrement Signatures (RDS), each corresponding to a different range of response amplitude, from which amplitude-dependent damping can be identified. The specific dependency it reveals depends on the nature of the response signal used as input. In other words, when applied to the displacement response, the Peak RDT will identify displacement-amplitude-dependent damping. Therefore, the legitimate application of the Peak RDT requires the system to exhibit amplitude-dependent damping [20].

This is conflicting with the fact that, the true damping mechanism in high-rise buildings is speculative and cannot be directly verified. It is therefore not known if the damping is truly *amplitude*-dependent. The reliability of damping estimates is questionable if the underlying damping mechanism is not truly amplitude dependent. This raises the question of the practical usefulness of damping estimates obtained through the Peak RDT.

As explained in the section 1.1, peak acceleration is the primary criterion for assessing occupant comfort in high-rise buildings. This chapter aims to demonstrate that the Peak RDT can estimate equivalent damping when applied to response signals of a system with non-amplitude-dependent damping. Damping is considered equivalent if the peak acceleration observed in the amplitude-dependent system's responses closely matches those of the non-amplitude-dependent system.

7.3.1. Approach

This section outlines the approach used to determine equivalent damping from response data of a system with non-amplitude-dependent damping. Furthermore, this section elaborates on the steps undertaken to assess equivalence using peak acceleration.

1. Define damping mechanism $\xi(x(t))$

   The damping mechanism considered is dependent on instantaneous displacement $x(t)$, and is hereafter referred to as instantaneous-displacement-dependent damping $\xi(x(t))$. The bi-linear shape of the instantaneous-displacement-dependent damping is chosen to be the same as the shape of amplitude-dependent damping for convenience rather than physical principles. The manner in which damping is defined in the initial value problem formulation (see section 3.5) governs its behaviour in the derived response.

2. Derive $x_1(t)$, using $\xi(x(t))$

   Derive N_{sim} displacement responses of the system exhibiting instantaneous-displacement-dependent damping, excited by zero-mean, stationary Gaussian white noise. In the derivation of the re-

sponse, the damping value is updated at every time step and the response is derived without the oscillation tracking algorithm.

3. Estimate $\hat{\xi}(A(t))$ by applying the Peak RDT to $x_1(t)$

   Apply the Peak RDT in combination with Least Squares Minimization, as outlined in the methodological framework (see section 3.2), in order to estimate mean damping as a function of displacement amplitude $\hat{\xi}(A(t))$.

4. Fit polynomial function to $\hat{\xi}(A(t))$

   Fit a polynomial function to the mean damping estimates $\hat{\xi}(A(t))$. The fitted polynomial function is hereafter referred to $\xi_{new}(A_x)$.

5. Derive $x_2(t)$, using $\xi_{new}(A_x)$

   Derive N_{sim} displacement responses of the system exhibiting amplitude-dependent damping, excited by zero-mean, stationary Gaussian white noise. In the derivation of the response, the damping value is updated using the oscillation tracking algorithm, which ensures that damping is dependent on displacement amplitude. The relationship between damping and amplitude is given by the polynomial function $\xi_{new}(A_x)$.

6. Verify the equivalence of $\xi(x(t))$ and $\xi_{new}(A_x)$ using the peak acceleration

   For the $2 \times N_{sim}$ displacement responses of $x_1(t)$ and $x_2(t)$, differentiate twice to compute the acceleration responses $a_1(t)$ and $a_2(t)$. For each acceleration response, identify the peak acceleration and determine the distribution of peak accelerations across both simulations.

7.3.2. Similarity Assessment

In this section, the results obtained using the approach described in 7.3.1 are discussed. Figure 7.9 illustrates the bi-linear target function $\xi(x(t))$, the mean damping estimates $\hat{\xi}(A(t))$, and their respective 95% confidence intervals, obtained by applying the peak RDT to N_{sim} displacement responses $x_1(t)$, as well as the polynomial function $\xi_{new}(A_x)$ fitted on the mean damping estimates. The figure thus illustrates steps 1 to 4 of the approach described in 7.3.1.

Figure 7.10 shows the distribution of peak accelerations for the two cases discussed: the peak accelerations from the acceleration responses of the system with instantaneous-displacement-dependent damping ($a_1(t)$ in blue) and those of the system with displacement-amplitude-dependent damping ($a_2(t)$ in yellow). The mean and median values of both distributions indicated. The equivalence of damping functions $\xi(x(t))$ and $\xi_{new}(A_x)$ is assessed based on the similarity of the peak accelerations observed in figure 7.10.

The poor fit between the target function $\xi(x(t))$ and the mean damping estimates $\hat{\xi}(A(t))$, displayed in figure 7.9, proves that the Peak RDT fails to capture the exact non-linearity of damping when its underlying mechanism is not amplitude-dependent. Although there is a clear increase in damping with increasing normalized displacement amplitude, the mean damping estimates do not accurately reflect the ground truth. This highlights the difficulty of assessing the reliability of damping estimates when the actual damping mechanism does not conform to the assumptions of the identification method. It would not be accurate to say that the damping estimates are incorrect. Rather, the Peak RDT seeks to identify a dependency that is not defined.

The distributions of peak acceleration for both simulations, illustrated in figure 7.10, show that most peak acceleration values are located in the same range (between 4.5 and 6 m/s^2). The distribution of peak acceleration, corresponding to the system with instantaneous-displacement-dependent damping ($\xi(t)$)), exhibits a higher peak between 5 and 5.7 m/s^2, whereas the distribution of peak values corresponding to the system with displacement-amplitude-dependent damping ($\xi_{new}(A_x)$) is wider with a lower peak spanning 5 to 5.9 m/s^2. Both the mean and median values for the instantaneous-displacement-dependent damping system are slightly lower than those for the displacement-amplitude-dependent system, although the difference is minimal. This indicates that the peak accelerations derived from the system with instantaneous-displacement-dependent damping and those from the system with displacement-amplitude-dependent damping are equivalent for the investigated case.

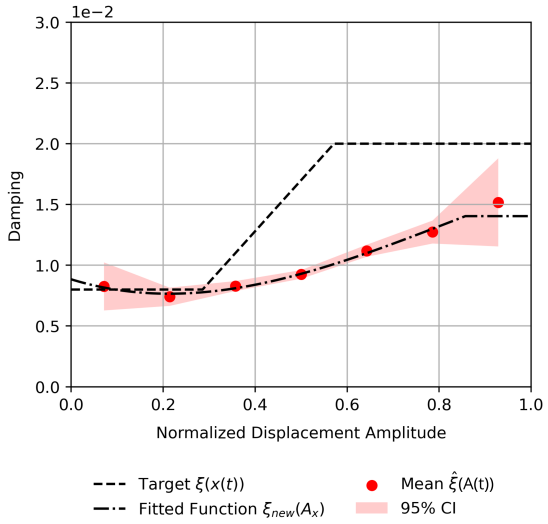

Figure 7.9: Mean damping obtained by applying Peak RDT (+LSM) to displacement responses of a system exhibiting instantaneous-displacement-dependent damping excited by stationary loading conditions; the bi-linear target function and polynomial fit are also depicted

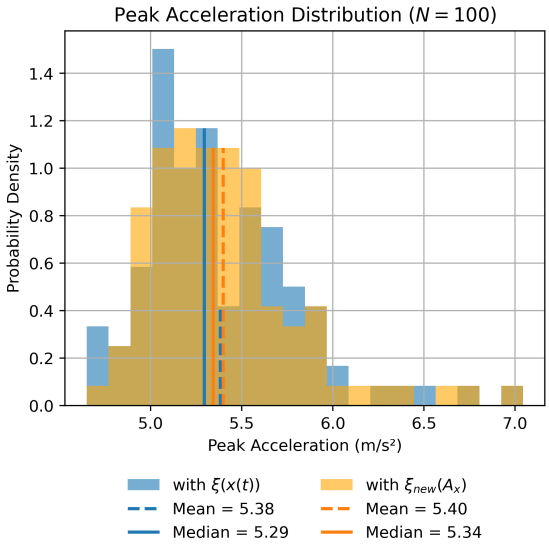

Figure 7.10: Distribution of peak accelerations for the system with instantaneous-displacement-dependent damping (blue) and the system with displacement-amplitude-dependent damping (yellow)

7.3.3. Conclusion

Section 7.3 aimed to contextualize the use of the Peak RDT in a more realistic setting and evaluating whether the Peak RDT can be effectively applied to real systems, where the amplitude dependency of damping can only be speculated and not directly verified.

It was demonstrated that, for the two cases considered, similar peak acceleration values were obtained which suggests that, for the purpose of comfort assessment of wind-induced responses in high-rise buildings, the precise nature of the damping mechanism might be less critical. This is because for the case considered in this thesis, the Peak RDT can estimate equivalent damping which does depend on amplitude, even if the original damping mechanism does not.

While the original damping mechanism, examined in this section, is dependent on instantaneous-displacement, it would be interesting to investigate whether the Peak RDT might produce equivalent amplitude-dependent damping based on other non-amplitude-dependent damping mechanisms. Additionally, the two systems analysed in this section are excited by zero-mean, stationary white noise. Section 7.2 showed that non-stationarity can introduce significant accuracy and precision errors. Therefore, it cannot be guaranteed that similar peak accelerations could be produced for other non-amplitude-dependent damping mechanisms or under non-ideal excitations.

Moreover, the impact of measurement noise was not addressed in this section. Consequently, when applying the Peak RDT to response data polluted by noise, there is no guarantee that the estimated amplitude-dependent mean damping would be reliable and could be used to produce an equivalent amplitude-dependent damping that would yield in similar peak accelerations.

Overall, it is important to emphasize that the findings from this particular study are specific to the cases studied and therefore cannot be generalized to all damping mechanisms. The interesting results, however, indicate that further investigation into this topic would be valuable.

8

Discussion, Recommendations for Further Research & Conclusion

This chapter aims to provide some closing remarks regarding the research objectives, summarize and discuss the key insights of this study and present recommendations for practical application as well as further research.

8.1. Discussion

This thesis investigates the reliability of damping estimates derived using the Peak RDT under ideal and non-ideal conditions by means of a series of numerical simulations. Damping is identified for systems with constant and amplitude-dependent damping, excited by stationary and non-stationary loads.

It is important to emphasize that all conclusions presented in this thesis apply specifically to the damping identification method employed. As noted in the section 2, Literature Review, Operational Modal Analysis (OMA) is a broad term relating to many methods. Although the Random Decrement Technique (RDT) is often referred to as an OMA method, it is technically not, as its direct output is not damping but rather an approximation of the system's free vibration response. In this thesis, damping is estimated using the Least Squares Minimization method, which relies on its own assumptions and carries its own limitations. Therefore, the conclusions drawn in this thesis are applicable to this specific sequence of methods, the Peak RDT and the Least Squares Minimization (LSM), rather than to the Peak RDT alone.

The Peak RDT and LSM produce reliable damping estimates for both the linear and non-linear system considered, when they are excited by a stationary load and when the method is used stochastically, as described in section 3.2. There is a significant difference in reliability between individual damping estimates, based on 1-hour response time traces, and mean damping estimates, derived from approximately 100 hours of response data. Compared to mean damping estimates, the precision of individual estimates is particularly poor, making them nearly unusable especially at low and high amplitude ranges. It should be noted that 100 hours of response data represents a substantial data requirement, which may not always be feasible in practice. In a way, this thesis evaluates two extreme cases: damping estimates based on very short time series and their average corresponding to much longer durations. It would be valuable to perform a convergence study to evaluate the expected accuracy and precision associated with varying amounts of response data.

The Peak RDT and LSM perform particularly well in the case of linear systems excited by stationary loads. This is because in that specific case, the Random Decrement Signatures (RDS) produced by the Peak RDT realistically approximate the free vibration response of a linear system, aligning precisely with the assumptions of the LSM. Tamura and Suganuma [20] acknowledge that Random Decrement Signatures, computed from response data with amplitude-dependent damping, do not represent the free vibration of the non-linear system nor a linearized system evaluated at a specific amplitude. Nonetheless Tamura and Suganuma estimate damping by curve fitting the theoretical decay of a linear

system to the signatures exhibiting non-uniform decay, which introduces fitting errors. A practical way to mitigate these fitting errors is to reduce the number of cycles used in the computation of the RDS, thereby capturing the response only within a specific amplitude range. However, this approach comes at the cost of discarding valuable information. Rather than fine-tuning the methods' settings to mitigate errors, it should be investigated whether the information in the non-uniform decay could be used to fit a non-linear function of damping. Since, according to Tamura and Suganuma, the RDS does not correspond to the free vibration response of the non-linear system, it is debatable whether fitting a non-linear damping function could reduce the fitting errors or whether it would still be considered as fine-tuning the method's settings. Exploring the reliability of damping estimates using this method could provide valuable insights.

Introducing non-stationarities in the excitation, and consequently in the response, significantly disrupts the RDT algorithm because the forcing component in the response is no longer properly cancelled out. In such cases, the RDS fails to approximate the free vibration response, making the damping identification largely meaningless due to large errors. The quantification of non-stationarity confirms that the response data are significantly non-stationary. However, the analysis of ambient acceleration responses by Entezami and Shariatmadar [51] raises doubts about whether ambient vibrations exhibit such pronounced non-stationarities in real-world conditions. Repeating the numerical simulation with more realistic excitation signals would be valuable to reassess the reliability of damping estimates. The current results might dismiss the reliability of damping estimates produced from non-level-stationary response data to quickly.

Lastly, this study was conducted without considering the effects of measurement noise. It is expected that the presence of noise would introduce additional errors, thereby reducing the reliability of the damping estimates or requiring longer response signals to achieve comparable reliability. To ensure that the findings of this thesis are realistically applicable in practice, it is essential to account for the influence of measurement noise.

8.2. Practical Recommendations

The third research objective of this thesis is related to the quantification of performance metrics. A variety of metrics are assessed in sections 7.1, 7.2, and 7.3, each corresponding to a different stage of the damping identification process.

Since the assessment of the reliability of damping estimates is ultimately needed in order to properly calibrate new damping prediction models, it is valuable to provide an indication of the errors that can be expected under specific levels of non-linearity or non-stationarity. Although the accuracy and precision of damping estimates is quantified for each of the cases in section 7, the results remain specific to these numerical simulations and should not be interpreted as definitive quantitative measures.

A more practically applicable outcome of this thesis is that it offers a range of qualitative insights into the behaviour of the Peak RDT under both ideal and non-ideal conditions. Since the reliability of damping estimates is highly dependent on the choice of identification method and its specific settings, engineers should not treat these estimates as absolute values. Instead, the engineer should have insights into the workings of the method and be able to flag intermediate results that do not look right, such as a Random Decrement Signature that is not strictly decaying, or a Random Decrement Signature whose segments do not convey similar free decay information. Of course, having insights into all the steps of an algorithm can be challenging and the Random Decrement Technique is comparatively simple and intuitive. Yet, it is important that engineers do not treat it as a black box.

8.3. Recommendations for Further Research

This section provides recommendations for further research which can help gaining insights into the reliability of damping estimates derived using the Peak RDT.

1. Tamura's damping model

   The amplitude-dependent damping model used in this thesis is modelled according to Jeary's model [19], where at high amplitudes, damping stays constant. However, Aquino and Tamura [16] speculate that damping values at very high amplitudes might decrease again. It is recommended to evaluate the performance of the Peak RDT using systems with various types of amplitude-dependent damping, to determine the method's reliability in identifying non-linear damping behaviour beyond the mechanism identified by Jeary [3]. Furthermore, it would be useful to perform the numerical simulation with Tamura's damping model to verify whether the Peak RDT can effectively detect a decrease in damping for very high amplitudes and to analyse its effect on the Random Decrement Signatures.

2. Mild non-stationarity

   The non-stationarity of the excitations considered in this thesis are significantly non-stationary, to a level that might be unrealistic with respect to wind-induced vibrations in high-rise buildings. While this thesis brought insights in the kind of non-stationary behaviour that can introduce significant errors to damping estimates, it might not be a quantification that is applicable to real scenarios. The investigation of this, more close to the non-stationarity observed in the response of high-rise buildings could deliver results which are more applicable. It is recommended to investigate the influence of mild-stationarity on the reliability of damping estimates and to find the threshold after which the non-stationarity introduces errors beyond the acceptable threshold.

3. Reliability of individual damping estimate

   In this thesis, the reliability of damping estimates was assessed based on the mean of the distribution of individual estimates obtained through Monte Carlo simulations. However, this stochastic approach relies on the availability of large amounts of response data, which may not always be practical. It is therefore recommended to investigate whether, based on the known distribution of damping estimates, it is possible to make informed statements about the reliability of a single individual estimate, without the need to repeat the entire numerical simulation. This could provide valuable guidance in practical applications where only limited data are available.

4. RDS with non-uniform decay

   Since the Random Decrement Signatures produced from vibration responses of a system with amplitude-dependent damping exhibit a non-uniform decay, it is recommended to investigate whether a non-linear function of damping could be introduced in the theoretical equation of the free vibration.

5. Equivalent damping with Peak RDT

   Section 7.3 investigates whether the Peak RDT can also be used when the underlying damping mechanism of the system is not amplitude-dependent. The study is focused only on instantaneous-displacement-dependent damping and under ideal conditions. It is recommended to explore this further and assess whether the damping identified by the Peak RDT is truly equivalent in other conditions.

8.4. Conclusion

The Peak RDT in combination with the Least Squares Minimization method showed promising results and reliable damping estimates when used stochastically in a scenario complying with both the linearity and stationarity conditions. Although the damping estimates derived from a single simulation, corresponding to 1 hour of response data, showed significant variability notably in the low an high amplitude ranges, the statistical mean of the distribution of damping estimates produces accurate mean damping estimates. The reduced precision in the low and high amplitude ranges are an artefact of the

method and are a repeatable phenomenon, meaning that it can be taken into account when estimating damping from in-situ measurements. The higher variance in the low amplitude range is a result of the segments not corresponding to a significant impulse. Therefore they do not convey sufficient free decay information and the resulting RDS is a poor approximation of the theoretical decay.

The application of the damping identification method to systems exhibiting amplitude-dependent damping proved to perform well given that the response truly corresponds to a system with amplitude-dependent damping. The derivation of response data exhibiting amplitude-dependent damping is achieved through the implementation of an oscillation tracking algorithm in the numerical derivation of the response. Minor accuracy errors are introduced when the system exhibits amplitude-dependent damping due to the difficulty of the method in detecting the exact shape of the target damping function. Additionally, accuracy errors are by curve fitting the theoretical free vibration equation of a linear system to a Random Decrement Signature exhibiting non-uniform decay. When the system at hand exhibits amplitude-dependent damping, the RDS are distorted by response data corresponding to the system's dynamic behaviour at other amplitude ranges, resulting in signatures with a non-uniform decay. The fitting errors introduced by curve fitting a model with constant damping, can be mitigated by reducing the length of the sampled segments in order to prevent contributions from other amplitude ranges.

Greater accuracy and precision errors are introduced when the systems are excited by non-stationary loading conditions. Especially the introduction of a non-zero mean in the displacement responses, used as input for the Peak RDT, introduces large bias in the damping estimates. In fact, a time-dependent mean trend in the excitation fundamentally conflicts with the underlying assumptions of the RDT, which is based on averaging out the forcing component. This component can only be averaged out if the mean is zero. While a reduction in precision is minor if the system is linear, the amplitude dependency of damping amplifies precision errors notably through a significantly large variance which is reflected in significantly wider confidence intervals.

For the levels of non-stationarity investigated in this study, none of the cases result in reliable damping estimates as the relative error is far greater than the threshold of 10%. However, while qualitatively similar accuracy and precision errors, it should be investigated whether more realistic loading conditions produce more nuanced results which could be translated to useable conclusions for in-situ measurements.

Bibliography

[1] DVP Smart concepts. *RISE Rotterdam*. 2025. URL: https://dvpsmartconcepts.nl/projecten/rise-rotterdam/.

[2] K. Heshmati et al. “Effects of wind-induced vibrations in tall buildings on cognitive work performance, comfort, and wellbeing of the occupants”. In: *Journal of Physics: Conference Series*. Vol. 2647. 25. IOP Publishing. 2024, p. 252032.

[3] A.P. Jeary. “Damping in tall buildings—a mechanism and a predictor”. In: *Earthquake engineering & structural dynamics* 14.5 (1986), pp. 733–750.

[4] T. Kijewski and A. Kareem. “On the reliability of a class of system identification techniques: insights from bootstrap theory”. In: *Structural Safety* 24.2-4 (2002), pp. 261–280.

[5] A.J. Bronkhorst, C.A. Van Bentum, and S.S. Gomez. *Wind-induced vibrations and damping in high-rise buildings*. Tech. rep. Tech. rep, 2018.

[6] TNO. *Hoge gebouwen vangen veel wind; monitorprogramma HiViBE van start*. June 2021. URL: https://www.tno.nl/nl/newsroom/2021/06/hoge-gebouwen-vangen-wind/.

[7] D. Boggs and J. Dragovich. “The nature of wind loads and dynamic response”. In: *Special Publication* 240 (2006), pp. 15–44.

[8] A.J. Bronkhorst and C.P.W. Geurts. “Slappe ondergrond dempt trillingen van hoogbouw. Demping in hoogbouwconstructies 2”. In: *Bouwen met Staal* December (2018), p. 40.

[9] R. Smith and M. Willford. “Damping in tall buildings–uncertainties and solutions”. In: *no. January* (2008), pp. 66–67.

[10] European Committee for Standardization. *Eurocode 1: Actions on structures – Part 1-4: General actions – Wind actions*. EN 1991-1-4:2005. 2005.

[11] NEN. *NEN 6702 (nl) – Technical Principles for Building Structures, TGB 1990 – Loadings and Deformations*. Dutch. https://www.nen.nl/. Normcommissie 351 001 Technische Grondslagen voor Bouwconstructies. Netherlands Standardization Institute (NEN), 2007.

[12] T.A. Wyatt. “Mechanisms of damping”. In: *Proceeding of a Symposium of Dynamic Behavior of Bridges at the Transpor and Road Research Laboratory, Crowthorne, Berkshire, England, May 19, 1977.* TRRL Rpt. 275 Proceeding. 1977.

[13] A.P. Jeary. *Designer’s guide to the dynamic response of structures*. CRC Press, 1998.

[14] Y. Tamura. “Damping in buildings for wind resistant design”. In: *International Symposium on Wind and Structures for the 21st Century, 2000*. 2000, pp. 115–130.

[15] S.S. Gomez, C.P.W. Geurts, and A. Metrikine. “On the importance of soil damping for tall buildings loaded by wind”. In: *Engineering Structures* 163 (2018), pp. 426–435.

[16] Y. Tamura. “Damping in buildings and estimation techniques”. In: *Advanced Structural Wind Engineering* (2013), pp. 347–376.

[17] D.Y. Yun et al. “LSTM-Based Approach for Stable Identification of Modal Damping Ratio in Building Structures”. In: *Structural Control and Health Monitoring* 2024.1 (2024), p. 6645626.

[18] C. Rainieri and G. Fabbrocino. “Operational modal analysis of civil engineering structures”. In: *Springer, New York* 142 (2014), p. 143.

[19] A.P. Jeary. “Establishing non-linear damping characteristics of structures from non-stationary response time-histories”. In: *Structural Engineer* 70.4 (1992), pp. 61–66.

[20] Y. Tamura and S. Suganuma. “Evaluation of amplitude-dependent damping and natural frequency of buildings during strong winds”. In: *Journal of wind engineering and industrial aerodynamics* 59.2-3 (1996), pp. 115–130.

[21] A. Cunha and E. Caetano. “From input-output to output-only modal identification of civil engineering structures”. In: *1st International Operational Modal Analysis Conference (IOMAC)*. 2005.

[22] Z. Fu and J. He. *Modal analysis*. Elsevier, 2001.

[23] F.B. Zahid, Z.C. Ong, and S.Y. Khoo. “A review of operational modal analysis techniques for in-service modal identification”. In: *Journal of the Brazilian Society of Mechanical Sciences and Engineering* 42.8 (2020), p. 398.

[24] Wikipedia. *Stationary process*. June 2024. URL: https://en.wikipedia.org/wiki/Stationary_process.

[25] A.P. Jeary. “The description and measurement of nonlinear damping in structures”. In: *Journal of Wind Engineering and Industrial Aerodynamics* 59.2-3 (1996), pp. 103–114.

[26] E. Reynders. “System identification methods for (operational) modal analysis: review and comparison”. In: *Archives of Computational Methods in Engineering* 19 (2012), pp. 51–124.

[27] T. Friis et al. “Operational modal analysis based linear system identification of systems with elasto-perfectly-plastic nonlinear behavior”. In: *Proceedings of the 8th International Operational Modal Analysis Conference*. 2019, pp. 481–488.

[28] Y. Tamura. “Amplitude dependency of damping in buildings and critical tip drift ratio”. In: *International Journal of High-Rise Buildings* 1.1 (2012), pp. 1–13.

[29] T. Kijewski and S. Kareem. “Reliability of random decrement technique for estimates of structural damping”. In: *8th ASCE Specialty Conference on Probabilistic Mechanics and Structural Reliability*. Vol. 1. 2000, pp. 1–6.

[30] H.A. Cole. “On-the-line analysis of random vibrations”. In: *9th structural dynamics and materials conference*. 1968, p. 288.

[31] S. Ibrahim. “The use of random decrement technique for identification of structural modes of vibration”. In: *18th Structural Dynamics and Materials Conference*. 1977, p. 368.

[32] J.K. Vandiver et al. “A mathematical basis for the random decrement vibration signature analysis technique”. In: (1982).

[33] J.C. Asmussen. “Modal analysis based on the random decrement technique: application to civil engineering structures”. In: (1997).

[34] K.K. Vesterholm, R. Brincker, and A. Brandt. “Random decrement technique for detection and characterization of nonlinear behavior”. In: *Mechanical Systems and Signal Processing* 143 (2020), p. 106841.

[35] R. Brincker and S. Amador. “On the theory of random decrement”. In: *Mechanical Systems and Signal Processing* 173 (2022), p. 109060.

[36] J. Wu et al. “Study on random decrement signature under different triggering level and length of time history”. In: *Topics in Modal Analysis & Testing, Volume 10: Proceedings of the 35th IMAC, A Conference and Exposition on Structural Dynamics 2017*. Springer. 2017, pp. 159–166.

[37] J.M. Joo. “Use of the Logarithmic decrement to assess the damping in oscillations”. In: *Revista de Investigacion de Fisica* 19 (2016), p. 161901551.

[38] Wikipedia contributors. *Logarithmic decrement*. Feb. 2023. URL: https://en.wikipedia.org/wiki/Logarithmic_decrement.

[39] V. Picozzi et al. “Uncertainty in the dynamic properties of tall buildings and propagation to the wind-induced response”. In: *The Structural Design of Tall and Special Buildings* 33.10 (2024), e2107.

[40] A.G. Davenport. “Damping in tall buildings: Its variability and treatment in design”. In: *Building motion in wind* (1986), pp. 42–57.

[41] L.E. Goodman. “Material damping and slip damping”. In: *Shock and vibration handbook* 36 (1976), pp. 1–28.

[42] C.F. Beards. “Chapter 5 - Damping in structures”. In: *Structural Vibration*. Ed. by C.F. Beards. Oxford: Butterworth-Heinemann, 1996, pp. 157–204. ISBN: 978-0-340-64580-2. DOI: https://doi.org/10.1016/B978-034064580-2/50007-7. URL: https://www.sciencedirect.com/science/article/pii/B9780340645802500077.

[43] R. Eyre and G.P. Tilly. “Damping measurements on steel and composite bridges”. In: *Proceeding of a Symposium on Dynamic Behaviour of Bridges at the Transport and Road Research Laboratory, Crowthorne, Berkshire, England, May 19, 1977.* TRRL Rpt. 275 Proceeding. 1977.

[44] S.R. Ibrahim, K.R. Wentz, and J. Lee. “Damping identification from non-linear random responses using a multi-triggering random decrement technique”. In: *Mechanical Systems and Signal Processing* 1.4 (1987), pp. 389–397.

[45] L. Wang and A. Kareem. “Modeling of non-stationary winds in gust-fronts”. In: *9th ASCE specialty conference on probabilistic mechanics and structural reliability*. Curran Associates NY. 2004, pp. 1–6.

[46] Weather Guys Editor. *What causes wind gusts?* Jan. 2012. URL: https://wxguys.ssec.wisc.edu/2012/01/09/what-causes-wind-gusts/.

[47] A. Tate. *Understanding the Importance of Stationarity in Time Series*. Dec. 2023. URL: https://hex.tech/blog/stationarity-in-time-series/.

[48] Statistics How To. *Stationarity Differencing: Definition, Examples, Types*. 2025. URL: https://www.statisticshowto.com/stationarity/.

[49] S. Prabhakaran. *Augmented Dickey Fuller Test (ADF Test)*. Apr. 2022. URL: https://www.machinelearningplus.com/time-series/augmented-dickey-fuller-test/.

[50] H. Bohn Nielsen. *Non-Stationary Time Series and Unit Root Tests*. 2005. URL: https://web.archive.org/web/20161130133316/http://www.econ.ku.dk/metrics/Econometrics2_05_II/Slides/08_unitroottests_2pp.pdf.

[51] A. Entezami and H. Shariatmadar. “Damage localization under ambient excitations and non-stationary vibration signals by a new hybrid algorithm for feature extraction and multivariate distance correlation methods”. In: *Structural Health Monitoring* 18.2 (2019), pp. 347–375.

[52] C. Dyrbye and S.O. Hansen. “Wind loads on structures”. In: (1996).

[53] C. Lin and D. Chiang. “Modal identification from nonstationary ambient response data using extended random decrement algorithm”. In: *Computers & Structures* 119 (2013), pp. 104–114.

[54] H. Pishro-Nik. *Linear Time-Invariant (LTI) Systems with Random Inputs*. URL: https://www.probabilitycourse.com/chapter10/10_2_2_LTI_systems_with_random_inputs.php.

[55] D. Tang et al. “Modal analysis of multi-degree-of-freedom dynamic system based on non-stationary response data”. In: *Journal of sound and vibration* 347 (2015), pp. 139–149.

[56] Z. Huang and M. Gu. “Envelope random decrement technique for identification of nonlinear damping of tall buildings”. In: *Journal of Structural Engineering* 142.11 (2016), p. 04016101.

[57] Wikipedia. *Runge–Kutta methods*. Apr. 2025. URL: https://en.wikipedia.org/wiki/Runge%E2%80%93Kutta_methods.

[58] The SciPy community. *solve$_ivp$—$SciPyv$1.15.3$Manual$*. 2025. URL: https://docs.scipy.org/doc/scipy/reference/generated/scipy.integrate.solve_ivp.html.

[59] J.H. Mathews and K.D. Fink. *Numerical methods using MATLAB*. Prentice Hall, Jan. 2004.

[60] Q.S. Li et al. “Field measurements of amplitude-dependent damping in a 79-storey tall building and its efects on the structural dynamic responses”. In: *The structural design of tall buildings* 11.2 (2002), pp. 129–153.

[61] Y. Quan, M. Gu, and Y. Tamura. “Experimental evaluation of aerodynamic damping of square super high-rise buildings”. In: *Wind and Structures* 8.5 (2005), pp. 309–324.

[62] Wikipedia. *Bias of an estimator*. Apr. 2025. URL: https://en.wikipedia.org/wiki/Bias_of_an_estimator.

[63] Adam Hayes. *What Is a Confidence Interval and How Do You Calculate It?* May 2025. URL: https://www.investopedia.com/terms/c/confidenceinterval.asp.

[64] J.A. Little and B.P. Mann. “Optimizing logarithmic decrement damping estimation through uncertainty propagation”. In: *Journal of Sound and Vibration* 457 (2019), pp. 368–376.

A

Computation Peak Acceleration

Appendix A presents the procedure for calculating peak acceleration a_{max} presented in equation A.1) according to Annex C of EN 1991-1-4 [10]. The goal is to assess how errors in damping estimates affect the resulting peak acceleration. Table A.1 lists and describes all variables appearing in the equations presented in section A.1.

A.1. Formulas according to Annex C of EN 1991-1-4

$$a_{max} = k_p \cdot \sigma_a \tag{A.1}$$

The peak acceleration is a product of the peak factor k_p (eq. A.2) and the standard deviation of the characteristic along-wind acceleration $\sigma_{a,x}(y,z)$ (eq. A.3).

$$k_p = \sqrt{2 \cdot \ln(\nu \cdot T)} + \frac{0.6}{\sqrt{2 \cdot \ln(\nu \cdot T)}} \tag{A.2}$$

$$\sigma_a(y,z) = \rho \cdot c_F \cdot I_v(z_s) \cdot v_m^2(z_s) \cdot R \cdot \frac{K_y \cdot K_z \cdot \Phi(y,z)}{\mu_{\text{ref}} \cdot \Phi_{max}} \tag{A.3}$$

The peak factor k_p depends, among other factors, on the up-crossing frequency ν (eq. A.4).

$$\nu = n_{1,x} \cdot \sqrt{\frac{R^2}{B^2 + R^2}} \tag{A.4}$$

The standard deviation of the along-wind acceleration $\sigma_{a,x}(y,z)$ depends, among other factors, on the resonance response R^2 (eq. A.5) and the size reduction function (eq. A.6).

$$R^2 = \frac{\pi^2}{4 \cdot \pi \cdot \xi} \cdot S_L(z_s, \eta_{1,x}) \cdot K_s(\eta_{1,x}) \tag{A.5}$$

$$K_s(\eta) = \frac{1}{1 + \sqrt{(G_y \cdot \phi_y)^2 + (G_z \cdot \phi_z)^2 + (\frac{2}{\pi} \cdot G_y \cdot \phi_y \cdot G_z \cdot \phi_z)^2}} \tag{A.6}$$

$$\text{with} \quad \phi_y = \frac{c_y \cdot b \cdot \eta}{v_m(z_s)} \quad \text{and} \quad \phi_z = \frac{c_z \cdot h \cdot \eta}{v_m(z_s)} \tag{A.7}$$

A.2. Effect of Damping on Peak Acceleration

Table A.1 identifies the parameters depending on the damping ratio ξ. Essentially the dependence on damping boils down to the resonance factor R^2, present in the expression for the up-crossing frequency as well as the standard deviation of the wind acceleration. Analysing first the expression for the up-crossing frequency ν (eq. $A.4$), EN 1991-1-4 mentions that the use of $B^2 = 1$ is conservative. Equation A.4 then simplifies to the expression shown in equation A.8. Finally, it can be concluded that the peak acceleration is proportional to the inverse of the square root of the damping ration (eq. A.9).

$$\nu = n_{1,x} \tag{A.8}$$

$$a_{max} \propto \frac{1}{\sqrt{\xi}} \tag{A.9}$$

To investigate the influence of damping uncertainty on the variability of peak acceleration, a range of ± 10 % around the damping value is considered. Equations A.10 and A.11 show that a variability of ± 10 % around the damping value propagates to a variability of approximately ± 5 % around the peak acceleration.

$$a_{max,upperbound} = \frac{1}{\sqrt{0.90}} \cdot \frac{1}{\sqrt{\xi}} = 1.054 \cdot a_{max} \tag{A.10}$$

$$a_{max,lowerbound} = \frac{1}{\sqrt{1.10}} \cdot \frac{1}{\sqrt{\xi}} = 0.953 \cdot a_{max} \tag{A.11}$$

A.3. Table of variables and parameters

Symbol	Equation	Description	Dependence on Damping
k_p	A.2	peak factor	dependent (ν)
T	A.2	averaging time for the mean wind velocity	independent
ν	A.2, A.4	up-crossing frequency	dependent (R^2)
R^2	A.4	resonance response	dependent (ξ)
B^2	A.4	background factor	independent
$\sigma_{a,x}(y,z)$	A.3	standard deviation of the characteristic along-wind acceleration	dependent (R)
c_f	A.3	force coefficient	independent
ρ	A.3	air density	independent
$I_v(z_s)$	A.3	turbulence intensity at the height z_s above ground	independent
$v_m(z_s)$	A.3	mean wind velocity at height z_s	independent
z_s	A.3	reference height	independent
K_y and K_z	A.3	constants	independent
μ_{ref}	A.3	reference mass per unit area	independent
$\Phi(y,z)$	A.3	mode shape	independent
Φ_{max}	A.3	mode shape value at the point with maximum amplitude	independent
R	A.3, A.5	square root of resonance response	dependent (ξ)
ξ	A.5	damping ratio	-
S_L	A.5	wind power spectral density function	independent
$\eta_{1,x}$	A.5	natural frequency of the structure	independent
K_s	A.5, A.6	size reduction function	independent
G_y and G_z	A.6	constants depending on mode shape variation	independent
ϕ_y	A.6, A.7	mode shape in y-direction	independent
ϕ_y	A.6, A.7	mode shape in z-direction	independent
c_y and c_z	A.7	decay constants	independent
b and h	A.7	width and height of the structure	independent

Table A.1: Summary and description of variables in the computation of the peak acceleration, according to Annex C, EN 1991-1-4 [10]

B

Figures & Tables

Appendix B contains the detailed data used to generate the graphs in this thesis.

B.1. Statistical Evaluation of Response Data

B.1.1. Analysis of Response Signals

Figures B.1 and B.2 illustrate how the displacement response evolves under increasingly non-stationary excitation. Both figures show the system's response to excitation types 1, 2, and 3, respectively, as defined in section 3.4. P refers to the peak magnitude of the Gaussian pulse used in the derivation of the time-dependent mean function $\mu(t)$, as defined in section 3.4.3.

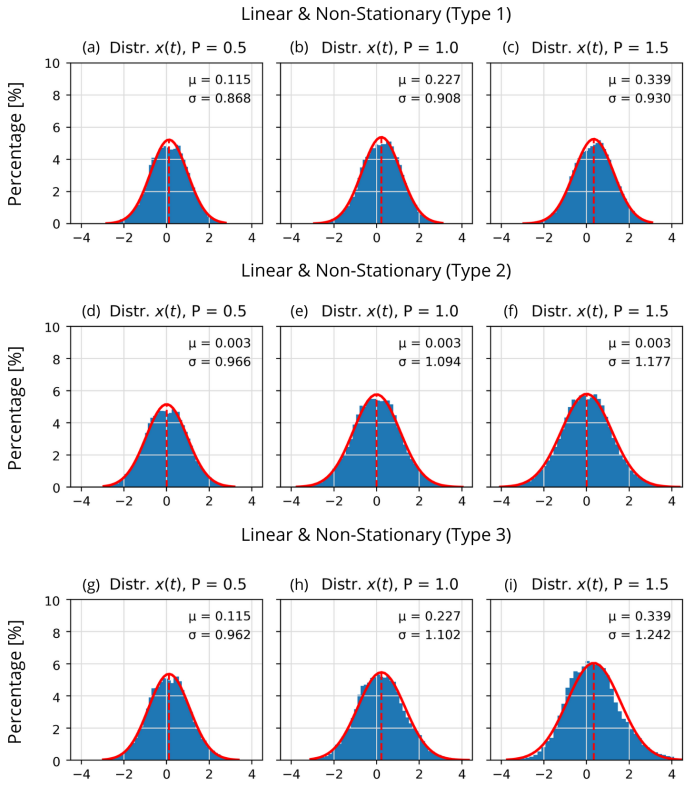

Figure B.1: Distribution of data points in displacement response derived on the linear system for the three types of non-stationary excitation; (a), (b) and (c) corresponding to excitation with time-dependent mean; (d), (e) and (f) corresponding to excitation with time-dependent variance; (g), (h) and (i) corresponding to excitation with time-dependent mean and variance

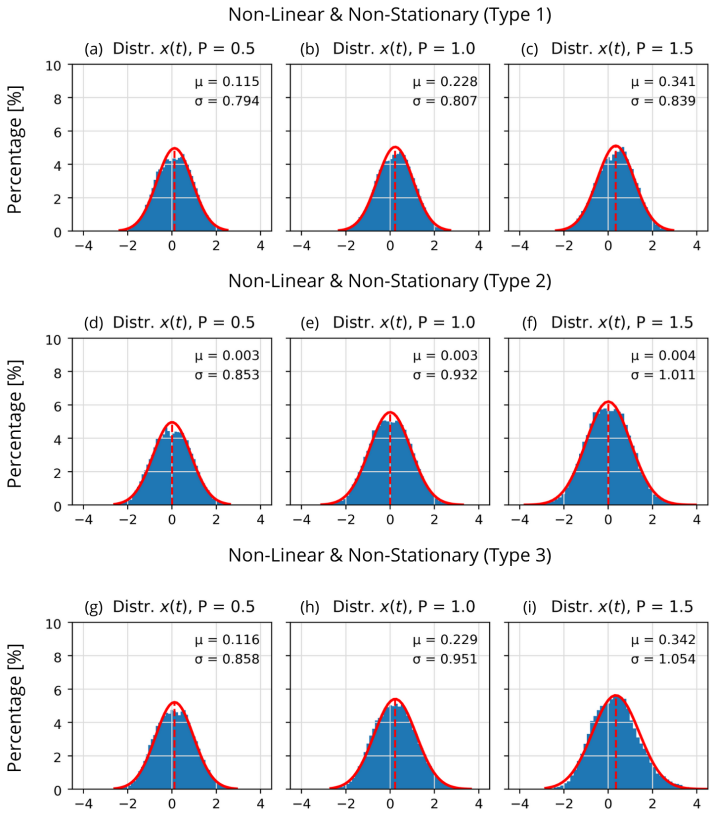

Figure B.2: Distribution of data points in displacement response derived on the system with amplitude-dependent damping for the three types of non-stationary excitation; (a), (b) and (c) corresponding to excitation with time-dependent mean; (d), (e) and (f) corresponding to excitation with time-dependent variance; (g), (h) and (i) corresponding to excitation with time-dependent mean and variance

B.1.2. Quantification of Non-stationarity

	S	NS1			NS2			NS3		
		P 0.5	P 1.0	P 1.5	P 0.5	P 1.0	P 1.5	P 0.5	P 1.0	P 1.5
Linear	100	0	0	0	100	100	100	0	0	0
Non-linear	100	0	0	0	100	100	100	0	0	0

Table B.1: Percentage of stationary response data for all cases, evaluated using the intersection of the ADF and KPSS stationarity tests

B.2. System Non Linearity

B.2.1. Sensitivity Analysis

Table B.2 summarizes the statistics of the damping distributions obtained by varying the RDS length in the Peak RDT algorithm.

Cycles	**Amplitude Ranges [%]**					
	0 - 16.7	16.7 - 33.3	33.3 - 50	50 - 66.7	66.7 - 83.3	83.3 - 100
			Means [10^{-2}]			
1	1.20	0.71	1.11	1.62	2.00	2.30
3	0.88	0.79	1.13	1.54	1.89	2.10
5	1.09	0.87	1.14	1.48	1.79	2.02
7	1.10	0.92	1.15	1.44	1.73	1.90
10	1.08	0.96	1.17	1.40	1.66	1.80
			95% Confidence Intervals [10^{-2}]			
1	$\pm$0.22	$\pm$0.08	$\pm$0.05	$\pm$0.06	$\pm$0.14	$\pm$0.53
3	$\pm$0.19	$\pm$0.07	$\pm$0.03	$\pm$0.04	$\pm$0.09	$\pm$0.44
5	$\pm$0.15	$\pm$0.06	$\pm$0.03	$\pm$0.03	$\pm$0.08	$\pm$0.38
7	$\pm$0.15	$\pm$0.06	$\pm$0.03	$\pm$0.03	$\pm$0.08	$\pm$0.39
10	$\pm$0.14	$\pm$0.06	$\pm$0.03	$\pm$0.03	$\pm$0.08	$\pm$0.45
			Variance [10^{-5}]			
1	12.83	1.77	0.64	0.94	4.62	10.08
3	9.07	1.11	0.26	0.34	1.92	6.70
5	6.21	0.91	0.21	0.26	1.65	5.01
7	5.49	0.90	0.20	0.22	1.60	5.27
10	5.37	0.85	0.21	0.20	1.49	7.29
			Bias [10^{-3}]			
1	4.01	-0.86	0.11	-0.76	-0.03	3.05
3	0.76	-0.14	0.30	-1.61	-1.11	1.01
5	2.91	0.70	0.41	-2.21	-2.11	0.23
7	2.98	1.18	0.53	-2.62	-2.69	-0.97
10	2.81	1.56	0.70	-3.01	-3.38	-2.00
			Relative Error [%]			
1	50.17	10.72	0.97	4.45	0.14	15.24
3	9.46	1.69	2.77	9.47	5.56	5.07
5	36.35	8.78	3.69	13.01	10.57	1.17
7	37.27	14.73	4.78	15.42	13.47	4.85
10	35.12	19.51	6.33	17.68	16.88	10.00

Table B.2: Summary statistics of the damping distributions obtained with varying RDS length in the system with amplitude-dependent damping under stationary excitation, corresponding to figures 6.3 and 6.4

B.2.2. Effect of Segment Length

Linear										
Cycles	1	2	3	4	5	6	7	8	9	10
Mean estimate [%]	0,93	0,93	0,93	0,93	0,93	0,93	0,93	0,93	0,93	0,93
LD estimate [%]	0,87	0,92	0,96	1,00	0,87	0,95	0,91	0,80	0,84	0,85
Ratio	0,93	0,99	1,04	1,07	0,94	1,02	0,98	0,85	0,90	0,91
Non-Linear										
Mean estimate [%]	0,96	0,96	0,96	0,96	0,96	0,96	0,96	0,96	0,96	0,96
LD estimate [%]	0,65	0,82	0,95	1,11	0,96	1,12	1,06	1,01	1,13	1,08
Ratio	0,68	0,86	1,00	1,16	1,01	1,17	1,11	1,06	1,18	1,13

Table B.3: Point A, Mean estimate obtained through curve fitting in comparison with damping estimates obtained with the Logarithmic Decrement method

Linear										
Cycles	1	2	3	4	5	6	7	8	9	10
Mean estimate [%]	1,02	1,02	1,02	1,02	1,02	1,02	1,02	1,02	1,02	1,02
LD estimate [%]	1,09	1,00	1,02	1,00	1,05	1,00	0,97	1,00	0,98	1,05
Ratio	1,06	0,98	1,00	0,98	1,03	0,98	0,95	0,98	0,96	1,03
Non-Linear										
Mean estimate [%]	1,66	1,66	1,66	1,66	1,66	1,66	1,66	1,66	1,66	1,66
LD estimate [%]	1,97	1,79	1,61	1,62	1,52	1,56	1,44	1,31	1,42	1,26
Ratio	1,19	1,07	0,97	0,98	0,91	0,94	0,87	0,79	0,85	0,76

Table B.4: Point B, Mean estimate obtained through curve fitting in comparison with damping estimates obtained with the Logarithmic Decrement method

Point A				
	Cycle 10		**Cycle 3**	
	Linear	**Non-linear**	**Linear**	**Non-linear**
Target Damping [%]	1.00	0.80	1.00	0.80
Mean Damping [%]	1.02	0.96	0.92	0.78
Ratio	1.02	1.20	0.92	0.98
Point B				
	Cycle 10		**Cycle 3**	
	Linear	**Non-linear**	**Linear**	**Non-linear**
Target Damping [%]	1.00	2.00	1.00	2.00
Mean Damping [%]	1.02	1.67	1.06	1.89
Ratio	1.02	0.84	1.06	0.95

Table B.5: Target and mean damping values compared for all cases

B.3. Performance Assessment

Section **??** - Effect of Amplitude-dependent damping on reliability of damping estimates

Relative Amplitude Range	$[10^{-2}]$	0-12.5	12.5-25	25-37.5	37.5-50	50-62.5	62.5-75	75-87.5	87.5-100
Target	$[10^{-2}]$	1.00	1.00	1.00	1.00	1.00	1.00	1.00	.
Mean	$[10^{-2}]$	1.00	0.93	1.00	1.00	1.03	1.08	1.05	.
95% Confidence Intervals	$[10^{-2}]$	$\pm$0.18	$\pm$0.06	$\pm$0.03	$\pm$0.03	$\pm$0.04	$\pm$0.08	$\pm$0.20	.
Variance	$[10^{-5}]$	8.28	1.03	0.32	0.20	0.50	1.43	2.72	.
Bias	$[10^{-3}]$	-0.05	-0.69	0.02	-0.02	0.26	0.79	0.48	.
Relative Error	[%]	0.50	6.90	0.20	0.20	2.60	7.90	4.80	.

Table B.6: Statistical statistics corresponding to damping estimates of benchmark system (blue) in figure 7.5

Relative Amplitude Range	$[10^{-2}]$	0 - 16.7	16.7 - 33.3	33.3 - 50	50 - 66.7	66.7 - 83.3	83.3 - 100
Target	$[10^{-2}]$	0.80	0.80	1.10	1.70	2.00	2.00
Mean	$[10^{-2}]$	0.88	0.79	1.13	1.54	1.89	2.10
95% Confidence Intervals	$[10^{-2}]$	$\pm$0.19	$\pm$0.07	$\pm$0.03	$\pm$0.04	$\pm$0.09	$\pm$0.44
Variance	$[10^{-5}]$	9.07	1.11	0.26	0.34	1.92	6.70
Bias	$[10^{-3}]$	0.76	-0.14	0.30	-1.61	-1.11	1.01
Relative Error	**[%]**	9.5	1.7	2.8	9.5	5.6	5.1

Table B.7: Statistical statistics corresponding to damping estimates of non-linear system (orange) in figure 7.5

B.4. Reliability of Damping Estimates

Figures B.3, B.4 and B.5 present the summary statistics of the damping estimates correspondsing to the linear and non-linear systems excited by the three different types of non-stationary excitation.

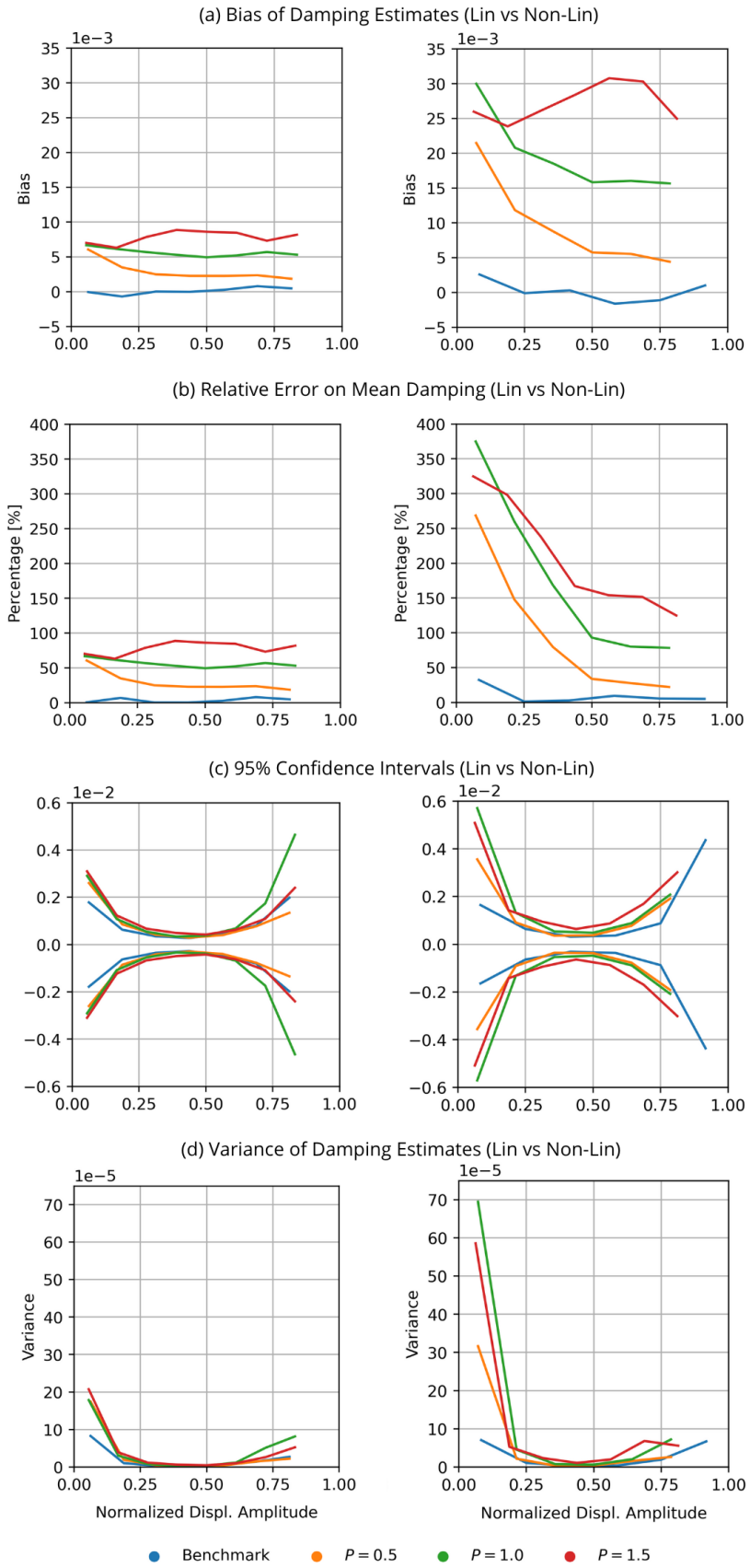

Figure B.3: Linear and non-linear systems under non-stationary excitation of type 1 (time-dependent mean), the left row shows the summary statistics of the linear system and the right side those of the system with amplitude-dependent damping for different levels on non-stationarity; (a) Bias of damping estimates; (b) Relative error on mean damping; (c) 95% Confidence Intervals on mean damping; (d) Variance of damping estimates

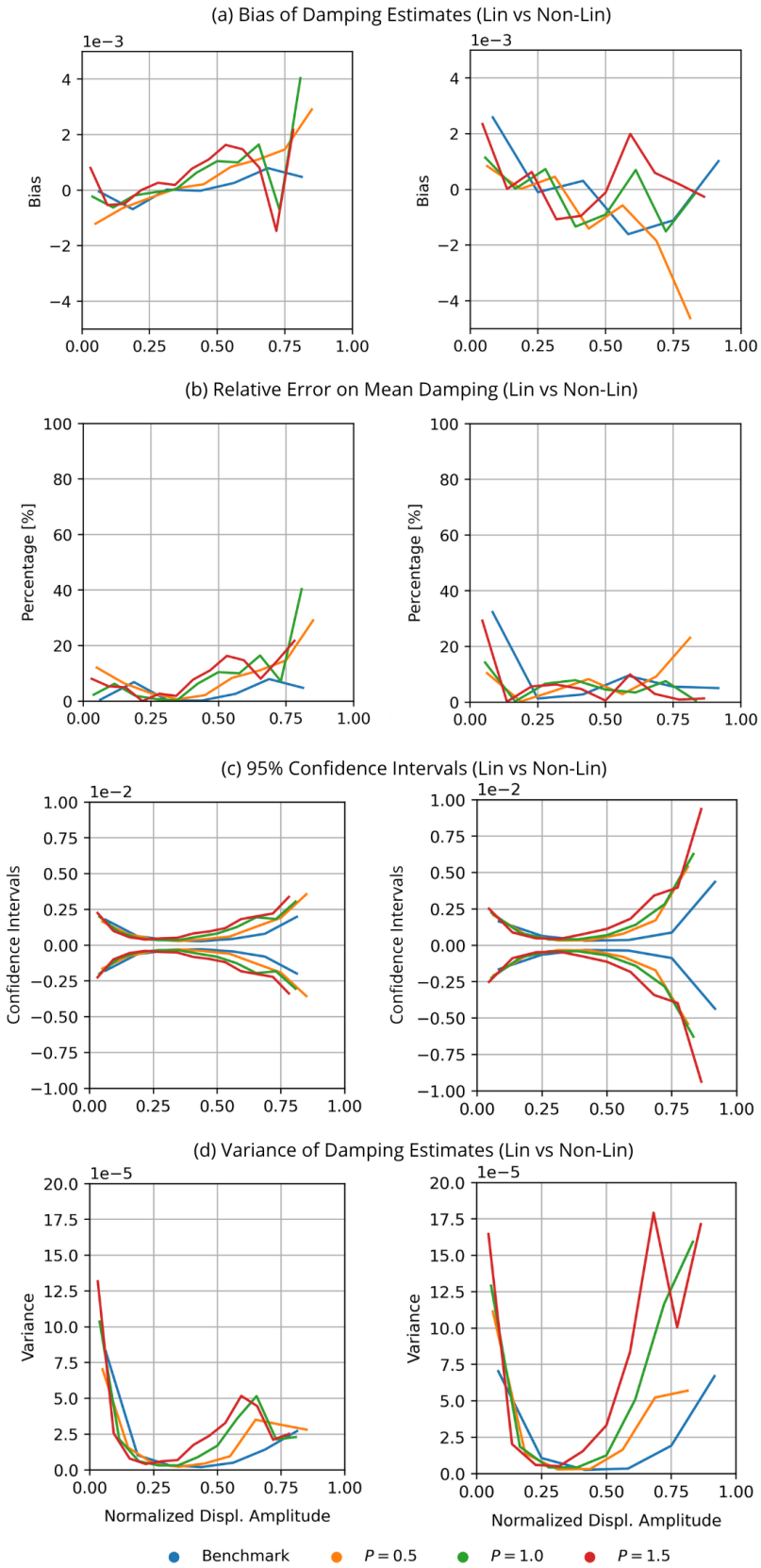

Figure B.4: Linear and non-linear systems under non-stationary excitation of type 2 (time-dependent variance), the left row shows the summary statistics of the linear system and the right side those of the system with amplitude-dependent damping for different levels on non-stationarity; (a) Bias of damping estimates; (b) Relative error on mean damping; (c) 95% Confidence Intervals on mean damping; (d) Variance of damping estimates

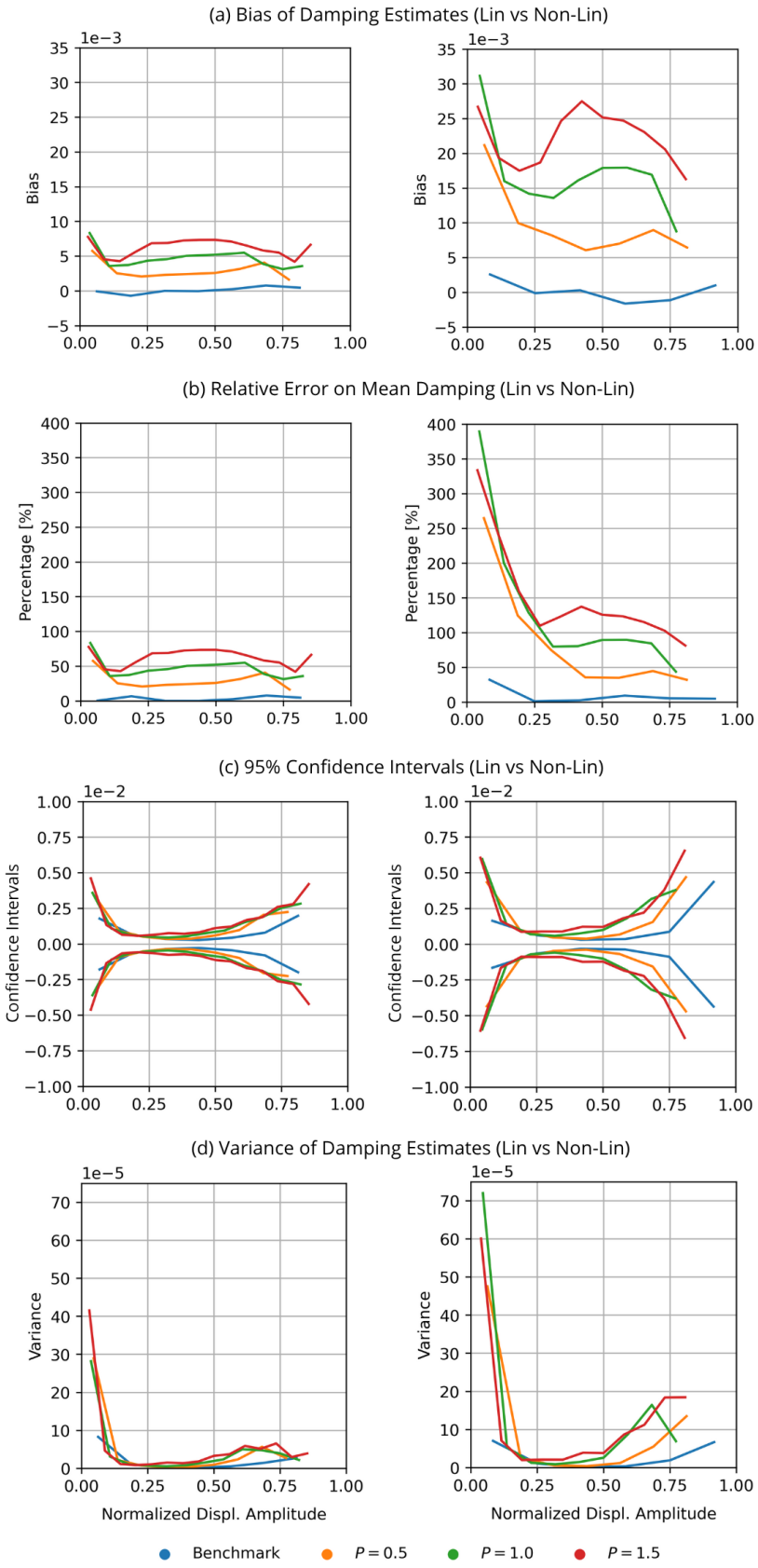

Figure B.5: Linear and non-linear systems under non-stationary excitation of type 3 (time-dependent mean and variance), the left row shows the summary statistics of the linear system and the right side those of the system with amplitude-dependent damping for different levels on non-stationarity; (a) Bias of damping estimates; (b) Relative error on mean damping; (c) 95% Confidence Intervals on mean damping; (d) Variance of damping estimates